

THE UNBC BEDLOAD MOVEMENT DETECTOR:
CALIBRATION, INITIAL RESULTS AND ANALYSIS

by

Jon Tunncliffe

THESIS SUBMITTED IN PARTIAL FULFILMENT OF
THE REQUIREMENTS FOR THE DEGREE OF
MASTER OF SCIENCE

in

NATURAL RESOURCES AND ENVIRONMENTAL STUDIES

© Jon Tunncliffe, 2000

THE UNIVERSITY OF NORTHERN BRITISH COLUMBIA

July 2000

All rights reserved. This work may not be
reproduced in whole or in part, by photocopy or
other means, without the permission of the author.

**UNIVERSITY OF NORTHERN
BRITISH COLUMBIA
LIBRARY
Prince George, BC**

Table of Contents

Table of Contents	iii
List of Tables	vi
List of Figures.....	vii
Acknowledgements	xi
Acknowledgements	xi
Abstract.....	xii
Introduction.....	1
CHAPTER 1 BEDLOAD TRANSPORT AND ITS MEASUREMENT	6
1.1 Bedload Transport.....	6
1.1.1 The Entrainment Threshold	7
1.1.2. The Role of Turbulence	9
1.1.3 The Effects of Relative Protrusion, Clusters and Bed Armouring.....	10
1.1.4. Multi-phase models of transport	12
1.2 Measuring Bedload Movement.....	13
1.2.1 Direct Measurement.....	13
1.2.2 Indirect Measurement	19
1.3 Stuart-Takla Bedload Studies	21
1.4 New Bedload Sampling Technology	22
CHAPTER 2 THE UNBC BEDLOAD MOVEMENT DETECTOR.....	24
2.1 The Sensor	24
2.2 The Housing Unit.....	26
2.3 Data Acquisition	28
2.4 Power Supply	29

2.5 The Study Site.....	30
2.5.1 Sediment Supply	31
2.5.2 Lithologies	34
CHAPTER 3 TIME SERIES AND FREQUENCY ANALYSIS	36
3.1 Identification and Characterization of Signals and Frequencies.....	37
3.1.1. The Influences of Clast Velocity On a Signal	42
3.1.2 The Influences of Clast Size On a Signal	44
3.2 Random Passage of Sediment.....	47
CHAPTER 4 ANALYSIS OF THE FLOOD DATA RECORD	50
4.1 Nival Flood, 1998	52
4.2 Nival Flood, 1999	55
4.3 Sediment Transport Patterns	62
4.3.1 Marginal Transport	62
4.3.2 Clustered Transport.....	63
4.3.3 Continuous Transport.....	64
4.3.4 Sand Streets.....	65
CHAPTER 5 PATTERNS OF BEDLOAD TRANSPORT	68
5.1 Discussion of Sediment Transport in O’Ne-ell Creek	68
5.2 Temporal Variation in Transport	68
5.3 Pulsations in the 1999 transport record.....	72
5.4 Lateral Instability - The Shifting Locus of Transport.....	73
5.5 Transport Volumes – A Transport Estimate from the 1999 Nival Event	75
5.5.1 Magnitude of Error	81
5.5.2 Stream Efficiency.....	82
5.6 Comparison with Existing Data	84
CHAPTER 6 FUTURE DIRECTIONS AND CONCLUSION	86
6.1 Flume Studies.....	86
6.2 Device Installation	86

6.3 Automation and Signal Processing	87
Conclusions	89
References	91
Appendix A – Glossary	100
Appendix B – Gravel sampling data	104
Appendix C – Laboratory calibration data	117

Definitions for terms in **bold type** throughout the text can be found in Appendix A – Glossary, on page 100.

List of Tables

Table 1 – Representative lithologies found in the bed material at O’Ne-ell Creek, N=234.	34
Table 2 - An estimate of the total number of grains per kilogram of bed material from O’Ne-ell Creek, based on 4 bulk samples taken at the study site.	80
Table 3 - Daily particle counts, with associated bulk sediment transport estimates. The record from June 16 th is incomplete.....	81
Table 4 - Summary of hydraulic parameters at O’Ne-ell 1950.	83
Table 5 – Calculations of transport rates through three reaches in the Stuart-Takla Watersheds. Cut/Fill Volumes are taken from morphological estimates made by Poirier (2000). Morphological Step Lengths and Tracer Step Lengths provide two estimates of transport distances within the reach. Cut/Fill volumes are accordingly divided by the number of step lengths in the reach, providing two estimates of transport volumes.....	85
Table 6 - Freeze Core sample data.....	105
Table 7 - Bulk Sample (15cm deep) Sieve Data - cont on next page	106
Table 8 - Bulk sample (30cm deep) Sieve Data	108
Table 9- Sample of Magnetic Sampling Data (All clasts < 50mm).....	109
Table 10 - Characteristics of rock samples used in pendulum experiments.	117

List of Figures

Figure 1 - The Stuart-Takla Experimental Watersheds	2
Figure 2 – O’Ne-ell Creek hydrograph - 1994-1997. Measurements were taken at an MOF gauging station 300m downstream of the study site. The flows shown here include Tsitsutl Creek, (approx. 250m downstream of the BMD site) which adds some 40% to the discharge.	3
Figure 3 – Gluskie, Forfar, O’Ne-ell and VanDecar drainages along Middle River.	4
Figure 4 - Vertical variation in transported material. After Klingeman, 1981.	6
Figure 5 – Force moment balance diagram for the entrainment of a single-sediment grain.	7
Figure 6 – The VUV pressure difference sampler – top and side views (Hubbell, 1967)	14
Figure 7 – The Helley-Smith portable sampler (Emmett, 1980)	15
Figure 8 – The initial bedload detector design by Ergenzinger and Custer (1983)	18
Figure 9 – Exploded view of the sensor (above), sensor dimensions and the assembled product.	25
Figure 10 – Voltage response as ferrous items pass at various points on the sensor.....	26
Figure 11 – Schematic diagram of the BMD installed in the creek bed	26
Figure 12 - Photo of the study site in early August. The instrument shed is located on the east side of the creek. The BMD is set within the streambed downstream of a group of mature sockeye salmon. A log and wire-rope cable provided access to the stream cross-section at all stages.	27
Figure 13 - The O’Ne-ell Creek watershed.	30
Figure 14 – Grain size distribution from four bulk sieve samples. Three samples were excavated to a depth of 15 cm and one (represented by a dashed line) went to 25 cm.	32
Figure 15 – Grain size distribution from freeze-core samples. Dashed lines indicate subsurface samples (below 15 cm) and solid lines indicate surface material.	32

Figure 16 – Texture of the stream bed at the study site, based on a 1998 topographic survey.....	33
Figure 17 – Time series $x(t)$ of a sensor’s response to a passing clast.....	37
Figure 18 – The signal trace $x(t)$ (black) with its corresponding Hilbert transform $h(t)$ (dashed) and signal envelope $A(t)$, shown in gray.....	38
Figure 19 – A sine pulse presented in time and frequency space. The relative brightness (z-scale magnitude) indicates the intensity of the frequencies. Note that the peak frequency response of the signal is located at $(31.6 \div 2 =) 15.8$ Hz, and occurs at $15/100$ s.....	40
Figure 20 – STFT spectrogram of a single sensor trace during a flood event.....	41
Figure 21 –The relationship of velocity and signal frequency for clasts of different sizes.	42
Figure 22 – Stage/Discharge rating graph for O’Ne-ell Creek 1950, June 1999.....	43
Figure 23 – Velocity profile at O’Ne-ell 1950, May-June, 1999. The exponential lines indicate the Universal Velocity Distribution Law for channel geometries based on low stage (May 17 th - 0.23m) and high stage (June 14 th - 0.68m). Four velocity measurements are indicated for each measurement period – two sets taken at 0.6 and 0.2 depth in the area of maximum flow.	44
Figure 24 –Signal amplitude diminishes and period increases with lower clast velocities	45
Figure 25– A comparison of signal envelopes for different sized clasts.	45
Figure 26 - A comparison of clast size versus the “apparent” clast size calculated from analysis of the voltage signal from a sensor.	46
Figure 27 - The probability function facing a particle as it approaches the device. The dashed line indicates the possible chord length of its transect across a sensor. The relative sensitivity of the sensor is outlined by the experiments introduced in Section 2.1.....	48
Figure 28 - The BMD Record consists of summing the voltage activity in absolute (positive) units for each channel in 30 second intervals. The resultant sums, showing the magnitude of activity across the channel width, are shown in the chart on the right.	51

Figure 29 - The sums for each 30-seconds interval are then plotted over the hours and days of the flood event. Here a 2.5 hour section of data from 20:00 to 22:30 on June 11 is shown.	51
Figure 30 - Stage readings during the 1998 nival flood. The gauge was swamped during the peak flows, and thus data from the night of May 25 have been reconstructed from readings taken just upstream of the station. Flow subsided quickly over the next three days.	52
Figure 31 - Data from the peak of the 1998 flood event, May 25 and 26.....	54
Figure 32 - Stage, bedload activity and suspended sediment readings from the 1999 flood.	56
Figure 33 - BMD Site Water Velocity Cross Section: contours based on maximum stage measurements in 1999 show the variation in velocity across the channel width. The vertical dimension is exaggerated threefold.	57
Figure 34 (following pages) - The BMD record from June 10 to June 17. The channel width is measured from the west side of the channel to the east. File lengths vary from one half hour to four hours. Gaps between the files are from maintenance and technical problems. Most of the record on June 16 was missed after a disk drive failure.	58
Figure 35 - Marginal transport.....	62
Figure 36 - Clustered transport.	64
Figure 37 - Transport at the height of the flood event.	65
Figure 38 - Steady discharge of sand and gravel along the bed.....	66
Figure 39 - The onset of a gravel street, 1.2 m wide. The steady passage of material lasted for over 10 minutes. This diagram shows the first 90 seconds of the transport event.....	67
Figure 40 - Figure from Ehrenberger's bedload measurements, taken with a basket sampler on the River Danube at Vienna National Bridge, 24 June 1931 suggest a pulsating movement of bedload. Sampling time=100-300s. Mean transport rate = 0.236 kg/s/m. (Ehrenberger, 1931 - Fig. 6). Taken from Gomez, 1991.	69
Figure 41 - Results from magnetic bedload detector at Squaw Creek, Montana (Bunte 1996).	70

- Figure 42 – Total transport rate versus time. Measurements were taken in a gravel-bed flume, showing transport fluctuations on the order of tens of minutes (Kuhnle and Southard, 1988)..... 70
- Figure 43 - Figure showing the pulsing nature of bedload transport. The upper portion of the graph displays the width of the stream over the course of 4 hours on June 15. The lower half of the graph is the voltage from a sensor located 3.4 meters from the right bank of the creek. 73
- Figure 44 – The wandering locus of transport – the locus of transport is defined here as the zone of maximum bedload activity throughout each data file from the 1999 Nival event. The locus of transport moved substantially throughout the event, starting within roughly 1 m of the right bank (see Figure 34, June 11th) and drifting to within 2 m of the right bank (June 15-16). 74
- Figure 45 - The total activity across each sensor is summed for every BMD file. File lengths are usually 3-4 hours. Summed values were divided by the length of the file to ensure compatible numbers. The cross section profile (see Figure 33) adds the context of channel geometry. 74
- Figure 46- Distribution of grain geometries based on a sampling of material >50 mm. The average sphericity of particles is 0.7..... 77
- Figure 47 - Size distribution of the theoretical bedload material used in the calculations. The proportions are based on the 4 bulk samples of bed material taken at the site. The coarsest material is 45 mm (5.5 ψ), and the assumed threshold of detection is 4 mm (2.0 ψ). 78
- Figure 48 – Rates of particle transport (number of events per second) over the course of the flood. 79
- Figure 49 - The effect of two important parameters in the volumetric transport estimate. As the assumed threshold of detection by a BMD sensor increases from 0.5 mm to 8 mm, the estimate of transported material grows by several orders of magnitude. The assumptions regarding the largest particle in motion (y-axis) affect the volumetric estimate as well - as the assumed size moves from 8 mm to 64 mm, the estimate increases by a factor of 3. 82
- Figure 50 - Locations of gravel sampling sites at the BMD study site..... 104

Acknowledgements

I would like to first of all acknowledge Dr. Allen Gottesfeld for his expert guidance and contagious enthusiasm for the study of Northern BCs rich legacy of geomorphology. I would also like to thank Ron Poirier and Tim Dressel for helpful discussions and technical assistance.

For their helpful comments and encouragement with this study, I would like to thank my committee members, Moustafa Mohamed and Peter Jackson.

Thanks are due to Rob Huggins (Geometrics of Palo Alto, CA) and Dr. Tadeusz Ulrych (UBC) for advice, readings and encouragement in my crash course in digital signal processing. I am grateful to Michael Church for the opportunity to present and discuss the BMD project with graduate colleagues at UBC. For their support in the field, I would like to thank the staff at the DFO camp, including Erland MacIsaac, Herb Herunter, and John Heinonen. Pierre Beaudry provided assistance with the monitoring program at O'Ne-ell Creek. Thank you to Dev Khurana for help with the gravel sampling and site reconnaissance. I am also indebted to the people of the Tl'azten Nation, from whom I have had the good fortune to learn about the Middle River area, particularly Wally Joseph and Paul Williams.

Most importantly, thanks are due to my partner, Kristiann Allen, for seeing me through two field seasons and thesis writing with boundless encouragement, inspiration and magic.

This research was supported by a grant from the Ecosystems Research Program of Forest Renewal British Columbia, under research award # OP96043-RE.

Abstract

In September 1997 the UNBC Bedload Movement Detector was installed in O'Ne-ell Creek, a mountain gravel bed river in the northern headwaters of the Fraser River. The device is designed to measure coarse sediment flux by passive induction as bedload material (> 1 mm), containing natural ferrous minerals, passes over an array of electromagnetic sensors. The device consists of a series of 82 sensors, housed in an aluminum beam and placed across the stream, inserted such that its surface is flush with the gravel bed. The device can be raised or lowered to compensate for bed aggradation and scour. A data acquisition system collects signals from the device at 100 Hz, providing a continuous, high-resolution record of any bedload transport event. The device is sensitive enough to record the movement of most volcanic, metamorphic, granitic, and ultramafic clasts larger than a few millimeters.

The installation and operation of the device is described, as well as the calibration and development of signal processing routines for estimating transport rates. Nival event transport records are presented and discussed. Some of the phenomena apparent in the records include: a pulsating pattern of activity, discrete 'sweep transport' events, lateral movement of the transport zone, and a sudden onset of bed movement with a tapered cessation. An initial estimate of transport volumes compares favourably with existing measurements taken at the study site. It is anticipated that more sophisticated calibration work will continue in the future.

Introduction

The regime of a gravel-bed river system is the product of the complex interaction between stream morphology and water and sediment discharge. The transport of sediment along a channel is a critical linkage in this balance, and a decidedly difficult phenomenon to measure. Although some relations have been established between the fluid forces exerted by the flow and sediment transport, the relation is not uniform, and is subject to variations in time and space, even under conditions of steady flow.

Material that is carried along the channel originates from sources both within and outside the fluvial system. **Allocthonous** material is carried from hill slopes and colluvial sources, as well glacial deposits. **Autochthonous** sediments originate from within the channel, particularly from storage in banks and bars. The latter generally constitutes the majority of the transported load, however the mixture varies, reflecting the degree to which the river is coupled with external sources and the availability of the in-channel sediments.

The sediment transport characteristics of a stream are important determinants of channel equilibrium and stability. Since the coarser material in a channel provides both the structural framework of the channel as well as the medium that accommodates hydraulic forces, transport of this material is an important process in channel morphology.

A new device has been developed to quantify and characterize the movement of coarse sediment along a reach of an undisturbed, salmon-spawning creek. Using an array of highly responsive magnetic sensors embedded in the stream, passing clasts are detected by the ferrous minerals they contain. Voltage readings from the sensors are recorded and stored in a digital format. By processing this information a coherent picture of transport dynamics may be obtained. In particular, details of the conditions necessary

for entrainment, and the spatial and temporal variations of bedload transport become remarkably evident. The device is hereafter referred to as a Bedload Movement Detector, or **BMD**. It was installed in September 1997 at O'Ne-ell Creek, in the Stuart Takla Experimental Watershed area (Figure 1).

The present study was undertaken as a component of The Stuart Takla Fish-Forestry Interaction Project. Experiments have been undertaken and baseline data collected since 1990 on topics such as salmonid populations, riparian vegetation, thermal regime and hydrology. The area is located 150 kilometers north west of Fort St. James, in the drainages of the Stuart-Takla watersheds (Figure 1), in Northern BC.

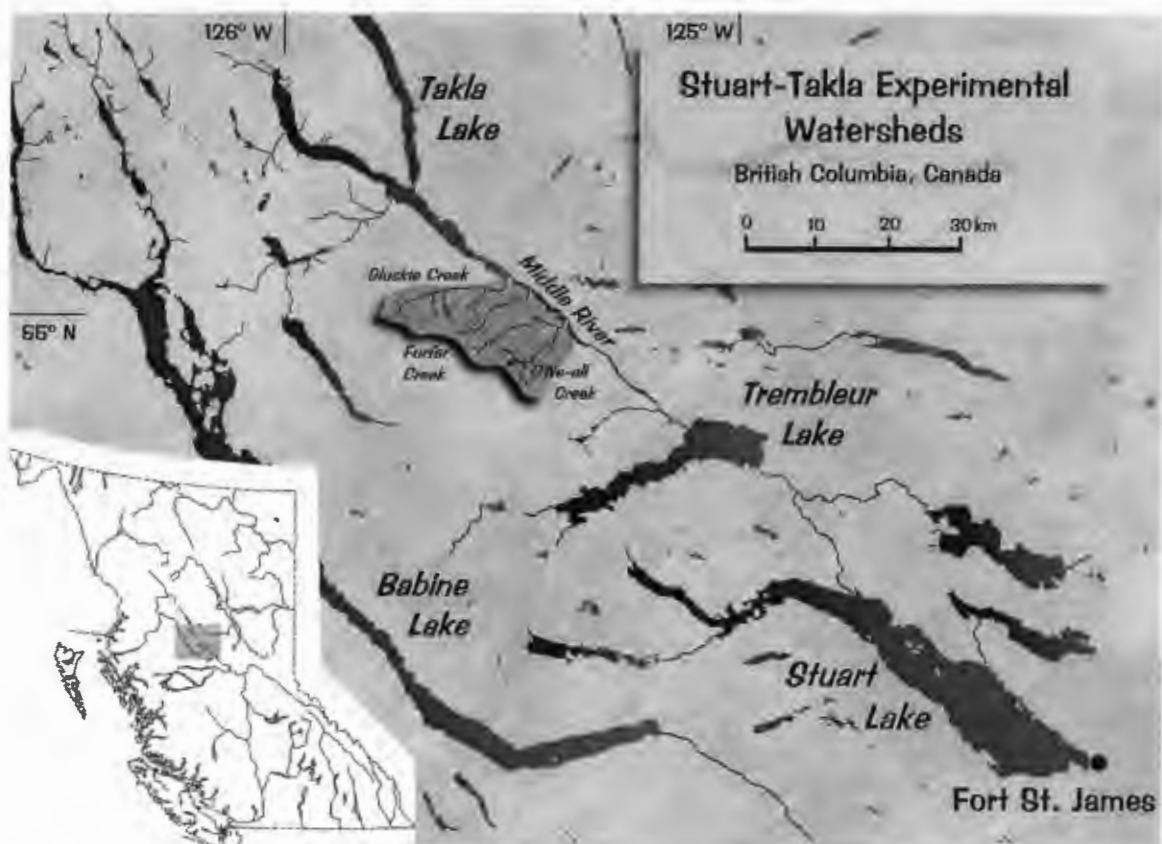


Figure 1 - The Stuart-Takla Experimental Watersheds

Sediment movement in the Stuart-Takla streams is extremely episodic. The majority of fine and coarse sediment moves during the spring snow-melt floods (Beaudry 2000; Gottesfeld, 1998). The discharge hydrographs from 1994-1997 (see Figure 2) illustrate the dominant role of **nival floods** in the annual flows. The flooding usually occurs in late May and early June. Brief summer and fall floods may be observed in the record, but the volume of coarse material transported during these events is relatively small.

Substantial amounts of coarse sediment are also moved by salmon **redd** excavation in the late summer. One of the initial goals of this project was to compare the quantity and timing of bedload movement measured in a nival flood event with that transported by spawning salmon. However, due to very disappointing returns of the Early Stuart Sockeye run in 1998 and 1999, there was insufficient spawner density to initiate full motion of the streambed.

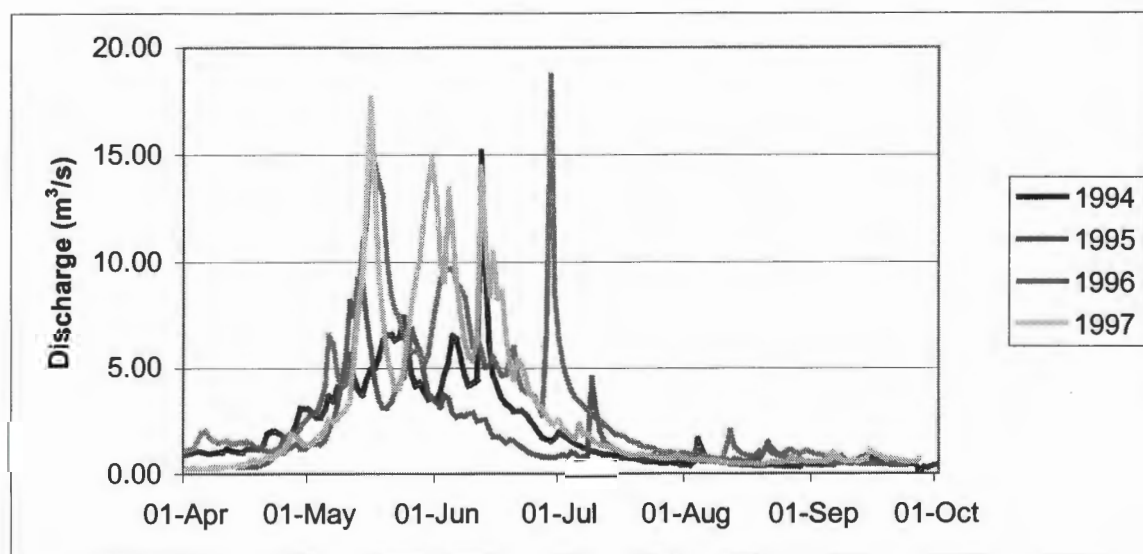


Figure 2 – O'Ne-ell Creek hydrograph - 1994-1997. Measurements were taken at an MOF gauging station 300m downstream of the study site. The flows shown here include Tsitsutl Creek, (approx. 250m downstream of the BMD site) which adds some 40% to the discharge.

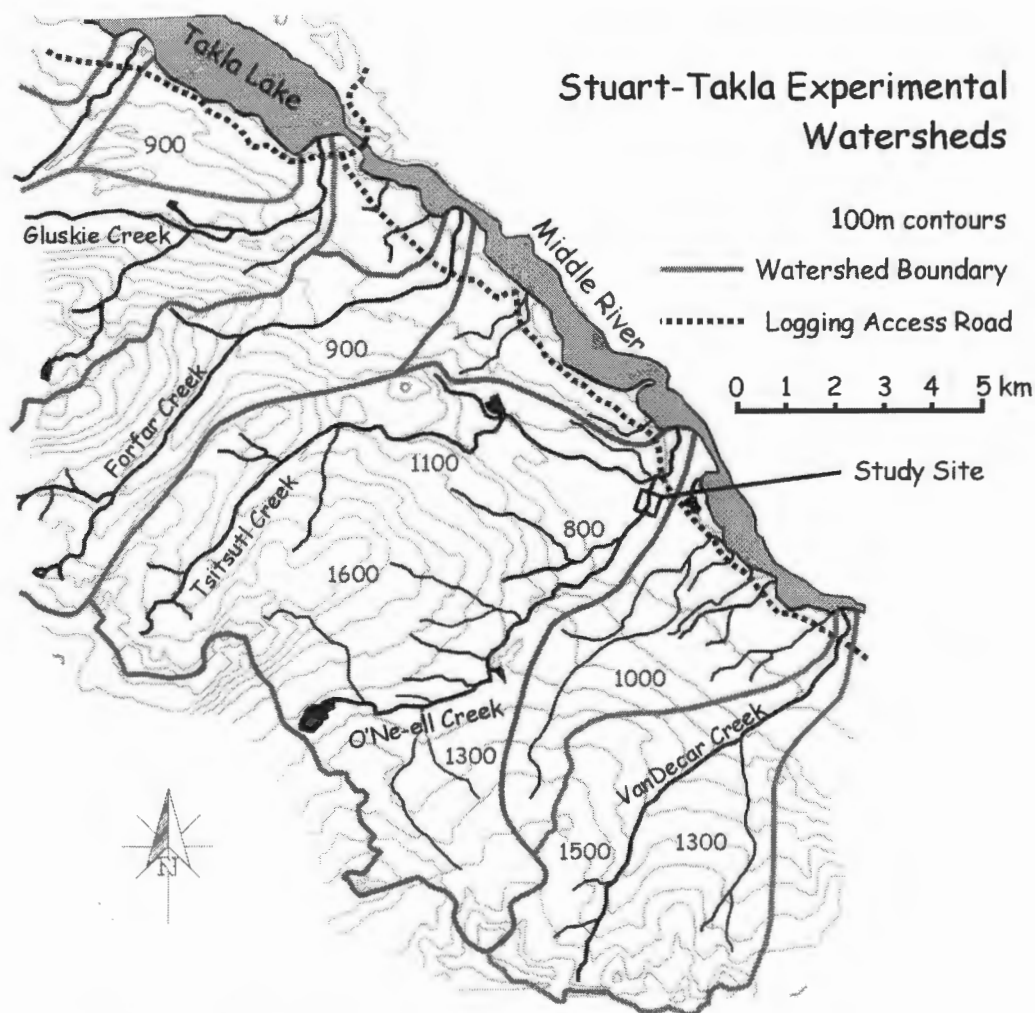


Figure 3 – Gluskie, Forfar, O'Ne-ell and VanDecar drainages along Middle River.

The scope of the present project is fourfold: **firstly**, the BMD is a novel instrument for the quantification of bedload movement. Therefore, I will:

- Discuss existing bedload sampling techniques (Section 1.2).
- Evaluate the relative advantages and disadvantages of the BMD as a means of achieving volumetric estimates of bedload transport (Section 1.4).
- Present a description of the BMD components, their installation and operation (Sections 2.1-2.4).

Secondly, calibration of the sensors used in the BMD was undertaken in the laboratory to determine their sensitivity and response. From the experimental results I will:

- Show how signals from the transport record vary with changes in particle velocity (Section 3.1.1).
- Describe the response of the sensors to rocks of varying sizes and lithologies (Section 3.1.2).
- Demonstrate the time series and frequency analysis of the signal traces from the BMD sensor (Section 3.1).

Thirdly, bedload movement was sampled with the BMD during the nival events of 1998 and 1999. From these data I will:

- Present the record of bedload movement for both flood events (Section 4.1 and 4.2).
- Compare and contrast examples of the record during periods of marginal transport, rising-stage and full-stage (Section 4.3).
- Discuss several ‘modes’ of transport, from marginal step-and-rest events to discrete ‘sweep’ and ‘cluster’ transport, to the movement of gravel and sand sheets along the channel (Sections 4.3).
- Estimate the volume of material transported, and compare this to existing measurements taken within the Stuart-Takla Watersheds (Sections 5.5).

Fourthly, the goal of this endeavour is to apply the device towards the investigation of a poorly understood phenomenon: the spatial and temporal variation in bedload transport rates. Some of the characteristics of transport activity during the nival event records are highlighted.

- Wave-like patterns in sediment transport rate are shown to exist on several time-scales (Sections 5.3).
- A “wandering” motion of the channel’s locus of transport is substantiated (Section 5.4).

Chapter 1 Bedload Transport and Its Measurement

1.1 Bedload Transport

Bedload is defined as that portion of the sediment load that rolls or slides along the bed, remaining in nearly continuous contact with the channel bottom at all times. In the relatively high gradient streams of the Stuart-Takla Experimental Watersheds, bedload seldom includes sediment that is finer than 1 mm in diameter, since finer sand particles are easily suspended in fully turbulent flows. Bedload thus comprises coarse sand, gravel, cobbles and boulders. Fine and medium sands represent a transitional grade, and may be carried as suspended load or bedload, depending on the channel geometry and hydraulic conditions (Beschta, 1987).

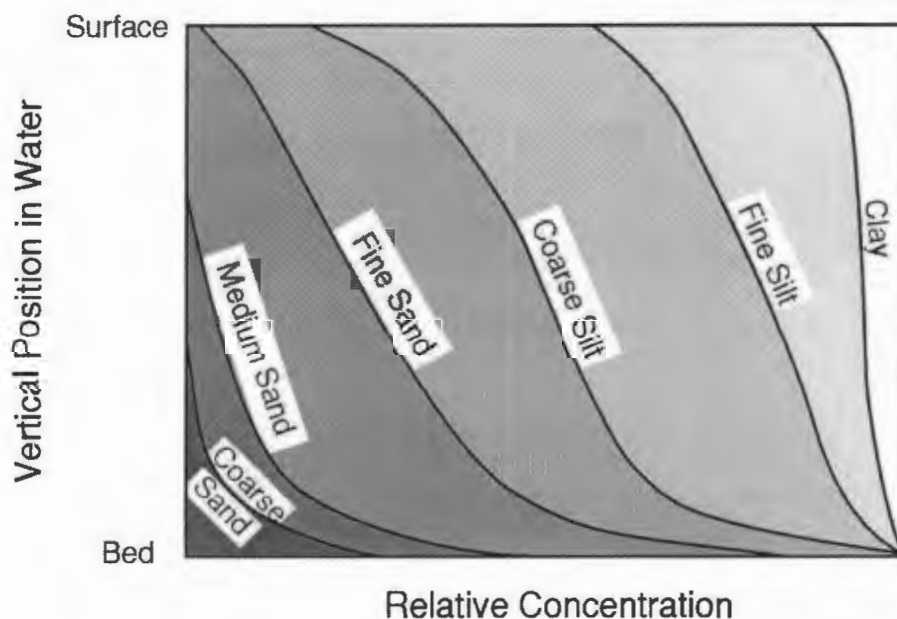


Figure 4 - Vertical variation in transported material. After Klingeman, 1981.

At lower flows, a step and rest pattern appears to be the principal mode of bedload transport (Andrews, 1983; Reid and Frostick, 1994). Observations indicate that this may

involve sporadic movement, with bursts of activity by neighbouring particles followed by a period of relative quiescence (Custer *et al.*, 1987; Reid and Frostick, 1994). Bedload transport does not always involve the full range of sediment sizes, however the patterns and mechanisms of entrainment are the subject of some debate. The effects of turbulence, relative protrusion, clustering and **imbrication** complicate the process a great deal. Any universal function for bedload transport remains a probabilistic, rather than a predictive, equation.

The following sections provide a brief summary of the theories on bedload entrainment and transport dynamics.

1.1.1 The Entrainment Threshold

The entrainment of a cohesionless grain, off of the streambed and carried along with the flow, may be considered the unbalancing of the frictional and gravitational forces that keep the grain on the streambed. Drag forces acting in a downstream direction, and lift forces, moving upward, pivot the grain about a point and move it out of position. Once in motion, the grain will roll or bounce along the streambed until it settles into a new resting position. Figure 5 illustrates the forces acting on a grain.

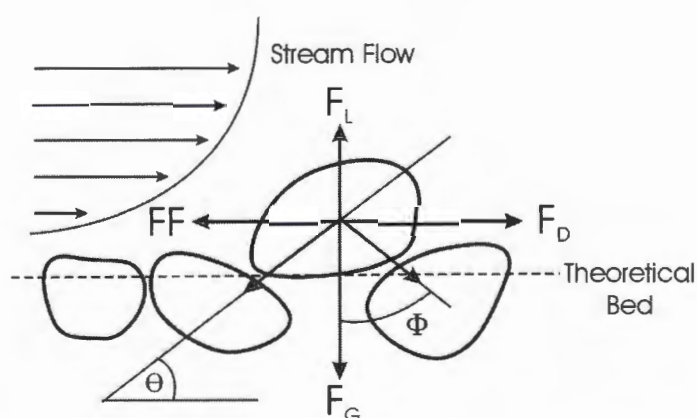


Figure 5 – Force moment balance diagram for the entrainment of a single-sediment grain.

F_G is the gravitational force. The drag force, F_D , is proportional to the cross-sectional area of the grain facing perpendicular to flow direction. Lift force, F_L , is proportional to the cross-sectional area of the grain parallel to the bed plane. The distribution of forces may depend on the pivoting angle, Φ (also referred to as the angle of repose). The steeper the angle of repose, the more the particle will tend to resist entrainment. For particles sitting at a low angle of repose, or for increasingly spherical particles, the force resisting particle motion is relatively small. Θ is the orientation angle, and FF is the frictional force acting to hold the grain in place.

The transporting ability of a stream has conventionally been described in terms of unit **stream power** (Bagnold, 1966; Leopold and Emmett, 1976) or **shear stress** exerted on the bed (Shields, 1936; Einstein, 1950). Unit stream power, ω , is defined as the product of the unit weight of water, velocity, depth and water-surface slope (γVDS). Shear stress at the bed, τ , is defined as the product of the unit weight of water, depth and slope ($\gamma DS = \omega / V$).

There have been many equations proposed to describe the shear stress conditions necessary for initial movement of a grain on the streambed, and many bedload transport equations assume that transport rates vary with some function of excess shear stress beyond this threshold.

Shields (1936) proposed that the critical shear stress for particle motion τ_{ci}^* was solely a function of the particle Reynolds number, R , which is described as

$$R = u^* d_i / \nu \quad (1.1)$$

where u^* is the shear velocity, d_i is the diameter of the i th particle fraction and ν is the kinematic viscosity.

The Shields equation describes the dimensionless function θ (Critical dimensionless shear stress) as the ratio of (erosive) fluid shear stress on the bed to submerged particle weight;

$$\theta = \frac{u_{*0}^2 D^2}{gD^3(\rho_s - \rho)} \Rightarrow \frac{\tau_o}{gD(\rho_s - \rho)} \quad (1.2)$$

where u_{*0} is the threshold shear velocity, τ_o is threshold shear stress (proportional to the square of the velocity), g is gravitational acceleration, D is grain diameter (usually taken as D_{50}), ρ_s is particle density and ρ is fluid (water) density. Shields calculated the typical value of this ratio to be 0.06 for spherical grains of equal size in a laboratory flume. Subsequent field evidence and flume studies have reported values ranging from 0.01 for an exposed grain on a cohesionless bed (Fenton and Abbott, 1977) to more than 0.25 for some natural streambeds (Church, 1978; Reid *et al.* 1985).

The relationship between shear stress and particle entrainment is complicated by several factors in natural streambeds, particularly in **pool-riffle** and braided channels.

The most significant of these are:

- Turbulence
- Imbrication, hiding and interlocking of particles
- The angularity of natural grains
- Width-wise variations in shear stress across the channel due to flow patterns

1.1.2. The Role of Turbulence

Sediment entrainment is a function not only of the shear stress acting on the bed, but also the intensity of turbulence above it. The role of turbulence in the entrainment process is not well understood, but numerous flume studies have shown that ‘burst-sweep’ cycles play a critical role in the initiation of transport (see Grass, 1971; Jackson, 1976). Bagnold (1966) reasoned that the upward thrust of turbulent flow must necessarily

be greater, on average, than the downward component; otherwise every suspended particle would drift back to the river bottom under the influence of gravity in turbulent flows. This has been shown to be consistent with experimental observations of turbulent boundary layer flows. Parcels of low-velocity fluid burst upwards within the outer layer to be replaced by quantities of high velocity fluid that sweep downwards towards the bed, disrupting the laminar sub-layer. Rapid fluid movements away from the bed are termed 'ejections' and accelerated flow events acting towards the bed are termed 'sweeps'. Thorne *et al.* (1989) and Williams *et al.* (1989) have shown that close to the threshold of bedload movement in marine tidal environments, most of the transport occurs during sweep events. Grass (1971) and Nino and Garcia (1996) have shown this in flume experiments as well. We can assume that, in streams, sweep events also move particles into suspension.

1.1.3 The Effects of Relative Protrusion, Clusters and Bed Armouring

Gravel bed rivers possess a number of sedimentological features that affect the threshold of entrainment. Depending on the bed material distribution and geometry, different packing arrangements may create hiding effects, clustering and imbrication. Particles may become constrained from motion as they are interlocked or 'hidden' from the shear forces acting on the bed. Therefore, gravel streambeds have susceptible particles that will move at a predictable threshold, while other particles may be entrained only as the force over the bed increases to a point where much larger surrounding material begins to move. The importance of the *relative* size of particles, as opposed to their absolute size has been explored extensively in the last 20 years.

In alluvial streams, the portions of the channel surface experiencing the highest flows are typically described as being **armoured**, i.e. the surface layer consists of clasts that are 2 or 3 times coarser than the average size of underlying material (Parker *et al.*, 1982; Andrews and Parker, 1987; Sutherland, 1987; Willetts *et al.* 1987). The armour layer develops after low and intermediate magnitude floods, when finer material is

selectively transported, leaving a residue of well-sorted, coarse immobile particles on the streambed. The armour layer is usually no more than one grain thick and overlies the sub-armour layer, which may be of variable thickness.

In its most pronounced form, the controlling effect of an armour layer is that particles are interlocked and thus restrained from motion. At extreme flows a critical point may be reached when the integrity of armour layer is diminished, the armour layer breaks up, and all sizes of grains are available for transport at the same time (Parker and Klingeman, 1982; Parker *et al.*, 1982; Andrews, 1983; Andrews and Parker, 1987).

Such conditions of **equal mobility** may occur in the Stuart-Takla creeks to some extent, however the effect is much less than we might observe in larger and hence deeper streams. There are at least some sections of the stream with coarser bed material that do become armoured after particularly high flows. These reaches did not change very much during the relatively low-magnitude nival events observed in the present study.

Entrainment of bedload material in the Stuart-Takla streams is dominantly size-selective. In many reaches, loose packing created by spawning salmon's annual **bioturbation** of much of the stream bed encourages selective entrainment. Downstream fining may be observed, which requires that there be greater mobility of the finer fraction (either as greater transport distances or more frequent transport). In O'Ne-ell Creek, the average diameter of cobbles decreases from 14 cm to 7 cm in the 1.5 km below the bedload detector site. This accompanies a decrease in gradient from 0.013 to 0.005. The effect of roughness elements such as log jams and gravel bars add further complexity to the entrainment model, as well.

1.1.4. Multi-phase models of transport

Bedload transport varies in character depending on the depth of flow and the nature of the bed material. Some authors have divided bedload transport in alluvial streams into two phases (Emmett, 1976; Jackson and Beschta, 1982). The first phase is the mobilization of smaller, loose material that is freely available for transport. Sand and fines are selectively carried from bars, channel margins, and pools. Gravel-sized particles, especially smaller sized ones, rotate out of the pockets in which they lie, and become entrained in the flow. Andrews (1983) points out that a significant portion of material may be transported during this first, marginal phase.

With much higher flows, a second phase of transport begins: the armour layer is disrupted. As the whole bed becomes mobile, the size distribution of the bedload coarsens. The velocities in pool sections exceed those at the riffles, and material is carried from one riffle to the next. Significant changes in bed morphology may occur during this period. It requires exceptional flow conditions to reach this stage of transport and large volumes may be moved.

Subsequent studies and field observations have shown that there are numerous degrees and variations of this two phase concept (Ashworth and Ferguson, 1989) depending on the size distribution of the bed material. At O'Ne-ell Creek, for instance, studies have indicated that a substantial portion of the bed is disturbed even in lesser flood events (Gottesfeld, 1998; Poirier, 2000). At flood stage, readings from the BMD indicate mostly finer material in motion, with the sporadic passage of cobbles. No doubt at sufficiently high flows (such as the 1990 flood) the stream bed is completely disrupted and equal mobility *sensu stricto* prevails.

Although the two-phase model is not quite adequate to describe the transport dynamics at O'Ne-ell Creek, it is a useful concept for understanding shifts in transport intensity throughout a flood event. It is anticipated that with the UNBC Bedload

Movement Detector, we may begin to better understand the factors that control sediment discharge in the creek.

1.2 Measuring Bedload Movement

Bedload movement is generally monitored using one of two techniques: *direct* (net samplers, pit traps, some form of sampling device placed on or above the bed) and *indirect* (tracer techniques, repeated channel surveys) .

1.2.1 Direct Measurement

Traps and pit samplers of various designs have been employed to sample the amount of sediment passing through a section of channel bed in a determined time. These measurements are generally recorded as weight per unit time per unit stream width, i.e. kg/m-s.

Direct sampling in high gradient mountain streams is often extremely difficult and hazardous, given the tremendous stream power required to transport cobble and boulder sized particles. Nevertheless, direct sampling has proven to be the most efficient and representative methodology.

Box, Basket and Net Samplers

Box and basket samplers have been used since the early 1900s, and the design evolved toward greater efficiency throughout the 40s and 50s, culminating in the development of the now standard Helley-Smith sampler (Hubbell, 1964; Helley and Smith, 1971; Gomez, 1991). Several of the most highly developed and tested basket samplers are those designed by Mühlhofer (Ehrenberger, 1932), Ehrenberger (1932), Nesper (1937) and the Swiss Federal Authority (1939). Essentially, these devices have

either a solid bottom, or a bottom of fine chain links that conforms to the bed. A mesh bag collects the coarser material, and water and fines escape at the rear of the device. Some versions of the basket sampler have weighted frames to keep it lower in the flow, or a vane mechanism to direct the aperture upstream.

Pressure-differential samplers, such as the Arnhem (Dutch), Károlyi and VUV, operate by causing the bedload-laden flow passing through the device to slow sufficiently to deposit material. Water then issues out the rear of the sampling box.

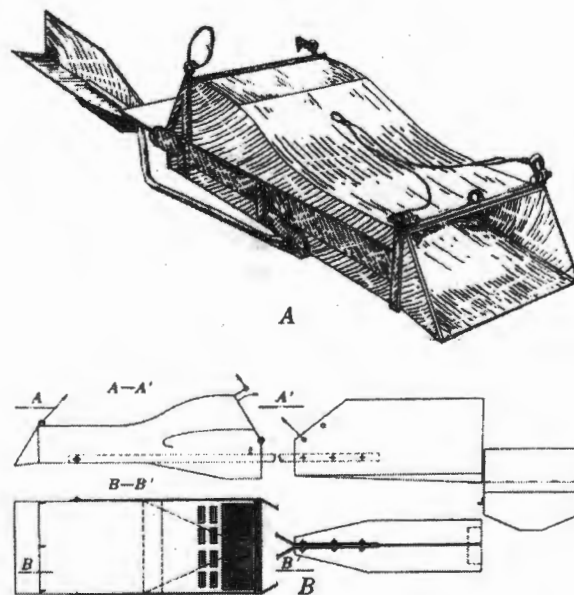


Figure 6 – The VUV pressure difference sampler – top and side views (Hubbell, 1967)

Since the mid 1970s, the standard portable sampler for bedload has been the Helley-Smith pressure-difference sampler. This device has a square 7.62 cm entrance nozzle (a 15.24 cm model is also available) and a 46 cm long sample bag constructed of 0.2 mm mesh polyester that holds about 10 kg of sediment. A **hydraulic efficiency** rating of 1.54 over a range of flows was determined by the calibration work of Emmett (1980). The trapping efficiency is considered to be 90 to 100 percent efficient for particle sizes from 0.5 to 32 mm at current velocities up to 1.5 m/s (Hubbell, 1987). Others have found that since the sampler must sit on the streambed, the geometry and placement of the

intake nozzle tends to alter the flow pattern, and thus affect the bedload discharge estimate. Furthermore, it is particularly difficult to maintain contact with the stream bed at flood stage.

It is often a considerable challenge to find the proper sections of channel to sample in order to account for the random or short-term, often “quasi-cyclic” temporal and spatial variations in bed load transport rates. Since the rates of transport can change dramatically even at constant-flow conditions, it is difficult to determine what constitutes a representative sample. Gomez and Troutman (1997) suggest that a representative sample of bedload activity should involve four or five traverses of a river, and the collection of 20-40 samples at a rate of five or six samples per hour.

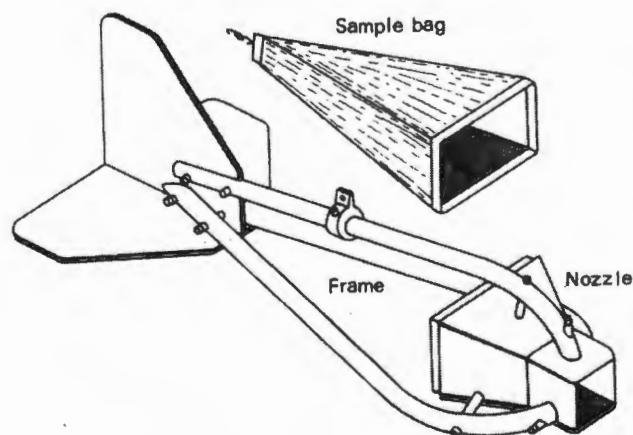


Figure 7 – The Helley-Smith portable sampler (Emmett, 1980)

Other researchers have rigged mesh nets over a solid frame that spans part of the stream, and these are emptied periodically throughout an event (Bunte, 1996). Clearly, net samplers give the best representation of pebbles in motion. They do not, however, gather any of the finer material. They also require a substantial effort, and yet the samples may not be large enough to be statistically representative and/or frequent enough to characterize the short period variation.

Pit and Bucket Traps

Hollingshead (1971) was able to monitor sediment transport along the Elbow River in southwestern Alberta by making an excavation 50m long, 20m wide and 1m deep. As the pit was refilled over the course of a nival event, successive surveys were taken to determine the total sediment deposition. Smaller traps have been developed, consisting of a bucket or tube sunk vertically into the bed (Church *et al.*, 1991; Powell and Ashworth, 1995), usually with an inner sleeve that can be emptied. Sampling by this method can yield a good estimate of the total mass of sediment moved during the flood event. It provides an estimate of the gross yield, though it provides little information on the timing and rate of transport. One successful modification of this technique was the placement of a pressure pillow within the trap well to weigh sediment as it accumulated (Reid *et al.*, 1980; Kuhnle, 1991; Harris and Richards, 1995). The main disadvantage of pit and bucket traps is that they may fill up quickly and, unless closely monitored, have little use in sampling at high rates of sediment discharge. It is also a challenging operation to remove, empty and replace the buckets in flood conditions.

The largest of pit samplers belongs in a category unto itself. That is the USGS bedload trap, installed in the East Fork River, Wyoming. A conveyor belt is set within a large concrete slot, placed perpendicular to the river flow, such that large quantities of passing sediment could be collected in flood conditions. In this fashion, a continuous record of bedload transport volume was maintained (see Leopold and Emmett, 1976). This device set a standard for bedload measurement by which other devices were compared and calibrated.

Acoustic and Seismic Equipment

Acoustic devices have been tested in Switzerland to estimate bedload transport in a mountain torrent by recording the sound generated by gravel collisions (Banziger and Burch, 1990).

Acoustics systems that measure sediment generated noise (SGN) in an ocean environment have been developed by several researchers in the UK. Results from these experiments have shown that the SGN spectrum is composed of band-limited noise, with a frequency range inversely proportional to particle size, and an acoustic intensity proportional to the mass of the mobile material. Williams *et al.* (1989; see also Thorne, 1989) collected acoustic measurements in a broad (4 km) ocean channel at West Solent. Gravel movement was detected by suspending a hydrophone 0.25m above the bed and recording the sounds of interparticle collisions. In conjunction with several current meters and video equipment, some relation between SGN and gravel transport was resolved.

Rouse (1994) reported further calibration of hydrophones recording intergranular collisions as particles moved over a fixed flume bed. This could then be related to the mass flux rate passing through the flume.

In the Italian Alps, Govi *et al.* (1993) used a series of seismometers along an alluvial channel to detect the motion of sediment within the reach. Microseismic data recordings provided a continuous record of the transport events.

Vortex Tube Traps

Vortex tube traps were originally designed for ejecting sand and silt from irrigation canals and ditches in agriculture (Hayward, 1974). Their use for measuring bedload transport rates was pioneered by Klingeman and Milhous (1970) at Oak Creek. By emptying the collection trap at regular intervals during a storm, they were able to measure transport rates and particle distribution. This data set remains one of the best continuous records of transport available anywhere. Similar devices were designed by Hayward (1974) in New Zealand, and Tacconi and Billi (1987) in Italy.

The device can recover bedload material continuously, with up to 90 percent efficiency. The construction and implementation of the concrete installation, however, is a substantial undertaking.

In Situ Magnetic Detection Devices

These devices record the magnetic signals of clasts with implanted magnets or, in the case of more sensitive instruments, the faint signals from remanent magnetism in naturally-occurring minerals. Ergenzinger and Conrady (1982) installed a device consisting of four large coils, 250 mm in diameter, attached to an aluminum frame 0.8 m above the water surface at Buonamico, Italy. It registered the passage of 100 cobbles with implanted magnets. The Birkbeck Bedload Sampler, installed at Turkey Brook, Enfield Chase, UK (Reid *et al.*, 1984) employed a metal detector circuit with a single 2.3 m long sensor installed within the streambed. This device was sensitive enough to detect movement of 100 artificial clasts tagged with ferrite rods.

Ergenzinger and Custer (1983) reported a more sensitive instrument consisting of two 1.25m coils buried horizontally in the streambed at Squaw Creek, Montana. This device could detect naturally magnetic pebbles and cobbles > 32 mm at a rate of 2 per second. Since only a portion of the stream was instrumented, bedload volumes were estimated for the total stream cross section.

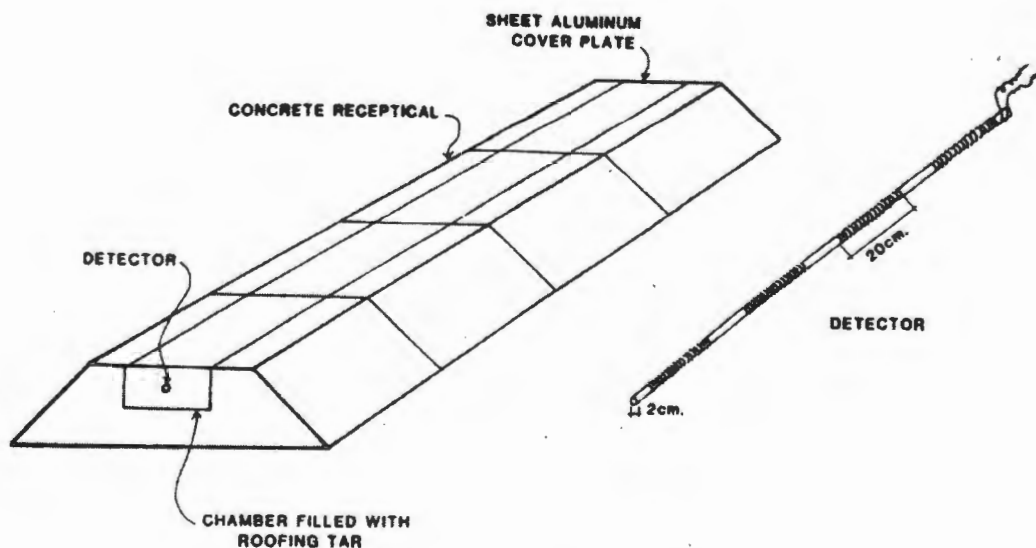


Figure 8 – The initial bedload detector design by Ergenzinger and Custer (1983)

In 1986 a more sophisticated device was installed in Squaw Creek (Bunte 1996, Custer *et al.* 1986). The device consists of 5 sets of paired multiple choke-coil units mounted in a beam set lengthwise across the stream. Each module is 1.55 meters long. It thus provides some spatial resolution for different sections of the channel. The placement of two arrays of microcoils 15 cm apart permits the determination of the travel time of passing clasts (Custer *et al.* 1987; Spieker and Ergenzinger, 1987). The sensitivity of this device permits detection of an estimated 40% of the coarse material (>32 mm) at Squaw Creek (Bunte, 1996).

All of these devices have used strip chart recorders, which limit their utility to several signals/second and a few sensor circuits. Impulses must be evaluated and counted visually and are usually summed over intervals ranging from 10 minutes to one hour. The practical limit of resolution of the strip recorder system in use at Squaw Creek may be 200/hr (Bunte 1996). Consequently, the passage of many clasts may be missed due to limitations of the data logging system. Although the device is well suited to recording the relative intensity of bedload activity, it remains an onerous task to quantify volumes.

1.2.2 Indirect Measurement

Sediment transfer volumes may be inferred after a transport event by several means, including tagged sediment tracers, morphological estimates, sonar surveys, and scour chains.

Tagged Sediment

Tracer studies are one of the most popular tools for tracing the paths and timing of gravel movement during a flood event. This method generally involves painting a number of rocks that represent the most common sizes and shapes within the bed material, numbering them, and then recovering and surveying their positions after a bedload

movement event (Crickmore, 1967; Rathbun and Nordin, 1971; Laronne and Carson, 1976). Distance of travel and patterns of deposition may then be inferred. Some of the strategies for locating the rocks afterward include painting the stones with fluorescent waterproof paint, inserting a magnet in the rocks for later retrieval with a magnetometer (Butler, 1977; Hassan, 1990; Gintz *et al.*, 1996; Gottesfeld, 1998), or exposing the rocks to radioactive treatment (Sobocinsky *et al.*, 1990)

Chacho *et al.* (1989) presented a methodology whereby radio transmitters were implanted into rocks in an extraordinarily active glacier-fed river, and then tracked for kilometers. The monitored particles typically traveled over 1500 m in 8 days time. Similarly, Schmidt and Ergenzinger, (1992) used their Pebble Transmitter System (PETSy) to track to movement of grains along the Lainbach, a step-pool mountain river in southern Germany.

Morphological Estimates

Comparing volumes of aggradation and degradation in a channel by repetitive cross-section or topographic surveys provides some insight into the rates of sediment exchange within a river system. Griffiths (1979) was one of the first to use this method, taking cross sections every 1.6 km along a 50 km reach of the braided Waimakariri River in New Zealand. The density of surveyed sections employed depends on the purpose and scale of the investigation and practical considerations. For instance, Poirier (2000) developed a methodology for fine-scale topographic measurements and volume estimation, taking repetitive surveys at an average density of 4 points per square meter along several 50 m channel reaches. Lane *et al.* (1994) recommend at least 3.5 points per m² to detect the subtler morphological changes within a stream reach.

The transport estimates provided by repetitive surveys are necessarily a minimum, since several cycles of scour and deposition may have occurred throughout the course of a flood. The final volumetric measurements are therefore the net transport rate. Loci of erosion and deposition may be matched, providing some indication of transport distance

and volumes. When this is not feasible, transport rates may be estimated using reach-average erosion or deposition and a mean transfer distance (Ashmore and Church, 1999).

Sonar Surveys

A variant of the morphological method worth mentioning is the use of sonar to measure instantaneous elevation changes in a portion of streambed. This is a particularly useful method for monitoring the passage of larger-scale bedforms. This method was successfully used by Dinehart (1989, 1992) at the North Fork Toutle River, Washington. The channel had a **bankfull** width of 60m with peak flows up to 330 m³/s. Coarse gravel dunes, up to 40 cm high, were observed migrating under a fixed sonar observation point during a flood. A multitransducer sonar altimeter was suspended on a boom, and held 1 meter above the streambed near the center of the channel **thalweg**.

Scour Chains

Scour chains have been employed in a variety of studies to determine the total scour and fill occurring during a flow event (Colby, 1964; Leopold *et al.*, 1966; Carling, 1987 and Hassan, 1990). A length of chain, fastened to an anchor, is inserted through a steel rod and driven into the streambed. The rod sleeve is then removed and a length of chain lies along the bed. After a scour and fill event, the chain is located beneath the fresh deposition with a metal detector. The depth of scour can be inferred from the distance below the initial datum that the chain length is found (see Laronne *et al.* 1994).

1.3 Stuart-Takla Bedload Studies

Several studies (Gottesfeld, 1998; Poirier, 2000) have been undertaken in the last 8 years to establish the rates and magnitude of bedload movement in two streams within the Stuart-Takla study area. Forfar and O'Ne-ell Creeks (see Figure 3) were chosen as suitable sites to compare the effects of flooding and salmon spawning activity on bedload

movement. Both creeks see an average returning population of approximately 12,000 salmon each year during the Early Stuart sockeye run.

Studies with over 1000 tracer stones were undertaken from 1992 to 1998 (Gottesfeld, 1998). Some 13,000 recoveries of tagged clasts were made after flood events or sockeye redd excavation. The results from this study posited that the amounts of bedload moved by spawning salmon bioturbation are similar to those of floods, although sockeye bioturbation of the streambed did not move the rocks as far as flood events.

A series of intensive total station surveys of stream reaches clearly showed the annual pattern of stream bedform change (Poirier, 2000). Computer-generated digital elevation models illustrated the morphological effects that each event exerted on the streambed, i.e. linearized features after a flood, and more prominent, hummocky features after the salmon had overturned the gravel substrate.

From these studies some understanding of the magnitude of bedload movement, the distance of bedload transport and how it affects channel morphology was gained, but there was still a lack of information on the timing of the gravel movement. To this end, we developed a device that records the timing and magnetic intensity of individual particles passing the detector. In addition this device may offer some indication of how much gravel is passing a cross-sectional line on the bed.

1.4 New Bedload Sampling Technology

In light of the many inherent drawbacks of existing bedload sampling methodologies, we have sought to develop a system that will overcome some of these difficulties. The UNBC Bedload Movement Detector has been developed as an improvement on *in-situ* magnetic bedload detection technology, using a series of highly sensitive magnetic sensors, and an industrial data-acquisition system. By placing a row of these sensors across a streambed, flush with the gravel-bed surface, we will be able to

monitor the passage of sediment by recording the voltage signals from the sensors. This method provides several advantages over the methods previously discussed.

- *It will overcome the numerous concerns about a sampling regimen: how often to sample, how long to sample, what parts of the creek to sample.* The record is virtually continuous, across the channel.
- *There will be little interference with the water flows or the sediment stream.* The device will have negligible effect on the passing material, and it may be raised or lowered to accommodate the current bed elevation.
- *Monitoring will provide an instantaneous particle count, and some information about particle size.* The digital data record from flood events provides detailed information in the spatial, temporal and frequency domains, providing significant opportunities for analysis. Sediment passage can be observed on the scale of 1/100s of a second, to several weeks.
- *The device will have the potential of remote operation.* With a triggering mechanism installed, and sufficient power resources, the device can operate automatically.
- *No nets, baskets, pits or large installations.* The BMD is automated for the most part, and requires no retrieval of samples. The device is not particularly portable – it is intended as a semi-permanent apparatus. However, there is much less alteration of the channel and construction involved than an installation such as a vortex tube trap or conveyor belt.

The following chapter will give a detailed description of the device, its installation and operation.

Chapter 2 The UNBC Bedload Movement Detector

The Bedload Movement Detector was developed principally by Drs. Moustafa Mohamed and Allen Gottesfeld at The University of Northern British Columbia. Dr. Mohamed engineered the coil sensors; Dr. Gottesfeld designed the housing unit, wiring and mounts for the device. Several students (graduate and undergraduate) and technicians assisted with the device construction and installation at various stages, notably Patrick Hudson, Tim Dressel, Ronald Poirier, and Jeffrey Gottesfeld. The device was installed at the study site in September 1997.

2.1 The Sensor

The sensor (Figure 9) consists of a copper-wound coil mounted within a torus-shaped magnet. A soft iron casing confines the magnetic field of the sensor so that it is not influenced by magnetic bodies beyond the diameter of its sensing face. The elements are set and waterproofed within an epoxy resin. Positive and negative terminals from the device extend from the rear of the sensor casing.

As a rock, or any ferrous body, passes over the face of the sensor, the magnetic field of the sensor is distorted. This induces an electromotive force with a potential of 1×10^{-6} to 1×10^{-1} volts. In a laboratory environment with proper voltmeter equipment, signals from most rocks can be recognized. The rugged and portable data acquisition systems that are required in the field environment generate sufficient noise to mask weak signals such that voltage responses from clasts on the lower end of this scale (i.e. up to approx. 2×10^{-4} V) are therefore indiscernible from static.

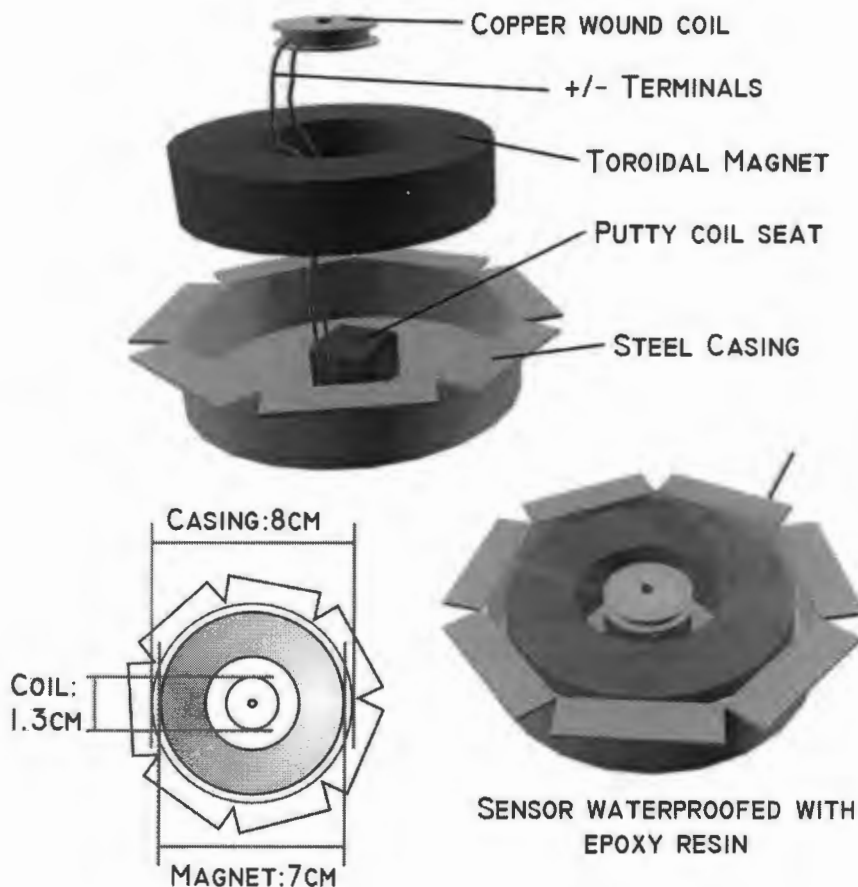


Figure 9 – Exploded view of the sensor (above), sensor dimensions and the assembled product.

Calibration experiments have determined that the response of the sensor drops off markedly as the clast moves toward the sensor's edge. Figure 10 shows the corresponding decline in signal strength as ferrous items are passed over points that are increasingly distant from the center of the sensor face, at a fixed velocity. Some of the implications of this will be discussed in Section 3.2.

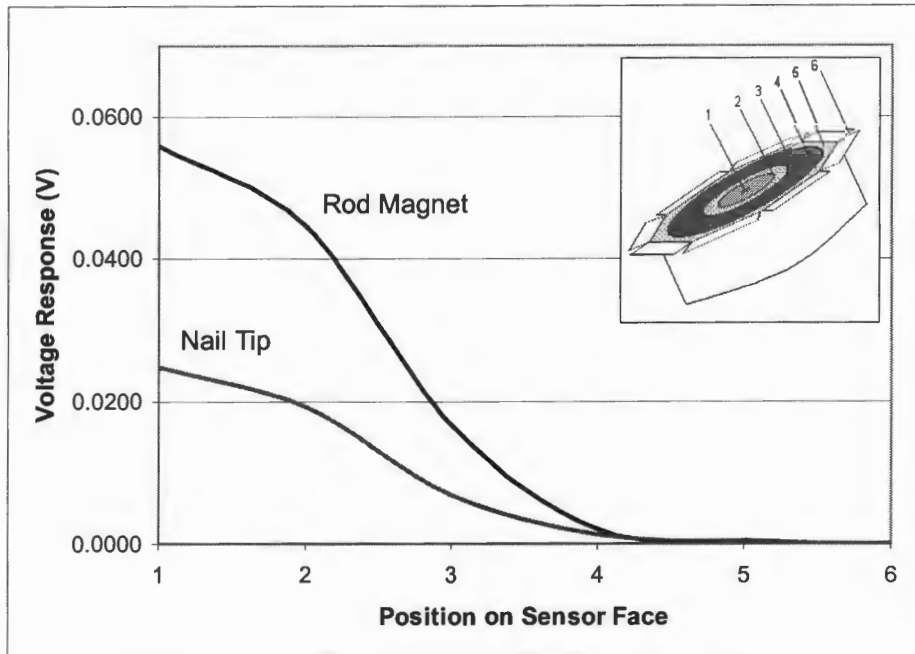


Figure 10 – Voltage response as ferrous items pass at various points on the sensor.

2.2 The Housing Unit

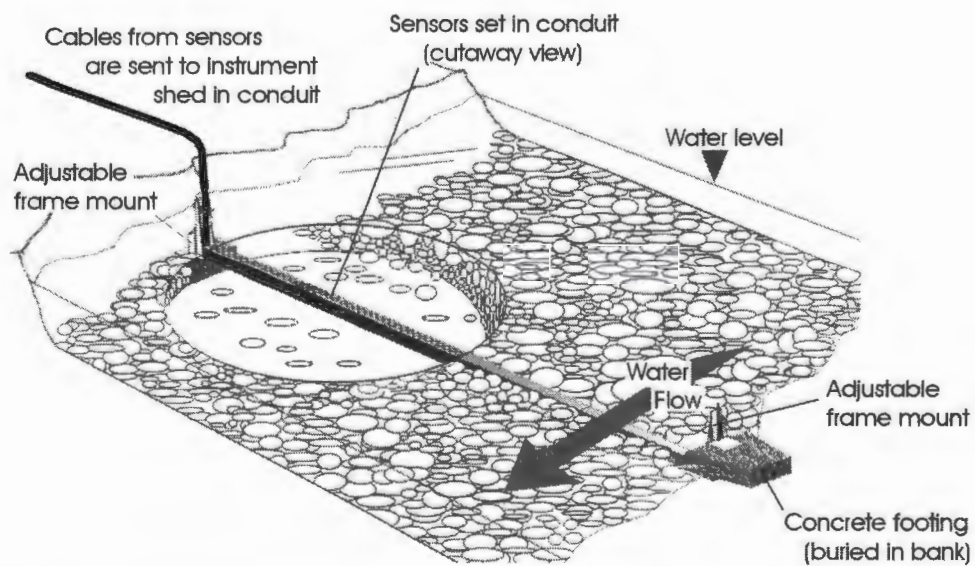


Figure 11 – Schematic diagram of the BMD installed in the creek bed

The sensors are set into a hollow aluminum beam (15 cm x 15 cm x 8.2 m) that is constructed of ¼ inch (0.64 cm) aluminum stock (Figure 11 and 12). There are adjusting mounts on each end of the beam, so that it can be raised or lowered to accommodate channel scour or fill. The device is set such that the sensing surface is placed flush with the streambed. Stream flow and sediment then pass over the device with minimal disturbance of near-bed fluid dynamics and sediment transport.



Figure 12 - Photo of the study site in early August. The instrument shed is located on the east side of the creek. The BMD is set within the streambed downstream of a group of mature sockeye salmon. A log and wire-rope cable provided access to the stream cross-section at all stages.

The device was custom built to the dimensions of the creek at the study site. This prototype spans a stream width of 8.4 meters. A similar design can be employed on most streams, to a maximum practical installation size of 30 m in width. The prototype contains 82 sensors, each 8 cm in diameter, spaced 10 cm from center to center. Wires from each sensor run the length of the beam and out to an instrument enclosure adjacent

to the stream. The conductors are housed in five strands of telecommunications cable, each one containing 50, 22-gauge insulated copper wires. At least 80 redundant wires were left in the housing unit as supplementary connections in the event of any wiring repairs or complications.

2.3 Data Acquisition

The instrument shed was constructed on the west bank of O'Ne-ell Creek adjacent to the BMD. It houses the data acquisition system and has modest facilities for sleeping and working. The cables from the BMD are routed to a protective enclosure where the sensor wires are distributed to their respective channels in the analog-to-digital (A-D) boxes.

In order to collect data from the array of sensors at a relatively high rate (100 Hz x 82 sensors) an industrial data acquisition system was acquired from Omega Engineering, Inc. of Stamford, Connecticut. The InstruNet™ (# iNet-100HC) data acquisition system consists of a 32-bit DSP PCMCIA card and a series of A-D boxes, each with 16 analog inputs (+ 8 digital). The PCI bus controller contains a 32-bit microprocessor with 256 Kb of RAM that manages the external network of the device. All real time tasks are off-loaded to this processor so that the host computer is not burdened with real-time issues. A 12V power adapter is also included. An optical isolation unit provides some noise reduction from high frequency disturbances such as the computer and Jaz™ drive operating nearby.

Each A-D box contains a signal conditioning amplifier for each channel, therefore voltage input from the sensor terminal is translated to a digital value which may then be recorded to a Jaz™ drive. Each channel has a programmable analog low-pass filter, as well as triggering capabilities. Signals are passed through a low-pass Butterworth filter, removing signals with a frequency greater than 40kHz. The filtered data are then recorded to disk for more sophisticated signal processing. A Jaz™ disk system was used

for this application, although a more reliable system is being sought. A high capacity disk drive system is required that can scan at least 20 Kbps, or 240 Mb per hour, without interruption. New media are inserted every two or three hours, and the written files are subsequently archived on recordable CDs for storage.

A portable data logger (StarLogger™) operates independently of the data acquisition system, recording creek stage and suspended sediment data every minute. Suspended sediment was measured using an optical backscatter (OBS) probe, measuring turbidity in Jackson Turbidity Units (JTU). These data are downloaded and processed on a weekly basis. During the Spring 1999 event, stage data were written to CD along with the BMD files.

2.4 Power Supply

The power requirements for the operation of the BMD are substantial. With two PC computers, two Jaz™ drives, data acquisition system, CD writer, data logger, and lights, roughly 13.3 kilowatt hours of energy are required daily while the BMD is running. To meet the needs of this system, three solar panels were acquired, as well as a 5500-watt generator. Three 12V telecommunications batteries were installed beneath the cabin to store power from these sources, and discharge them to DC appliances directly, and to AC appliances through inverters. Typically, the generator had to be run for several hours each day to maintain the battery array potential at 12.5 volts. While the solar panels provide up to 200 watts of power during sunny hours, many of the spring days were overcast and sunlight crested the tree line for only a few hours on clear days.

As we shall see in the presentation of results in Section 4, the generator tended to affect the signal acquisition by introducing low frequency (~10-40 Hz) noise to the system. However, the functioning of the data acquisition system deteriorated noticeably as the voltage potential dropped below 12 volts, so at some points it was necessary to use the generator despite the interference it created in the BMD record.

2.5 The Study Site

The bedload movement detector was installed on O'Ne-ell Creek (also known as Kynoch Creek), approximately 150 kilometers north of Fort St. James in central British Columbia. It is a **third-order tributary** of Middle River; Middle River drains Takla Lake, flowing southward to Stuart Lake, between the Omenica Mountains to the west and the Hogen Range to the east. The O'Ne-ell Creek watershed (Figure 13) encompasses about 68 km². The bedload movement detector site is located roughly 200m upstream of the Tsitsutl Creek confluence, where the drainage area is about 38.5 km².



Figure 13 - The O'Ne-ell Creek watershed.

The watershed above the detector site is undisturbed by human activities. Large amounts of woody debris, abundant riparian growth, and ample gravels in the bed make this river an important spawning locale for sockeye salmon. Frequent inputs of large woody debris create a forced **pool-riffle morphology** (Montgomery *et al.* 1995) throughout much of the stream. The study reach has a gradient of 1.3%, and though there is a large logjam 65 m upstream of the detector site, there is little woody debris adjacent to the bedload movement detector. The device is on a relatively straight reach of about

100 meters. Nival discharge through the reach ranges up to about $16 \text{ m}^3/\text{s}$. The average annual precipitation in the O'Ne-ell watershed is about 60 cm. Rainfall peaks in June and early July. Snowfall from November to April accounts for about 50% of the precipitation. Summer season temperatures frequently exceed 20° ; winter temperatures are frequently below -20° (MacDonald *et al.* 1992).

The upper reaches of the watershed are quite steep with alpine ridges up to 2000m. Outcrops of bedrock along the stream contribute granitic, ultramafic and metasedimentary rocks to the stream bedload. As the stream approaches its alluvial fan at about 900m, the gradient becomes increasingly subdued.

2.5.1 Sediment Supply

Numerous processes upstream of the study site determine the particle size distribution of the streambed and the material in transport. Contributions of tills and glaciofluvial materials from gullies and scarps are common throughout the course of O'Ne-ell Creek (Ryder, 1995). Colluvial inputs from bedrock outcrops a few kilometers upstream of the study site are common. Logjams and woody debris have a great influence on the patterns of gravel distribution as well (Rice, 1994). Bank failures occur in places throughout the system – the failure of a section of stream bank above the BMD was particularly noticeable in the record from the 1999 flood event.

Streambed sediments were sampled by collecting four bulk sieve samples and 12 cores of the streambed with a **freeze-core sampler** (see Thoms, 1992). The bulk samples were of the surface 15 cm of 1 m^2 plots, each weighing roughly 270 kg. The large samples are necessary to provide accurate estimates of the coarsest fraction of the streambed sediment (Church *et al.*, 1987). The freeze core samples are 30 cm deep, and weighed roughly 17 kg apiece. They were split into lower and upper 15 cm segments. The volume of each freeze core segment is approximately 0.01 m^3 . The surface 1-grain layer was not segregated in either sampling methodology.

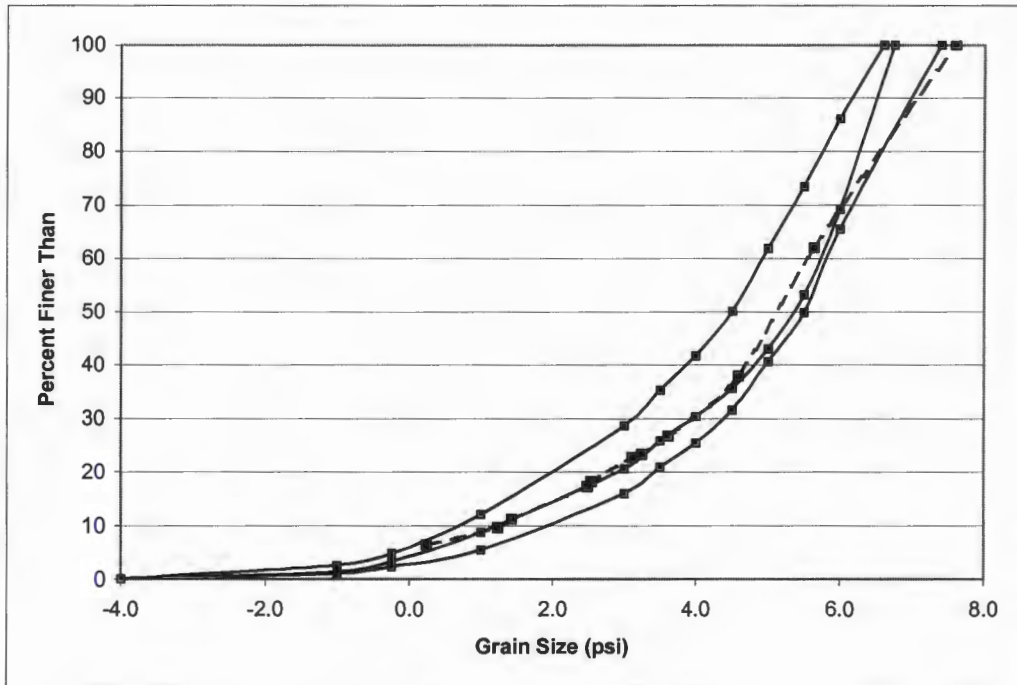


Figure 14 – Grain size distribution from four bulk sieve samples. Three samples were excavated to a depth of 15 cm and one (represented by a dashed line) went to 25 cm.

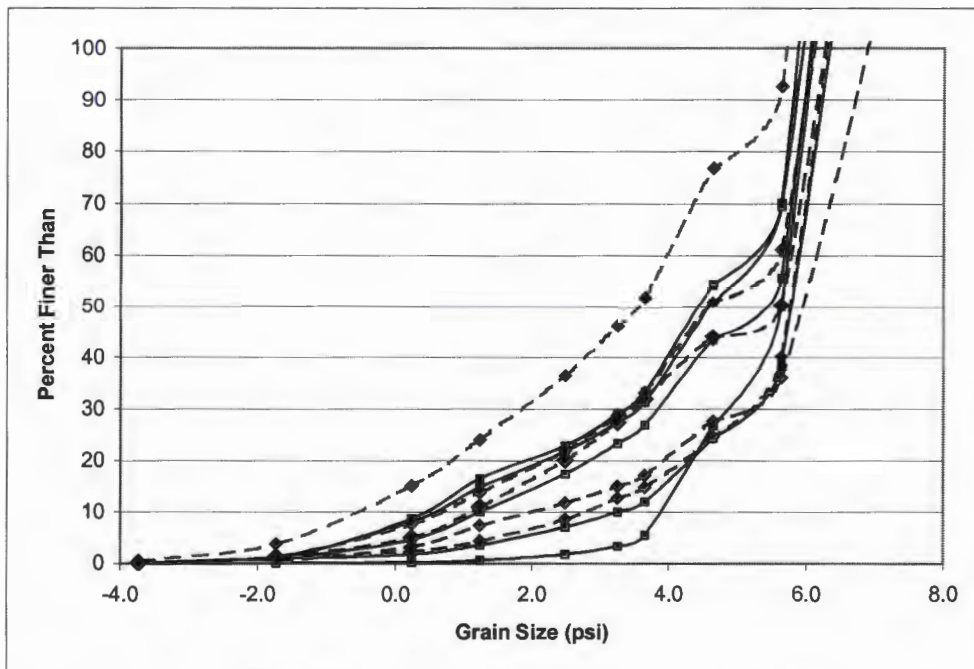


Figure 15 – Grain size distribution from freeze-core samples. Dashed lines indicate subsurface samples (below 15 cm) and solid lines indicate surface material.

Bed material ranges from coarse sand to small boulders with diameters up to 30 cm. Sediment finer than 1 mm makes up 1% to 10% of the streambed. Large pebbles and cobbles are the most abundant size material. The D_{50} of these sediments ranges from 3.5 to 6 ψ (11.3 to 64 mm). The average D_{50} is about 42 mm. The D_{90} ranges from 5.5 to 7.5 ψ (45.3 to 181 mm). The average value of the bulk samples is about 128 mm.

The pattern of textural variation on the streambed is complex. The bed material is coarsest in the deeper portions of the channel that experience the highest flow velocities such as along the thalweg and in pools. Areas removed from high velocities because of shallow depths or obstructions can accumulate finer material. The pattern of average grain sizes for the relatively linear portion of O'Ne-ell Creek above the BMD is shown in Figure 16.

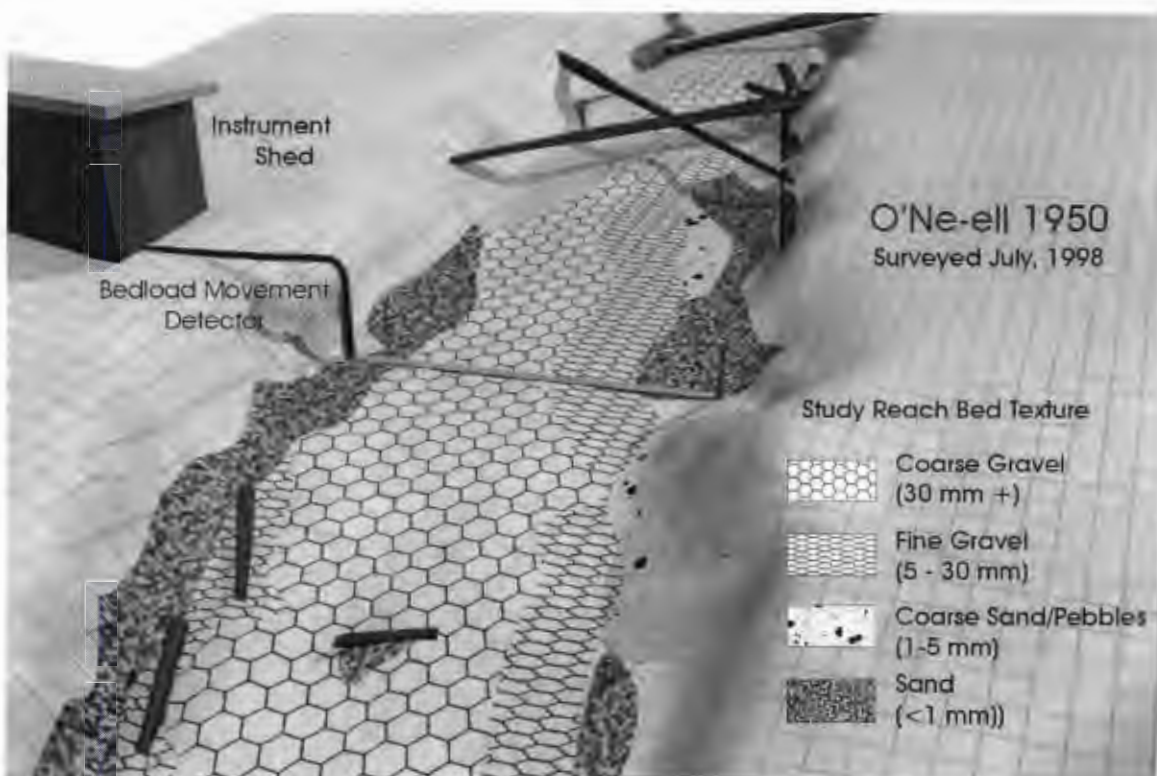


Figure 16 – Texture of the stream bed at the study site, based on a 1998 topographic survey.

2.5.2 Lithologies

The lithologic or mineral character of the bed material varies a great deal, but is dominated by granitic and metamorphic rock (Table 1). In part this diversity originates from past regional glacial transport and deposition. Ferromagnetic minerals such as the common iron oxide accessory minerals magnetite, ilmenite and hematite, and the iron sulfide, pyrrhotite, are found in many of the clasts in O'Ne-ell Creek. Paramagnetic and diamagnetic minerals such as pyroxene, biotite, chlorite and quartz are found in abundance, but seldom exert sufficient magnetic influence to trigger the sensors. For the purposes of this study, we have assumed that the distribution of magnetic minerals remains constant over all size ranges represented within the creek. It is, however, an important task to quantify the overall percentage of rocks within the study area that contain sufficient ferromagnetic material to elicit a response from a BMD sensor.

We have recorded the signals of 180 rocks in the laboratory ranging in mass from 0.5 to 1200g. This work and similar field experiments suggests that approximately 30% of the rocks in O'Ne-ell Creek yield sufficient ferrous material to obtain a voltage

<i>Lithology</i>	<i>Percent</i>
Granodiorite (+ diorites)	26.0%
Cache Creek group metamorphics	25.6%
Metasedimentary	14.1%
Ultra Mafic	9.0%
Dacite	8.1%
Andesite	5.5%
Arenaceous (conglomerates, greywacke)	5.3%
Rhyolite	3.4%
Quartz	3.0%

Table 1 – Representative lithologies found in the bed material at O'Ne-ell Creek, N=234.

response greater than 1.7×10^{-4} V (noise threshold of the data acquisition system) from a sensor. Clasts that yield strong signals include a variety of lithologies: volcanic rocks, granodioritic to gabbroic plutonic rocks, serpentinized ultramafic rocks, metasediments and metavolcanics.

Because of the high sensitivity of the BMD sensors, we expect that this device will operate effectively in most gravel bed streams, including most of the glaciated regions on North America and Europe, which have a component of glacially transported granitic and high-grade metamorphic rocks. Custer (1991) points out that naturally magnetic clasts can be found in any of the andesitic volcanic terranes of Western North America (Coastal and Cascade ranges), the Aleutian and Alaska Range in Alaska, the Andes of South America, and the mountains of the Philippines, New Zealand, and Japan. Basaltic terranes also yield magnetic material (e.g. Snake River Plain, Columbia Plateau, Iceland, Deccan Plateau of India), and other metamorphic and intrusive terrains may also contain particles that are sufficiently magnetic to be detectable.

Chapter 3 Time Series and Frequency Analysis

This section will examine some of the strategies that have been employed to characterize and quantify continuous time series signals from the BMD records. Since all the voltage information is stored in digital format, there are numerous strategies for manipulating, processing and visualizing the data. Signals can be analyzed through time, across the stream width, or in the frequency domain. They may be filtered with respect to amplitude and frequency or convolved with other signals.

Although these procedures have met with a certain degree of success, there remain some significant problems. At the simplest level these are due to the chaotic nature of sediment movement in turbulent flow, especially at high sediment transport rates. It is difficult to set the rules for particle counting when there seems to be so many exceptions and permutations. Problems that are more complex have arisen from the introduction of noise across the whole bandwidth of the system – due in part to the data acquisition system itself, and also from the operation of the power generator.

The bulk of the signal processing work was accomplished using LabView™ software, produced by National Instruments of Austin, Texas. The software uses a graphical programming format, which greatly shortens and simplifies the time one might otherwise spend generating thousands of lines of code for these applications. The tradeoff is that many of the signal-processing routines are somewhat of a ‘black box’, and thus the mathematical processing routines may only be customized to a certain degree.

The voltage data from the sensors are stored in an interlaced binary format. All channels are written continuously to one file. This way the hard disk writing head stays in one place on the platter when writing multiple channels, as opposed to moving back and forth between separate files for each channel. A matrix operation must then sort the written voltage values (v) and channels (c) so that $v_1c_1, v_1c_2, v_1c_3, v_1c_4\dots$ becomes $v_1c_1,$

$v_2c_1, v_3c_1, v_4c_1 \dots$ and so on. The values are stored as 32-bit floating-point data, in high endian format.

3.1 Identification and Characterization of Signals and Frequencies

As a clast passes over the device, a signal similar to Figure 17 is recorded. The signal amplitude, or intensity, is primarily a function of the magnetic properties of the clast. The period of the signal is a function of both the length of the passing axis of the particle, and the velocity with which it passes the sensing surface of the device. The

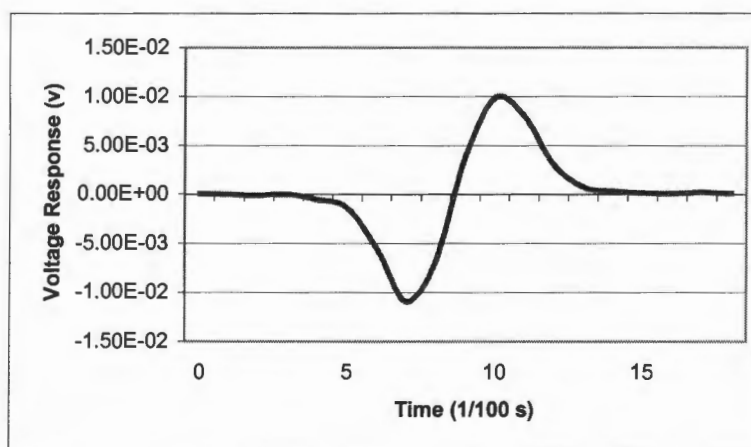


Figure 17 – Time series $x(t)$ of a sensor's response to a passing clast.

positive and negative excursions of the signal are related to the change in sign (+/-) for magnetic flux with respect to time. Although the sensor has a symmetrical magnetic field, the particles passing over the sensor often lack homogeneity in the distribution of magnetic elements, or else pass in an irregular fashion, resulting in an unbalanced signal; i.e., large positive component with little or no negative side, or vice versa. As we shall see, this presents a problem in terms of detecting and counting events in a continuous signal record $x(t)$.

The identification of singular pulses in a time series is fairly straightforward; there are threshold exceedance and peak detection algorithms that are able to detect exceptional peaks within a record. Peak detection algorithms typically function by fitting a quadratic polynomial to sequential groups of data points. For each peak, the quadratic fit is tested against a threshold level, in this case the maximum voltage noise from the data

acquisition system ($\sim 2 \times 10^{-4}$ V). Peaks with amplitudes lower than the threshold are ignored. Peaks are detected only after approximately 4 data points have been processed beyond the peak locations.

However, if the positive component of the signal is absent, a peak detection algorithm will likely fail (and similarly for the negative component with a valley detection algorithm). Although a routine might locate a peak followed later in time by a valley, it is difficult to assert that they come from the same impulse. A useful mathematical transform for representing a discrete sine pulse as a positive, singular wave function is the Hilbert Signal Envelope. To envelope a signal $x(t)$, the Hilbert Transform of the signal is calculated $h(t)$. This consists of the original signal with a 90° phase shift. Sines are therefore transformed to cosines and vice versa. These signals are then convolved to produce the envelope function $A(t)$.¹

$$A(t) = \sqrt{x(t) \otimes x(t) + h(t) \otimes h(t)}$$

Figure 18 shows the envelope function $A(t)$ of the sine wave from the first example (Figure 17).

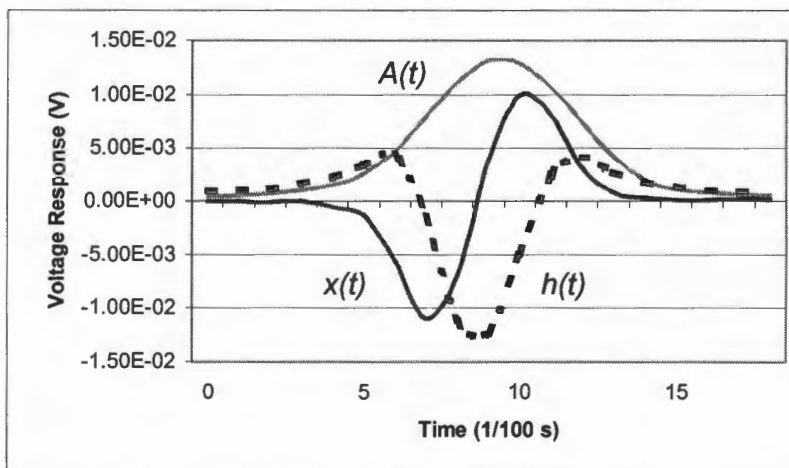


Figure 18 – The signal trace $x(t)$ (black) with its corresponding Hilbert transform $h(t)$ (dashed) and signal envelope $A(t)$, shown in gray.

¹ \otimes denotes convolution

This transform resolves the ambiguity of missing positive or negative signal components, and provides a signal that is easy to locate and quantify in terms of frequency. Of course, as multiple particles cross a sensor in rapid succession, signals are confounded and this signal processing strategy is no longer effective.

By taking the derivative of the Hilbert Transform, another sine wave is generated, with balanced components. By finding the “zero-crossing” at either end of this wave, the effective extents of the original signal may be determined. That is, we find the true beginning of the signal as it begins its upward trajectory, and the final point of the signal’s negative excursion. This has been an effective strategy for isolating impulse signals for frequency transforms. Otherwise, they are affected by larger signals within the time series that is windowed and analyzed.

National Instruments’ Joint Time-Frequency Analysis Toolkit (JTFA) TM provides another useful tool for the analysis of sine wave impulses. The approach used here is to divide the signal into several blocks that can be overlapped. Then, the **Fourier transform** is applied to every individual block of data to indicate the frequency contents of each. This is known as the Short Time Fourier Transform, or **STFT**. By squaring the STFT, the STFT spectrogram is produced. The spectrogram represents the signal in Time-Frequency or $[t,f]$ space, as illustrated in Figure 19. This representation is particularly useful for approximating the time of clast passage, and the associated signal frequency.

The **Gabor** expansion represents a discrete signal $s[i]$ as the weighted sum of the frequency modulated and time shifted function $h[i]$:

$$s[i] = \sum_m \sum_{n=0}^{N-1} C_{m,n} h[i - m\Delta M] e^{j2\pi i/N} \quad (3.1)$$

where the Gabor coefficients $C_{m,n}$ are computed by the STFT:

$$C_{m,n} = STFT[m\Delta M, n] = \sum_{i=0} s[i] \gamma^* [i - m\Delta M] e^{-j2\pi ni/N} \quad (3.2)$$

where N denotes the number of frequency points, or “bins” and ΔM indicates the time sampling interval.

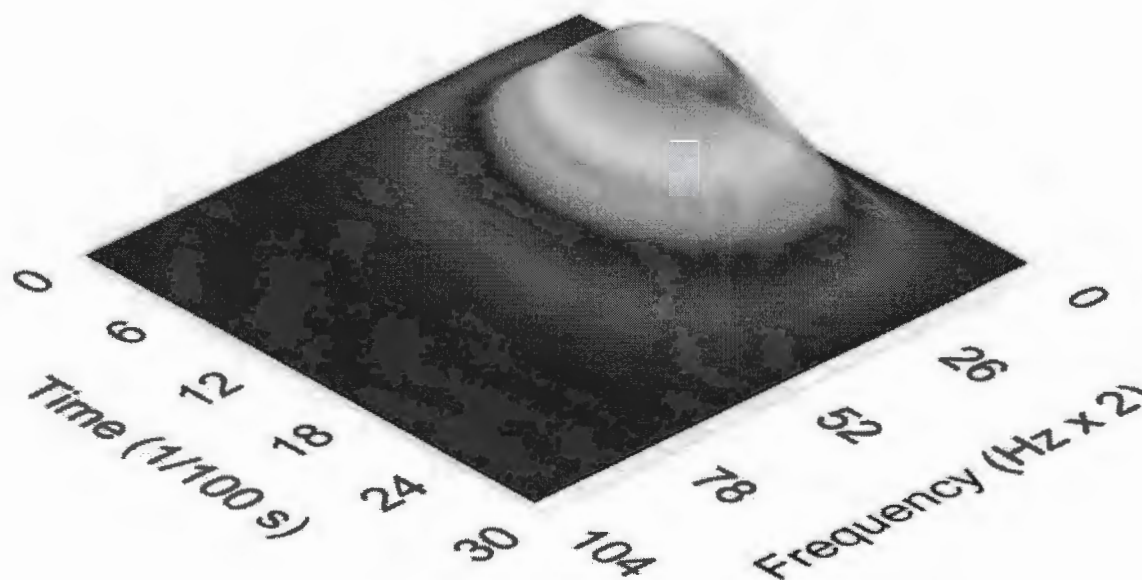


Figure 19 – A sine pulse presented in time and frequency space. The relative brightness (z-scale magnitude) indicates the intensity of the frequencies. Note that the peak frequency response of the signal is located at $(31.6 \div 2) = 15.8$ Hz, and occurs at 15/100 s.

An example of JTFA applied to a BMD signal is shown in Figure 20. Estimates of the frequency content of each impulse can be measured along the Y-axis of the graph, and the voltage intensity of each signal is indicated by the size and brightness of each point. The first signal, for instance, has a frequency of 6 Hz. The final signal, on the right hand portion of the chart, appears to have two frequency components – a different one for the positive and negative excursions of the signal.

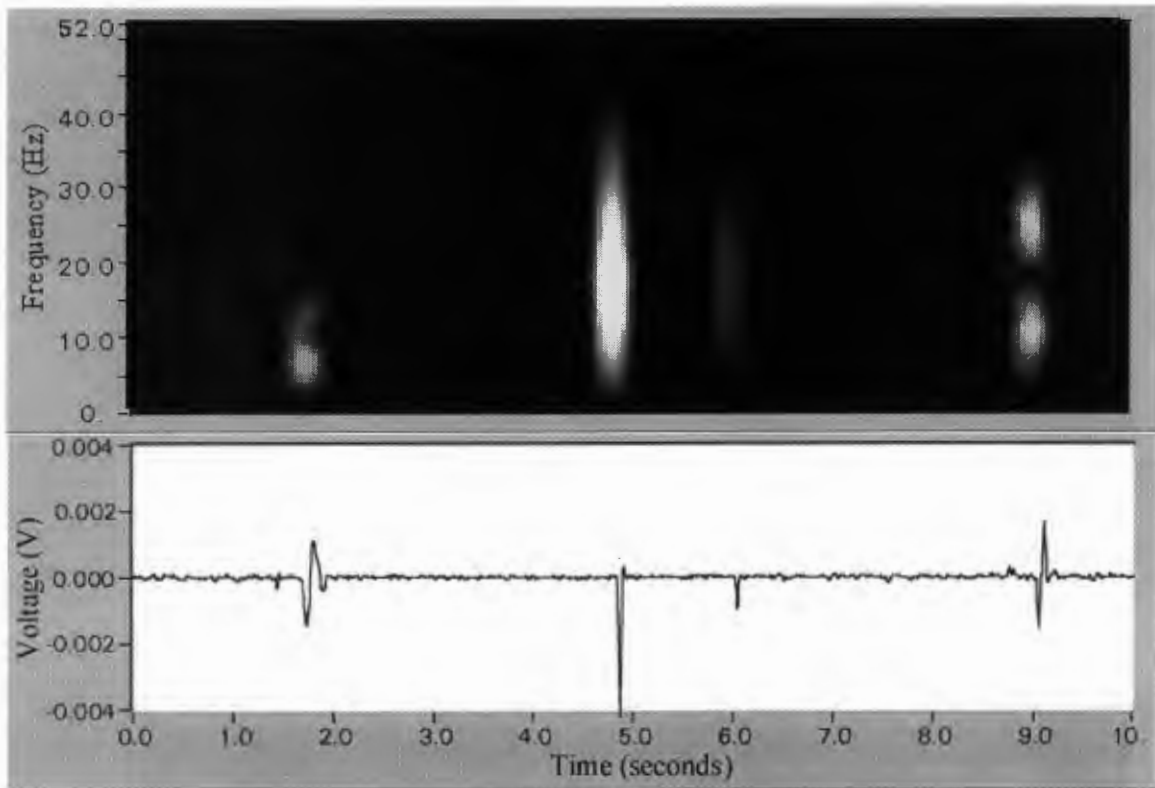


Figure 20 – STFT spectrogram of a single sensor trace during a flood event.

This example is taken from a ‘clean’ section of the data. The majority of the data shows varying degrees of background noise, which are particularly noticeable under JTFA analysis.

While Joint Time Frequency Analysis is a powerful tool, the cumbersome calculations involved with the JTFA Toolkit entail prohibitively long processing time. A single 4 hour file requires over 36 hours of processor time on a 450 MHz Pentium machine. In order to expedite processing at present, conventional **Fast Fourier Transform (FFT)** methodology has been applied to the signals.

3.1.1. The Influences of Clast Velocity On a Signal

The time required for a unitary particle (say of 1 mm diameter) traveling at 1 m/s, to cross the 0.07 m sensor face is .07s. The associated period of a sensor's output voltage signal would be 14.1 Hz. The general formula for calculating the period for a given particle moving across a BMD sensor is

$$f\{x(t)\} = \frac{1}{(D_x + 0.07)} \times v \quad (3.3)$$

where $f\{x(t)\}$ is the frequency of the signal, D_x is the length in meters of the particle axis nearest to its vector of motion (referred to hereafter as the *passing axis*), and v is the particle velocity in meters per second. We assume that the passing axis of a clast rolling along a streambed would be equivalent to the **B** or **C** axis.

Figure 21 illustrates the relationship between velocity and associated period for 5 different particle sizes. As the passing axis becomes longer, the size of the particle becomes increasingly important in determining the signal duration. For coarse sand and

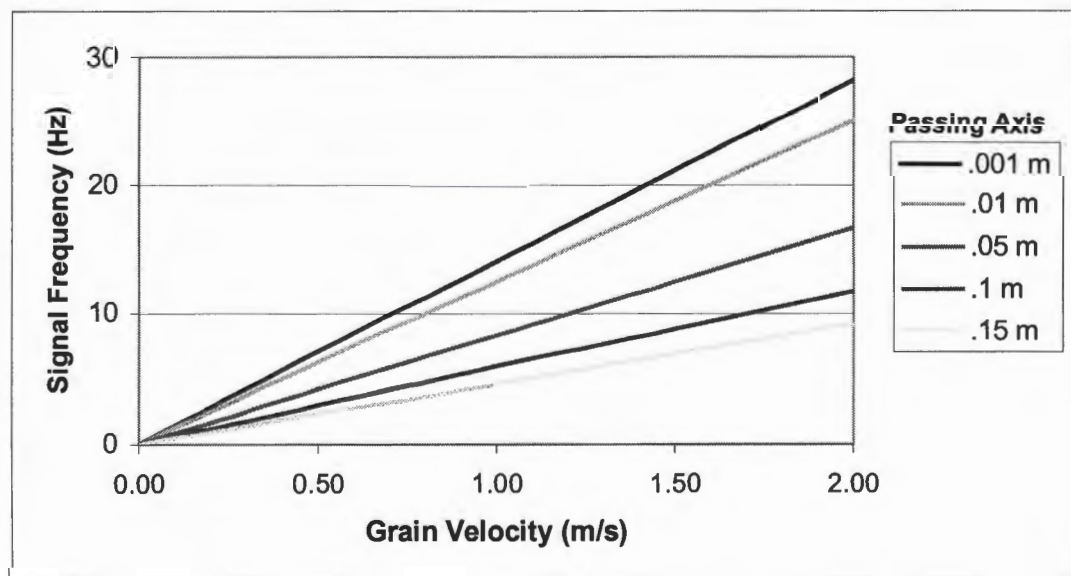


Figure 21 –The relationship of velocity and signal frequency for clasts of different sizes.

granule particles the signal frequency is proportional to the velocity divided by the width of the sensor face. As D_x becomes much larger (i.e. larger clasts), the length of the clast becomes a greater influence on signal length, and the relation departs from this proportionality.

To put this in a hydraulics perspective, Figure 22 and Figure 23 present the flow parameters at the study site. Figure 22 shows the stage/discharge graph, relating depth of flow with corresponding discharge.

Velocity measurements were taken throughout the 1999 flood event, and the readings are shown in Figure 23. Two sets of measurements, taken at 0.6 and 0.2 of the flow depth (measured from the bed), are displayed on the graph, and compared to velocities predicted from the Universal Velocity Distribution Law (Dingman, 1984). These velocity sampling elevations were erroneously selected (0.8 and 0.2, or 0.4 alone is generally preferred), however the measurements are still valid. At high stage the water velocities did not exceed 2.5 m/s, and the velocities in the bedload transport zone (lower 5 cm) could not have exceeded 1.3 m/s (likely < 1.0 m/s). One would expect the fastest moving particle in the transport zone to be moving at a velocity approaching that of the water.

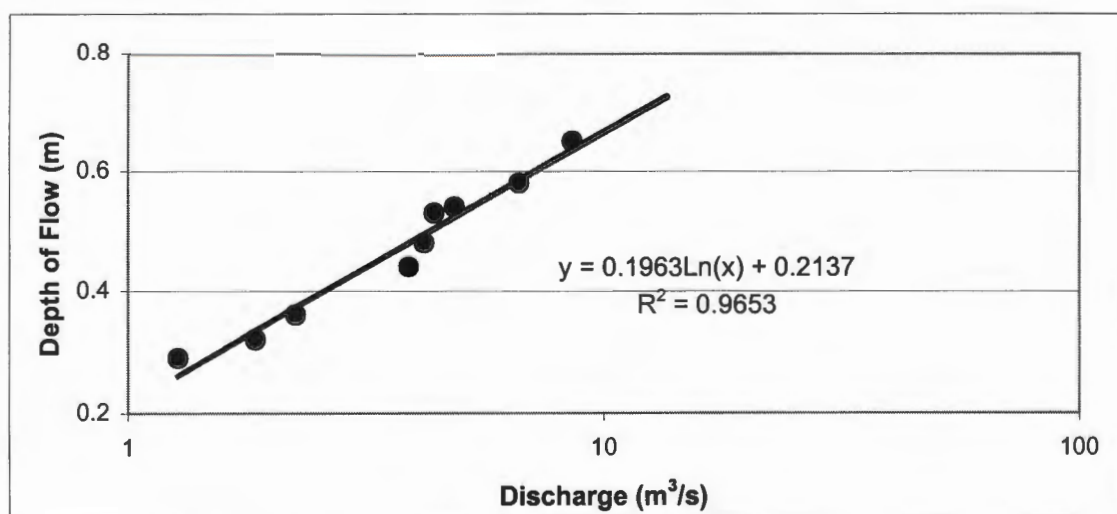


Figure 22 – Stage/Discharge rating graph for O'Ne-ell Creek 1950, June 1999.

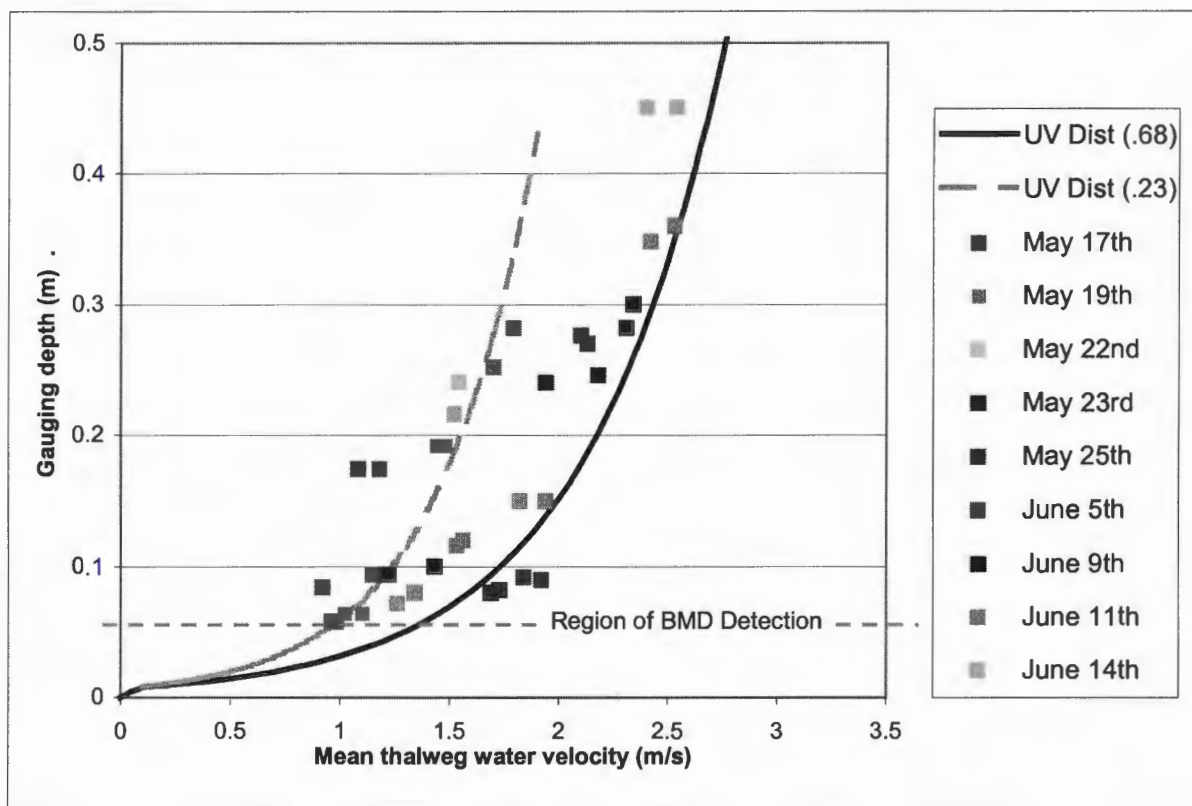


Figure 23 – Velocity profile at O’Ne-ell 1950, May-June, 1999. The exponential lines indicate the Universal Velocity Distribution Law for channel geometries based on low stage (May 17th - 0.23m) and high stage (June 14th - 0.68m). Four velocity measurements are indicated for each measurement period – two sets taken at 0.6 and 0.2 depth in the area of maximum flow.

From this reasoning, the shortest frequency signal we could expect to see in the BMD record from a grain passing the full width of a sensor would come from a 1 mm grain of sand traveling at 1.0 m/s, which would have an associated period of 14.1 Hz. This is substantially less than the **Nyquist frequency** of the sampling rate ($104.2 \div 2 = 52.1$) and less than the suggested threshold of 0.2 of the sampling frequency, which would be 20.8 Hz. Thus, a sampling frequency of 104.2 Hz allows plenty of bandwidth for digitizing signals from the passage of even the fastest particles.

3.1.2 The Influences of Clast Size On a Signal

Figure 24 shows the resultant signals from three trials of a single mafic rock passing over the sensor on a pendulum. The signals have been enveloped with the Hilbert

transform, as discussed above. As the velocity of the particle diminishes, the signal intensity is attenuated and the signal period increases. The area under each curve is roughly similar, but clearly the associated period changes substantially (see Appendix C).

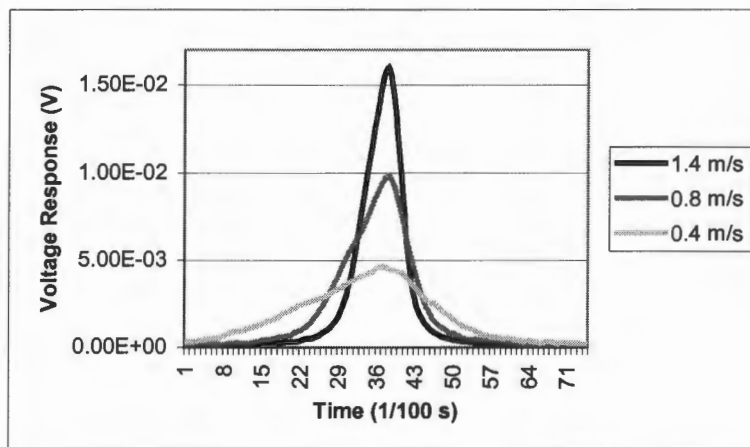


Figure 24 –Signal amplitude diminishes and period increases with lower clast velocities

In Figure 25, results are shown from the passage 8 particles, all of the same lithology and passed over a sensor at the same velocity. With the increasing length of the particles' passing axis, the period of the signal broadens correspondingly.

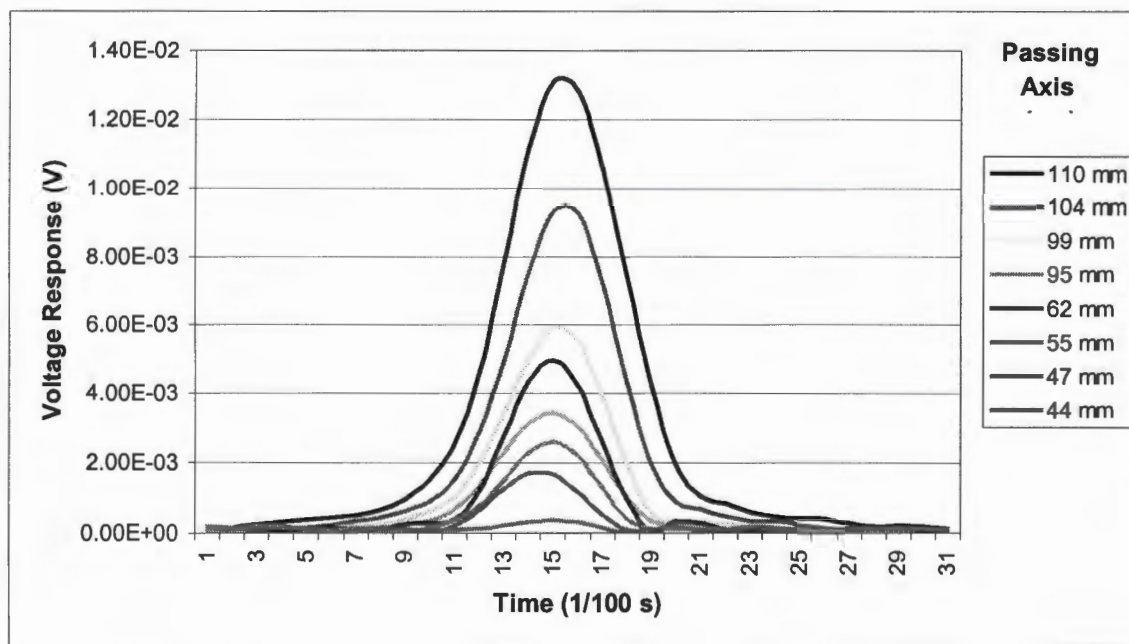


Figure 25– A comparison of signal envelopes for different sized clasts.

The amplitude of the signal is dependent on the strength of the magnetic field of the clast and its velocity. In Figure 25, the sampled particles are all ultramafic dunites and consequently have similar magnetic characteristics. The amplitudes of the sensor responses are roughly proportional to the third power of their lengths. The volumes of all the rocks may not be proportional and thus we see at least one exception, in the rank of the 95 mm particle; it has a lower amplitude value than the 62 mm sample.

Figure 26 shows a graph of 71 rocks passed over the sensors at a constant velocity of 2.25 m/s. By measuring the duration of the sensor's voltage response for each particle, an "apparent" size of the passing clast is calculated. Despite much experimental error the slope of the fitted curve (1.014) is very close to 1. Although some stones have complex magnetic properties with varying magnetic strengths across the clast, there is a direct relationship between the size of the clast and the duration of the voltage signal induced by its passage over the sensor

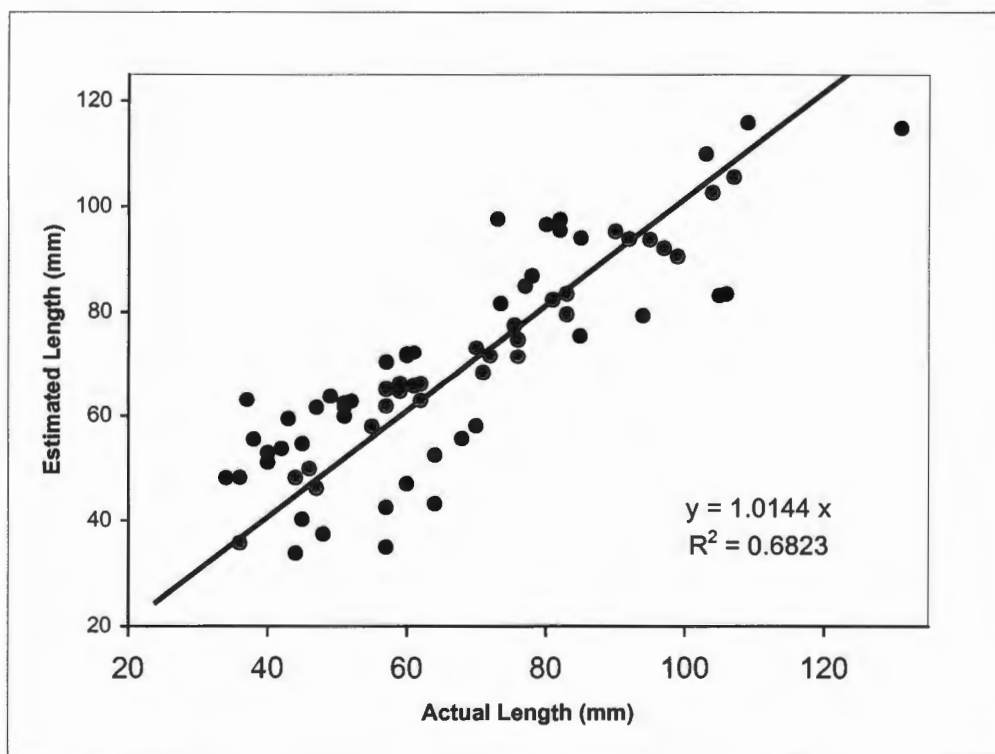


Figure 26 - A comparison of clast size versus the "apparent" clast size calculated from analysis of the voltage signal from a sensor.

Thus, the frequency of the signal from a passing clast is a function of both its size and velocity. Since we can neither assume that the size of the particles is constant, nor that their velocities are constant, we must develop some statistical algorithms to extract pertinent information from the data. Given that we know the size distribution of the bed material and can measure water velocities, the distribution of signal durations in a given period will likely inform us about the range of velocities and/or sizes of clasts in motion. Furthermore, when particles in the cobble range are entrained, we should expect that at least two adjacent sensors would peak at the same instant a cobble traverses the device, leaving another clue as to the range of sizes in motion.

3.2 Random Passage of Sediment

As stated earlier, the BMD signals are the product of the size and velocity of material moving over a sensor. While we can make some reasonable assumptions about both of these variables, the margin of error remains at least an order of magnitude.

There is also the matter of the trajectory of particles passing over the device. Particles that wobble in their course, or pass between sensors will not provide a representative signal. Figure 27 illustrates the results from laboratory test of the voltage response from a BMD sensor (see Figure 10) as various magnetic items are passed over the sensor at a fixed velocity. Although the sensor lane is 10 cm wide (i.e. the sensors are spaced every 10 cm) and the sensor face is 8 cm wide, the area of highest response is only 6 cm wide. Thus, the probability of a particle passing over the device and registering a substantial signal is only about 60%.

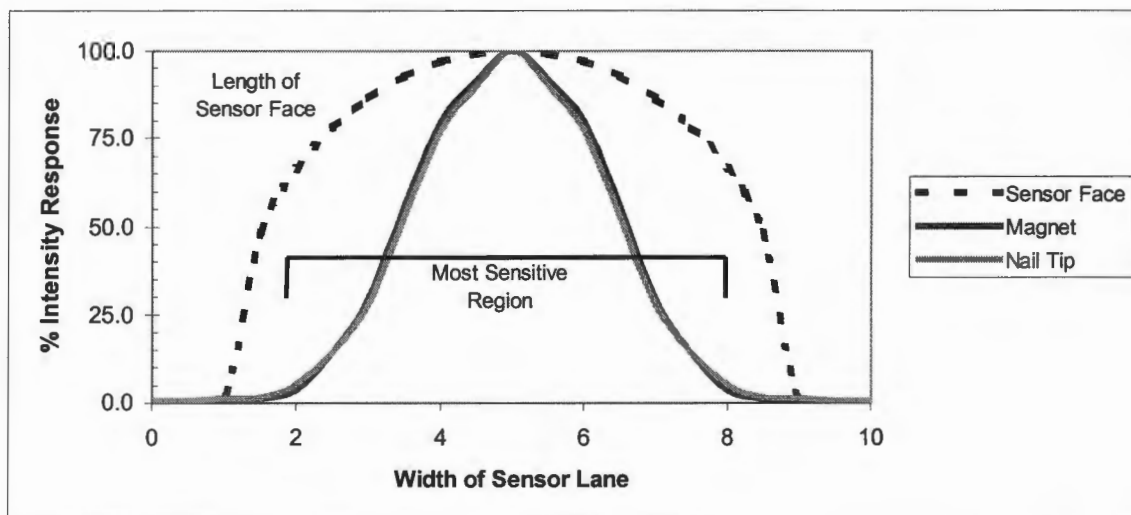


Figure 27 - The probability function facing a particle as it approaches the device. The dashed line indicates the possible chord length of its transect across a sensor. The relative sensitivity of the sensor is outlined by the experiments introduced in Section 2.1.

Another substantial problem for deciphering signals is the phenomenon of clusters and sweep events. In these cases, distinguishing individual clasts becomes a difficult task. Particles are frequently swept up in events that trigger up to half the device in one or two hundredths of a second. This signal-processing problem is small, however, compared to sections recording the passage of gravel sheets, when the transport record is all but static (the sensors are overwhelmed by multiple transport events). One would expect, though, that the total voltage recorded might bear a positive relationship with the total volume of sediment passing at this point.

Along with signals that can be assigned to a particle length and velocity, there are numerous high frequency signals in the record. These are signals greater than 12 Hz. These might arise from three circumstances:

- Passing grains not traversing the central part of a sensor. This is by far the most common reason, and presents the greatest problem in terms of estimating the total transport.

- Particles can move faster than the local mean fluid thrust at the bed. Instantaneous velocities may be as much as double the mean velocity due to high-speed sweeps.
- Noise from the system (considerable in some instances) generates discrete random signals that vary over the breadth of the BMD record's frequency spectrum. Extraneous signals from system noise will be the easiest problem to eliminate, with an improved power source and better data acquisition equipment.

As shall be discussed in the next section, longer signals arise from larger particles, but turbulence will also slow particles, and drag resistance increases with particle diameter. It is for these reasons that size estimates from the BMD sensor signals are considered *gross* estimates only.

Chapter 4 Analysis of the Flood Data Record

Two nival floods have been recorded to date with the BMD. The floods of 1998 and 1999 show considerable contrast in their timing, length, and sediment-moving capability. **DFO** data show that record low flows were reported in the Fraser River during the spring of 1998, while the flow volumes of 1999 were third highest on record (DFO, 2000). This is certainly consistent with the data presented here.

During the peak of sediment transport activity, the device may register over 200,000 signals per hour. The simplest method of depicting the relative amount of bedload transport activity across the channel throughout a flood event is to show the total voltage recorded at each sensor integrated over time. The voltage readings from the BMD are taken to be a reasonable proxy for the rate of sediment flux. It is emphasized that although this is not entirely accurate, it is reasonable for illustrative purposes. If it is assumed that the distribution of magnetic particles varies uniformly over time, then statistically these summations are a good approximation of the bedload activity.

Much of the initial data analysis has consisted of summing the many hours and days of data into 30-second voltage sums for each sensor. Sensor 1 is on the west bank and sensor 82 on the east. Charts of the total transport activity over time are then plotted onto graphs similar to Figure 29. Obvious spatial and temporal trends in transport activity then become evident, and the active periods of transport can be identified and further analyzed.

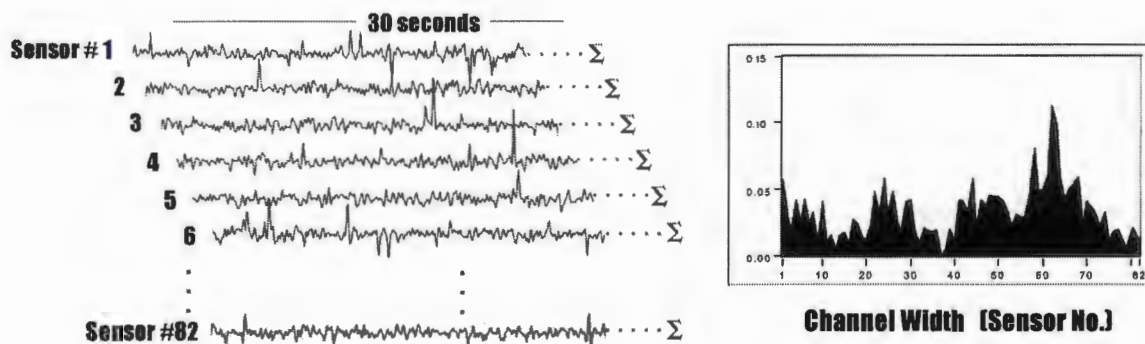


Figure 28 - The BMD Record consists of summing the voltage activity in absolute (positive) units for each channel in 30 second intervals. The resultant sums, showing the magnitude of activity across the channel width, are shown in the chart on the right.

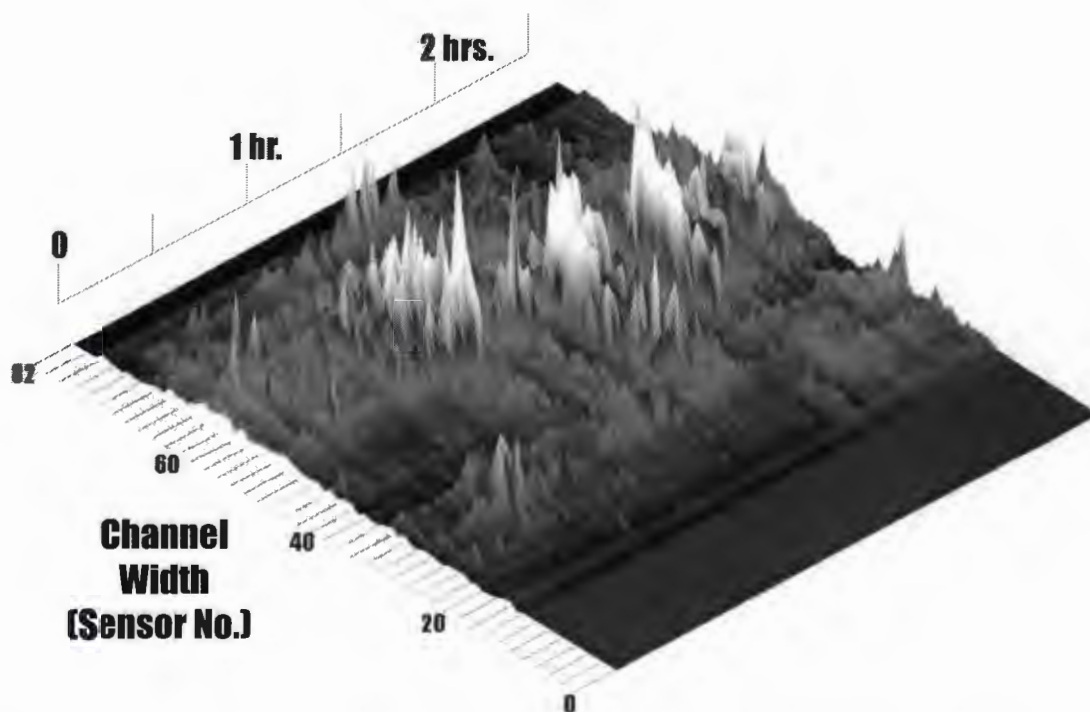


Figure 29 - The sums for each 30-second interval are then plotted over the hours and days of the flood event. Here a 2.5 hour section of data from 20:00 to 22:30 on June 11 is shown.

4.1 Nival Flood, 1998

The nival flood event in 1998 took place between May 17 and May 27. Intermittent transport activity was recorded for several days as the flood waters rose. Scattered activity across the channel consisted primarily of high frequency signals that are interpreted as clusters of sand and pebbles that were available for easy entrainment and were swept downstream along with loose organic debris and litter. On May 25, after a significant rain-on-snow event, a flood wave surged down the channel during the evening. The stage was on the order of a one in three year flood, but water levels rose very quickly. The great majority of sediment that moved in 1998 traveled within the ensuing 24 hours.

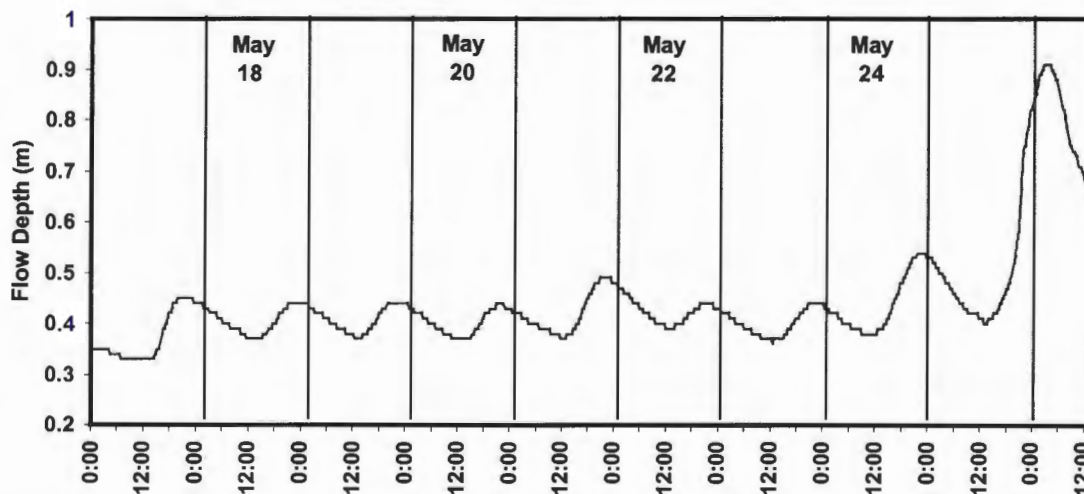


Figure 30 - Stage readings during the 1998 nival flood. The gauge was swamped during the peak flows, and thus data from the night of May 25 have been reconstructed from readings taken just upstream of the station. Flow subsided quickly over the next three days.

Figure 31 shows the BMD record from the peak of the flood event. Data were recorded at an acquisition rate of 30 Hz per channel. They are presented in the diagram as voltage values integrated over 30 seconds.

While shorter, more sporadic occurrences of activity could be seen before and after this period, by far the bulk of the activity took place in the May 25-26 segment. As the event began, most of the activity registered in the center-left bank section of the

channel. As the event progressed, approximately 80 percent of the channel width was mobilized, until the activity shifted to the right hand side at about 12:30 AM on May 26. Three large pulses can be discerned in the graph – one starting at midnight, the next at about 8:45 AM, and another, smaller one at about 4:45 PM. In each case the onset of activity is quite abrupt, and tapers off over the course of 8 hours or so. Gaps along the length of the transport record probably indicate obstruction of sediment transport, possibly due to boulders coming to rest upstream of the device.

A one-clast thick carpet of sediment 1.5m wide covered a section of the west part of the channel, which is seen in the chart as a gray zone in the lower part of the strip diagram. The low intensity is likely due to the increased distance of moving clasts from the sensors. Brighter, high intensity patches represent movement of clasts when patches of the covering layer were removed and/or unusually strong signals. At about 3:30 PM the cover was disrupted and normal signals resumed. At the end of the transport event, another blanket of sediment on the device in the same area was cleared off, and the device was raised approximately 12 cm to accommodate the slight aggradation in that section.

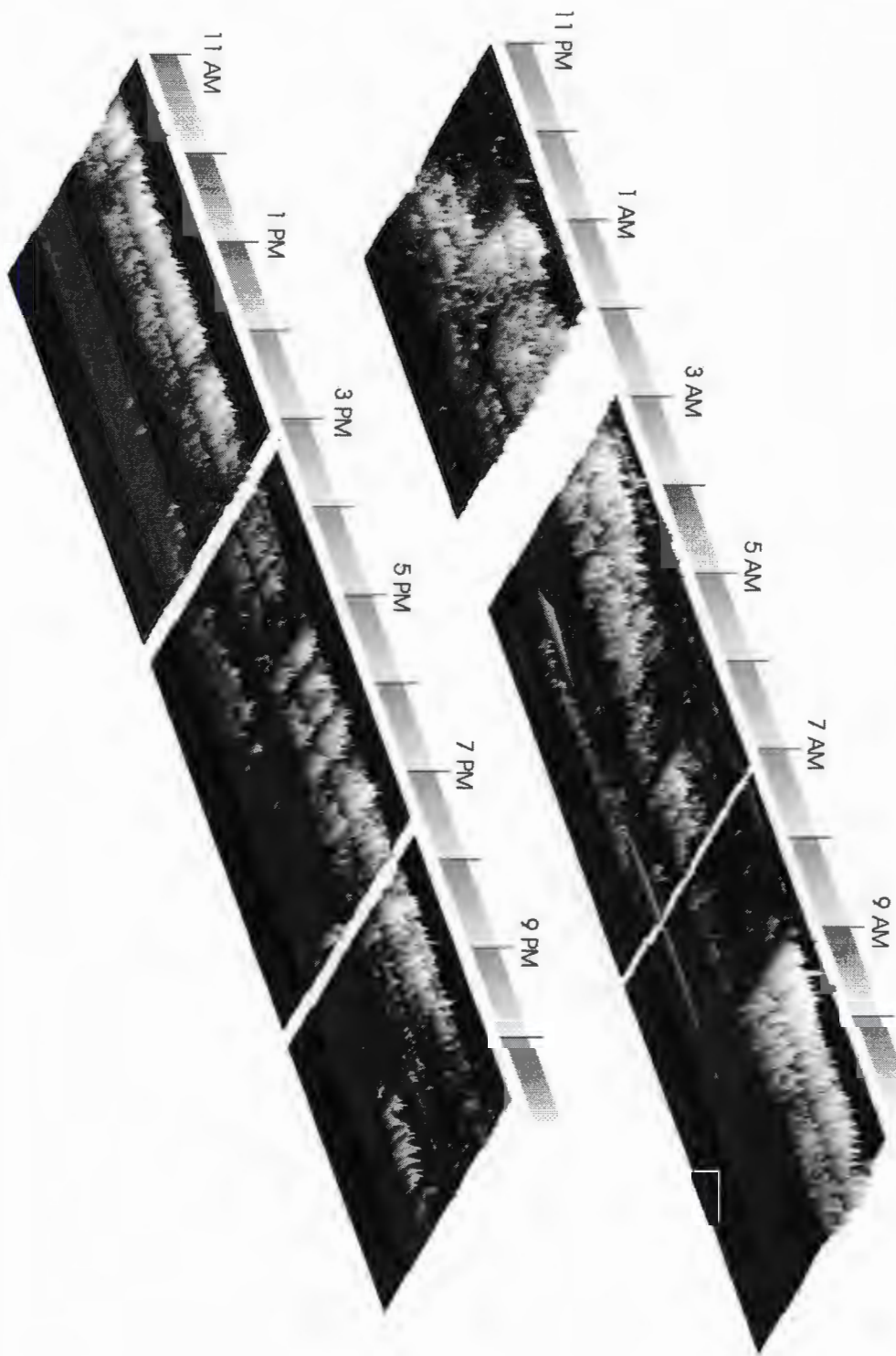


Figure 31 - Data from the peak of the 1998 flood event, May 25 and 26.

4.2 Nival Flood, 1999

The spring of 1999 was somewhat unusual. The accumulated snow pack was above normal, and the spring was mostly cool, with a few warm spells. The snow melt flow was spread over more than a month. When the weather did finally warm in early June, the floodwaters rose over the course of a week. Since the flood was attenuated over many days, we did not see a dramatic flood peak such as the 1998 event. The passage of sediment was monitored continuously, but the record shows significant movement only from June 9 to June 16. A wide range of flow conditions was observed over the course of the flood, enabling us to identify a number of distinct patterns or phases of sediment transport.

Figure 32 shows the hydrograph from this period, along with the total bedload activity and suspended sediment from June 9 to June 18, 1999. The strong diurnal signal is due to the higher altitude snowmelt events in the afternoon that create a flood wave, passing by the study site some 6 to 8 hours later. The suspended sediment index rises with discharge levels most days, although there is a subdued response on the night of the 13th, when the availability of fine sediment appears to decline following a period of prolonged bedload activity.

From May 23 to June 8, the transporting ability of the creek was relatively low. The bulk of the transport was sand-sized sediments, likely carried from storage in pools, channel edges and bar margins. Organic debris, clusters of fine material and a few small pebbles were also noted. By June 9 the stage rose to a point where larger clasts (up to 2 cm) were transported over the device. Throughout the flood the stage remained at about one half bank full, never quite reaching the point of picking up structural stones, but easily moving whatever small, loose material was available.

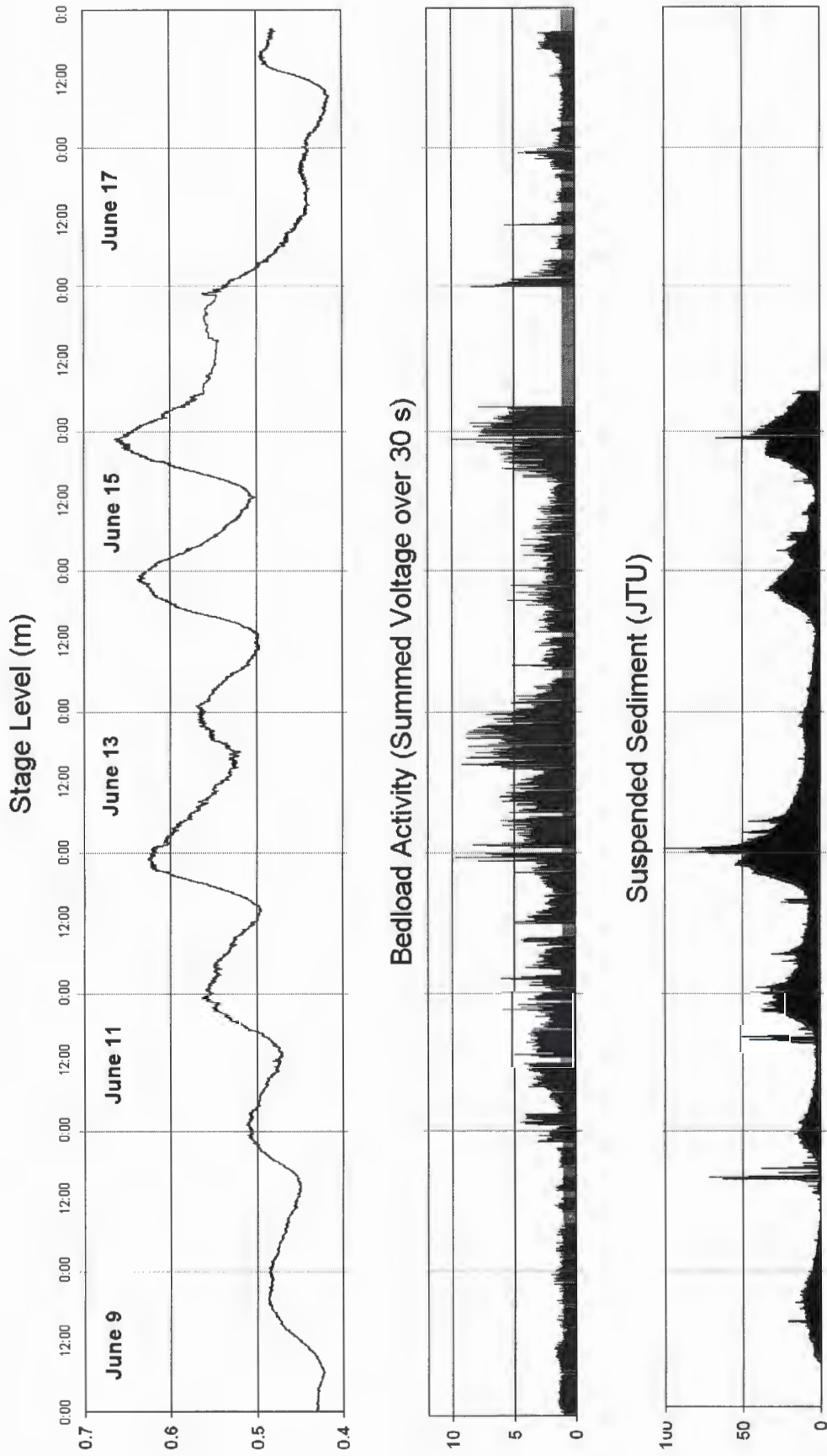


Figure 32 - Stage, bedload activity and suspended sediment readings from the 1999 flood.

O'Ne-ell creek has a remarkably low amount of fine sediment transport. Turbidity values remained low throughout the flood. At the highest turbidity levels, the streambed was visible (but yellowish), and between the turbidity episodes the streambed was clearly visible.

Discharge through the study section reached a peak of $8.6 \text{ m}^3/\text{s}$ on June 15. Instantaneous velocities in the creek were measured daily, and ranged up to 2.6 m/s . The channel cross section at peak discharge is shown in Figure 33. The depth and velocity measurements were taken roughly 30 cm downstream of the BMD, every $\frac{1}{2}$ meter at 0.2 and 0.6 depth. The relatively flat cross section of this spot was present before installation of the BMD.

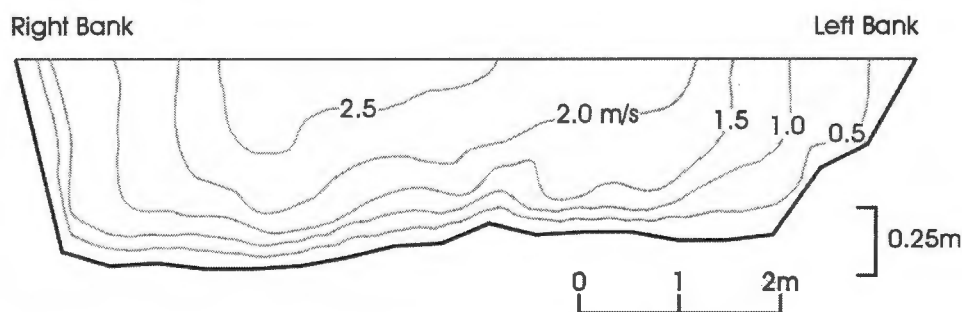


Figure 33 - BMD Site Water Velocity Cross Section: contours based on maximum stage measurements in 1999 show the variation in velocity across the channel width. The vertical dimension is exaggerated threefold.

The following figure shows the 8 days of bedload activity throughout the 1999 nival event. Gaps in the record are due to periods of maintenance and technical problems. Some portions of the record have been removed due to excessive noise levels. Most of the record on Jun 16 was missed after a disk drive failure.

By June 12, particles with an **a-axis** larger than 6 cm were being recovered from the flow with a small hand-held basket sampler. As the stage rose during the afternoon and evening of June 12, increasingly intense waves of sediment passed over the device.

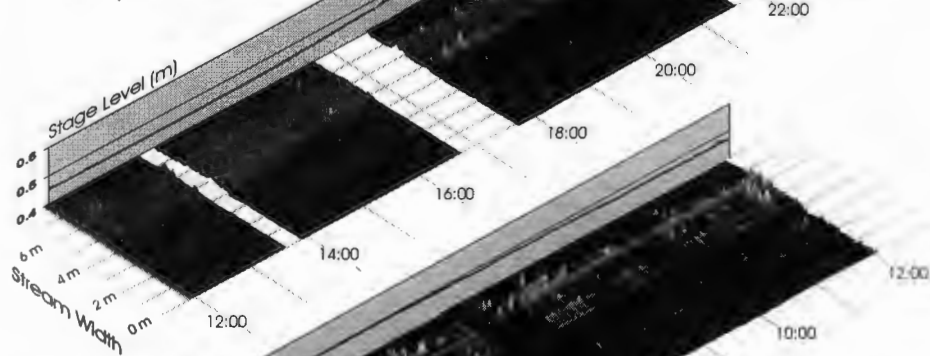
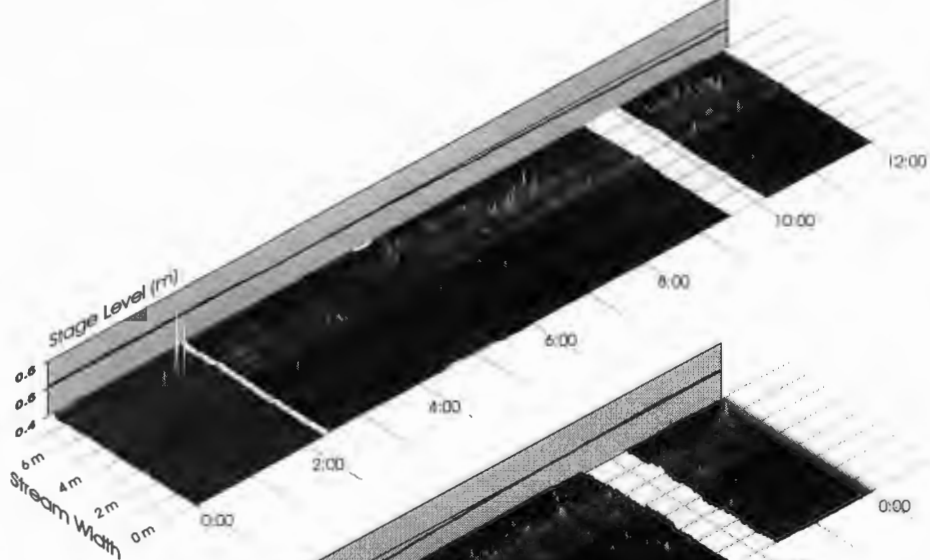
There is a lapse in the sampling record from about midnight to 1 AM, but we then see the activity continue past roughly 10 AM, when the amount of material in transit subsides.

There is a strong diurnal signal in the stage record and, quite clearly, the bedload transport pattern responds to this trend. There is an evident hysteresis effect, wherein the bedload discharge rate responds proportionately to the rising flow, but then continues at a high rate even as the stage level diminishes.

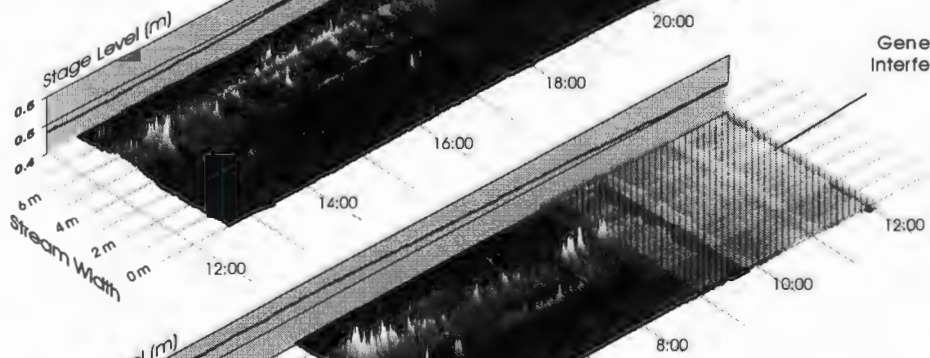
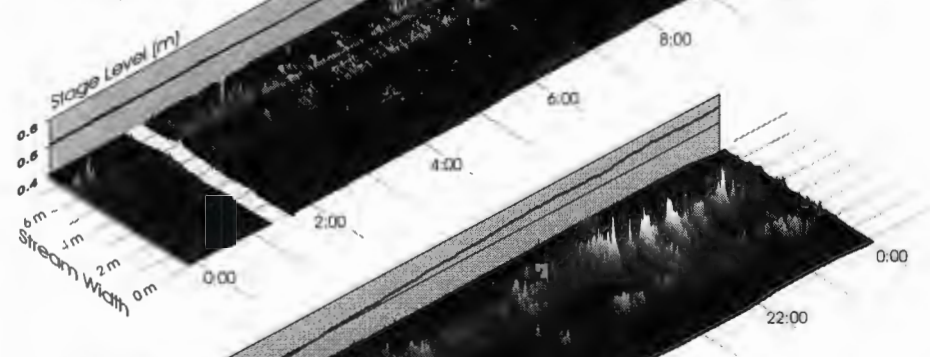
Interestingly, even with the lesser flows on June 13 (see hydrograph, Figure 32) the peak rates of bedload discharge were quite similar to the previous days' record. The duration of the transport event was much shorter, however.

Figure 34 (following pages) - The BMD record from June 10 to June 17. The channel width is measured from the west side of the channel to the east. File lengths vary from one half hour to four hours. Gaps between the files are from maintenance and technical problems. Most of the record on June 16 was missed after a disk drive failure.

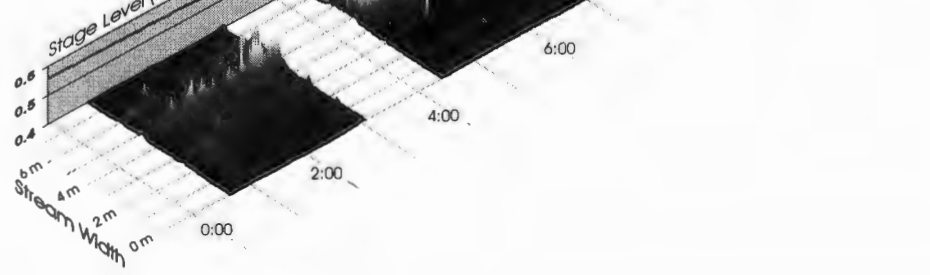
June 10



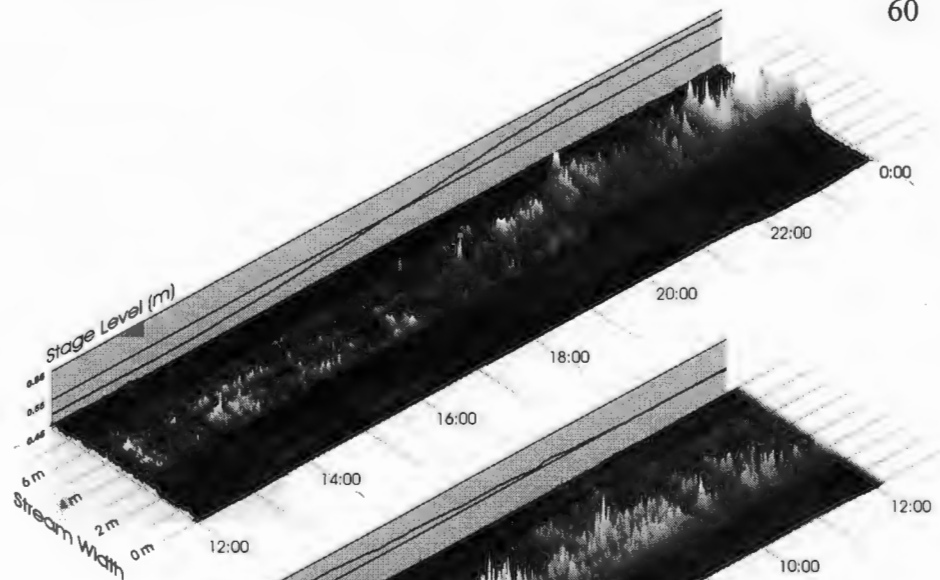
June 11



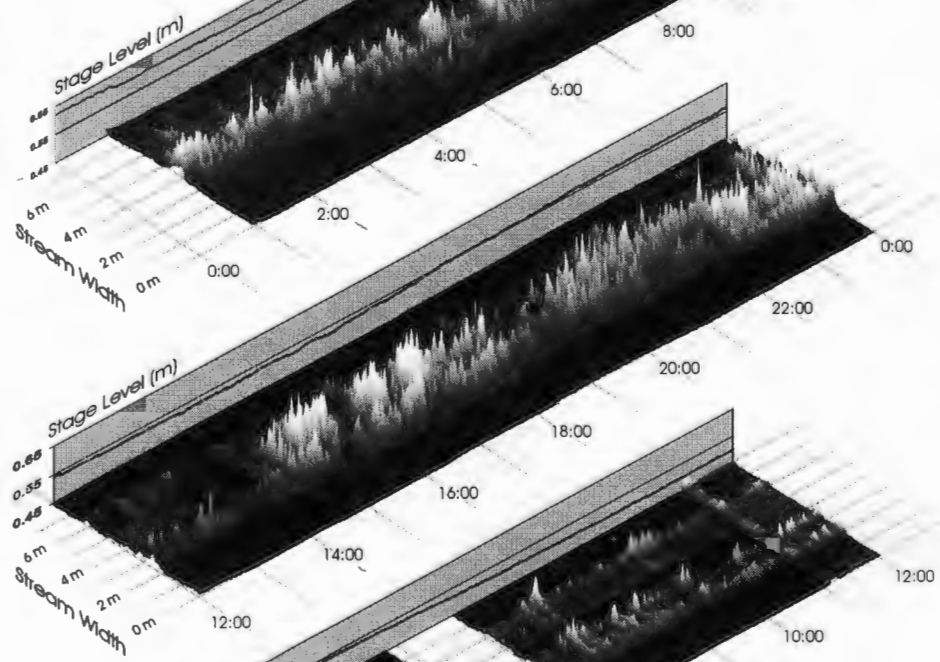
June 12



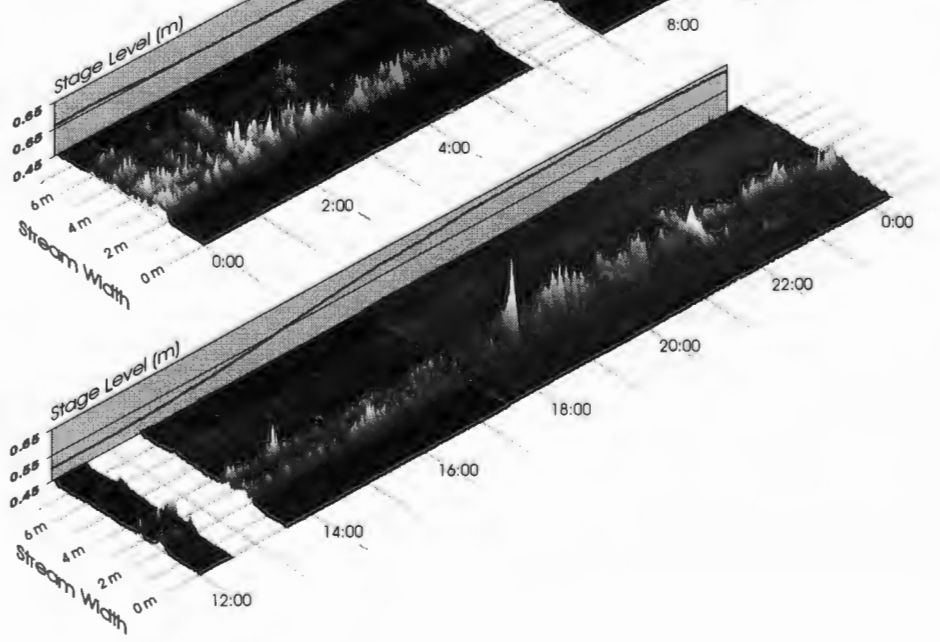
June 12



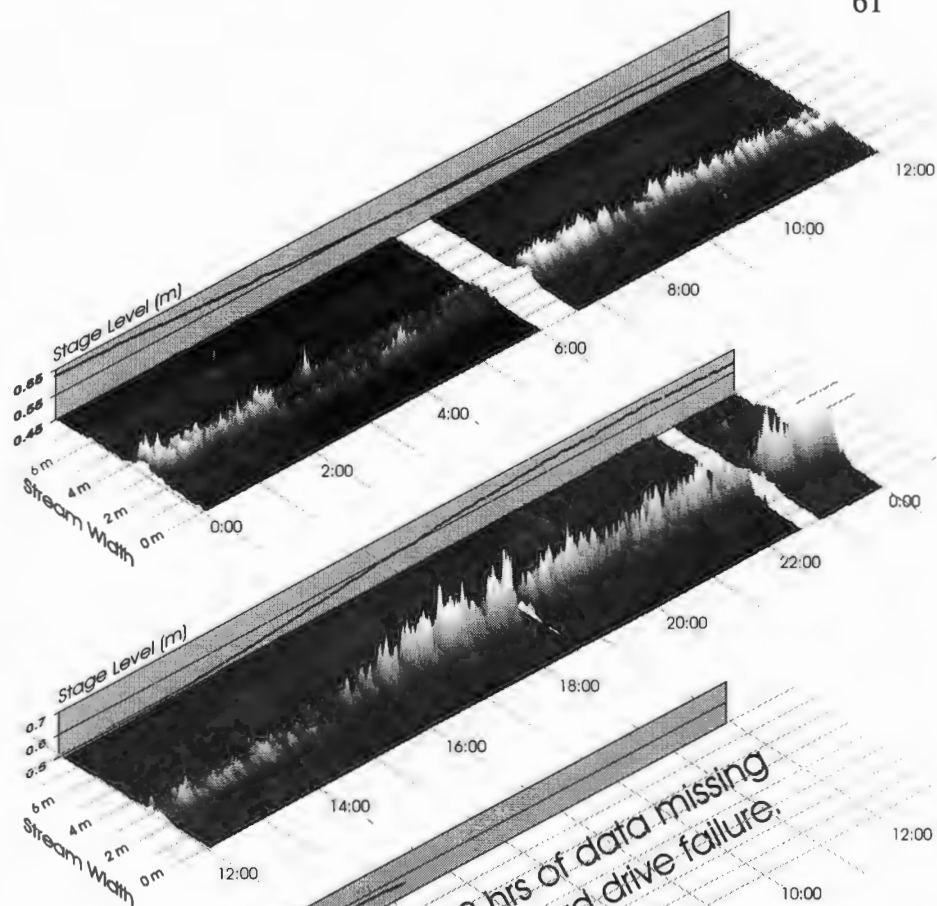
June 13



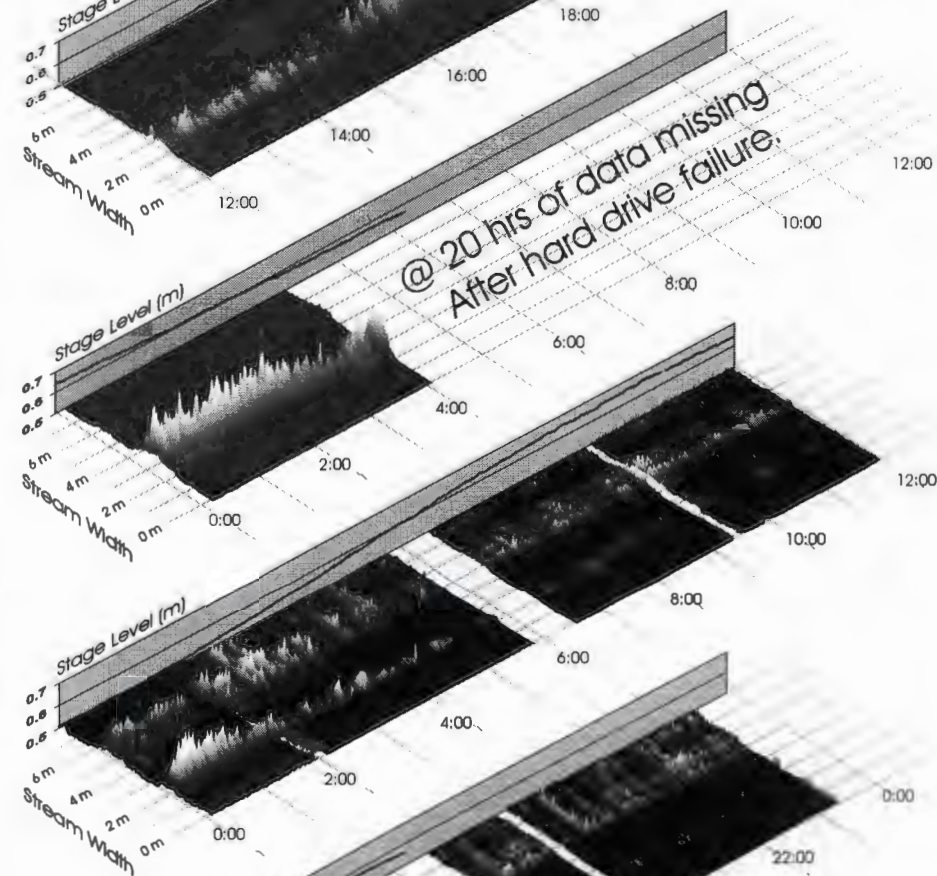
June 14



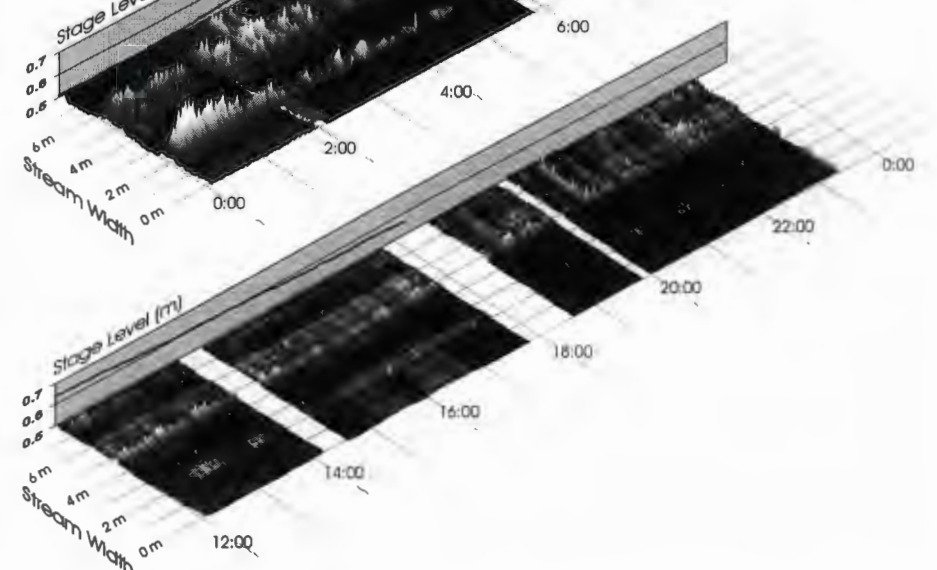
June 15



June 16



June 17



4.3 Sediment Transport Patterns

The 1999 flood data were recorded at a higher rate of signal acquisition (104.2 Hz per channel) than those in 1998 (30 Hz), thus presenting a clearer view of transport activity, and affording better signal processing resolution. As the data from the 1999 event were analyzed, at least four patterns or “modes” of transport became evident; these are explored in detail here.

4.3.1 Marginal Transport

From May 23 to June 10, the creek discharge was close to the threshold of **competence**. Only small amounts of organic debris, clusters of fine grains and pebbles were transported. For a few evenings between May 30 and June 5, the stage rose to a point where particles in the pebble range were transported, but it is mostly sand-sized particles that are evident in the record (i.e. generally few signal frequencies < 14 Hz). Transport was generally sporadic, and when the discharge and turbulence increased, particles showed a tendency to pass as clusters.

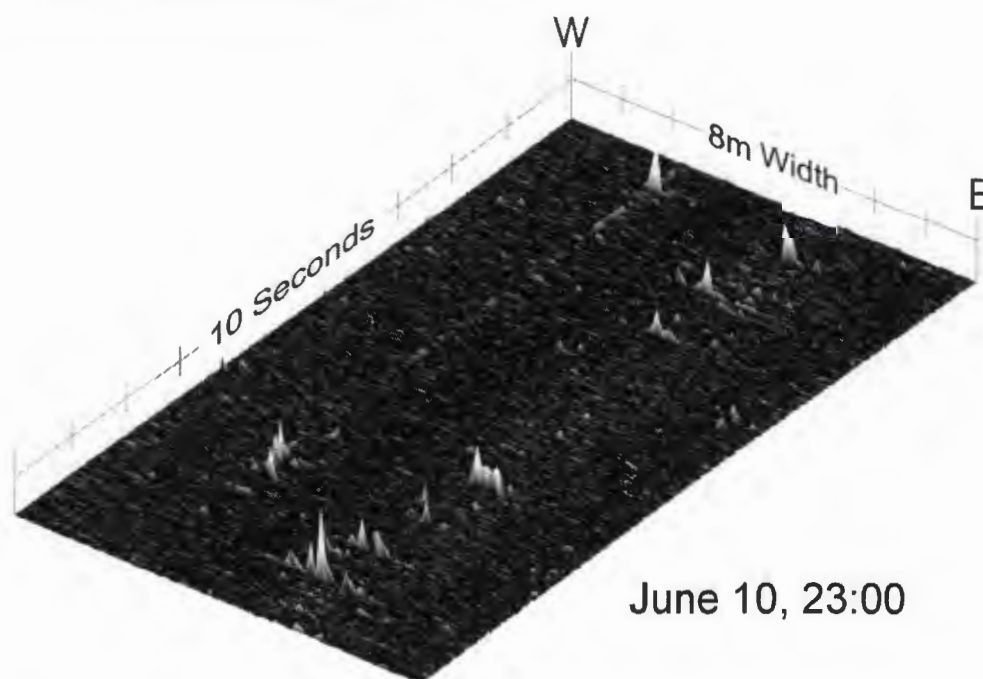


Figure 35 - Marginal transport.

Figure 35 shows a sample of the record during this early phase of transport. The majority of the transport activity was on the east side of the channel where flows were slightly faster. The narrow band of activity on the west part of the channel is sandy, easily transported material from a bar immediately upstream of the BMD. This portion of the record is the easiest to analyze, since the events are discrete, and usually affect only one sensor.

On June 9, a heavy rain fell for most of the morning. This contributed to the snowmelt flow, which was probably accelerated by substantial melt in the higher reaches of the basin. The stage rose to a point where larger clasts up to 2 cm were transported over the device. Two days later, temperatures rose to 25 C, and material began passing in greater volumes.

4.3.2 Clustered Transport

As increasing numbers of particles were picked up and carried along the bed, fluid turbulence and particle interaction caused grains to cluster together. There are many points in the record where it becomes difficult to distinguish among several particles passing at once.

Figure 36 shows an example of transport during clustered transport when material was moving faster, with particles ranging up to 2-3 cm diameter. Some of the bundles of sand and pebbles washed over the device in swaths up to 3m wide.

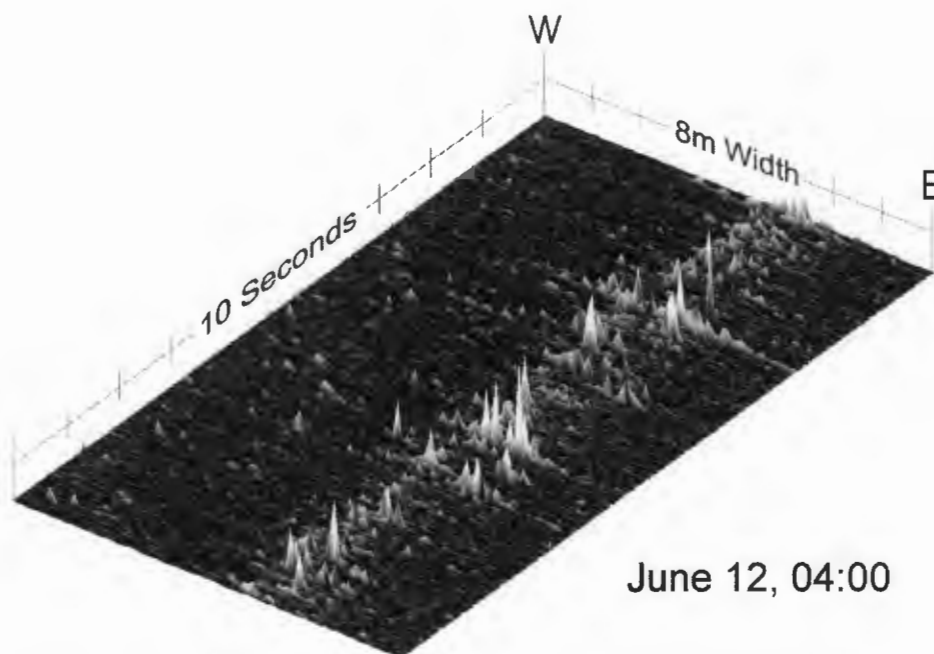


Figure 36 - Clustered transport.

4.3.3 Continuous Transport

As the stage rose during the afternoon and evening of June 12, increasingly intense waves of sediment passed over the device. Inter-granular collisions, and the sheer volume of material in motion, blur the distinction of passing clusters. At times, the material seemed to pass in steady sheets. The activity continued until about mid-day on June 13, when the amount of material in transit subsided for a few hours and then resumed and reached a maximum on the evening of June 13. There was clearly an abundant supply of material entrained by the high flows, and the bedload discharge continued even as the stage level dropped during the mid-day period of June 13.

With the ample availability of material for transport, the clustering effect becomes less pronounced, and we observe the onset of pulses lasting for 10-20 minutes. In the brief intervals between pulses, the transport rate drops almost to zero.

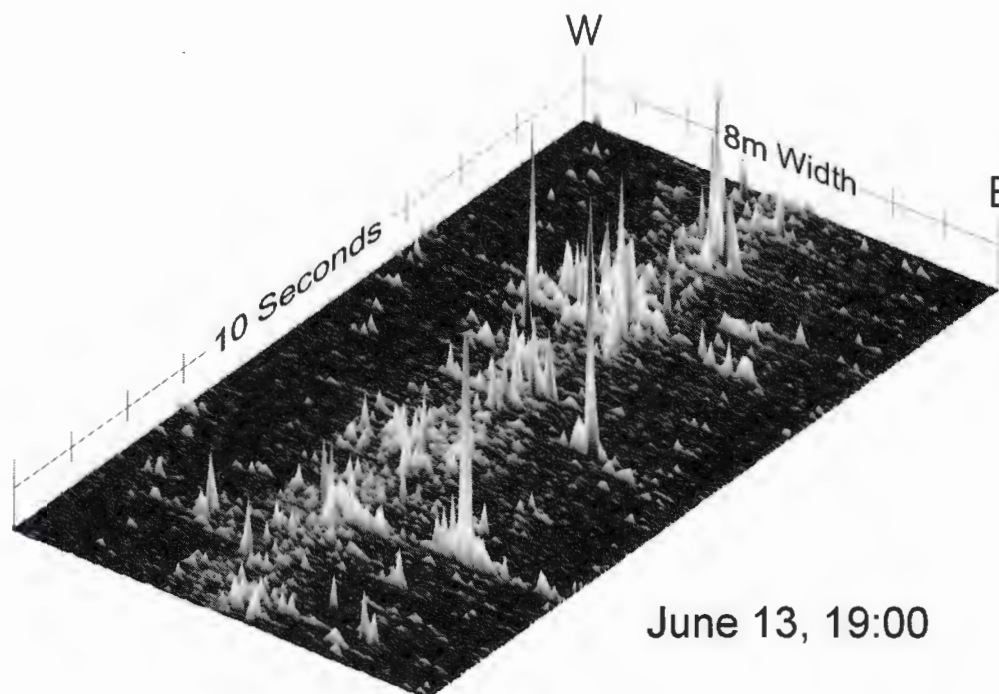


Figure 37 - Transport at the height of the flood event.

4.3.4 Sand Streets

The final piece of the record (June 14th to June 17th) was dominated by the passage of sediment stringers, originating from a collapsed section of the bank approximately 65 m upstream. A shift in a logjam diverted flow against the bank and caused a large failure, sending roughly 4 m³ of sandy material downstream. The transport was confined to one or two narrow transport zones, 1-2 meters wide, which migrated laterally by about one meter. Material was passing as sheets of finer material, as could be observed from the catwalk at the site. Portions of the device became draped in sediment, although this blanket of material moved laterally as the hours passed, indicating the active nature of these “streets.” The position of the transport streets is determined by newly developed minor bars upstream of the device and likely by individual small boulders. The width of the streets appears to vary from 10-20 cm to over a meter. The recorded signals indicate that the stringers were comprised mostly of sand and gravel material.

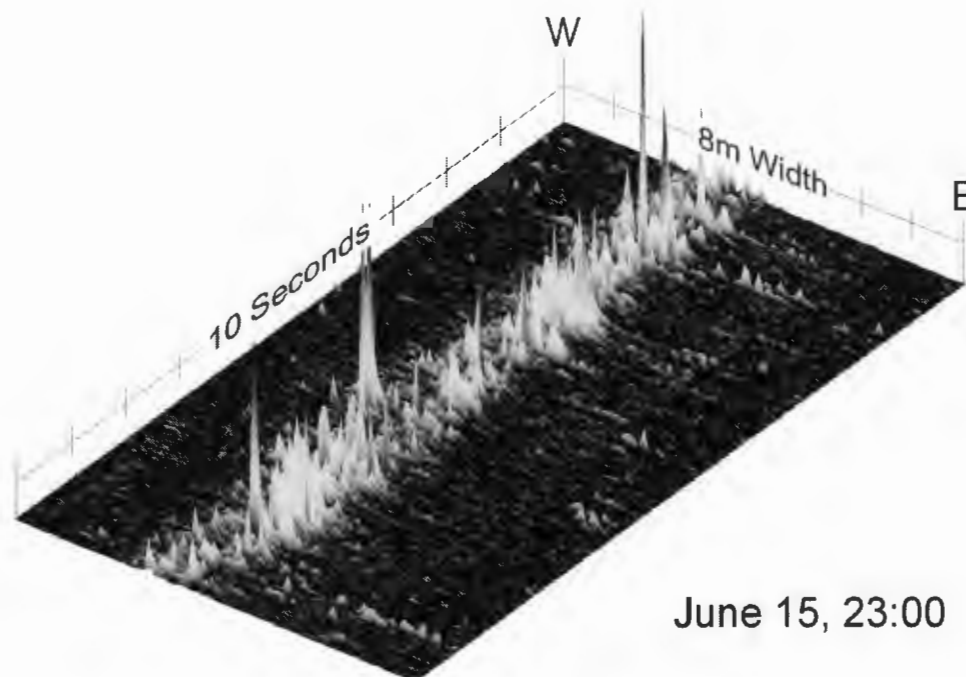


Figure 38 - Steady discharge of sand and gravel along the bed.

Figure 39 shows an excellent example of the onset of a gravel street, after a few minutes of relative quiescence. Once the material was set in motion, it continued in an uninterrupted stream for approximately 10 minutes. The width of this street is approximately 1.2 m.

By June 18th, the waters subsided to lower levels, and the transport of material gradually diminished to nothing. As the water level dropped, it became evident that a few larger clasts immediately downstream of the device had been transported leaving somewhat of a 'drop' at the site, roughly 15 cm deep and 2 m wide. A small hydraulic jump was evident in this area during the last portion of the flood. By placing some boulders, the scoured portion could be filled; however, this did highlight the necessity of maintaining the site.

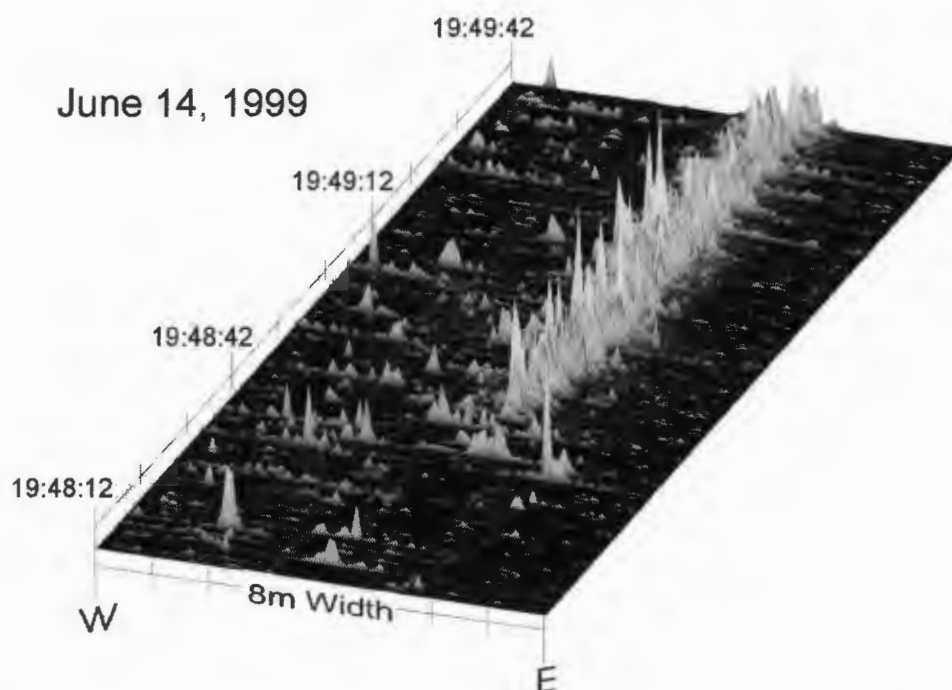


Figure 39 – The onset of a gravel street, 1.2 m wide. The steady passage of material lasted for over 10 minutes. This diagram shows the first 90 seconds of the transport event.

Otherwise, there seemed to have been little geomorphic work done on the stream throughout the 1999 nival flood. The flood was unusual in that it was so protracted and that the peak discharge was relatively low. The 1998 flood had a short period but with significantly higher flows. Larger floods (> 10 year return interval) will have a larger transporting capacity with greater, and more stochastic, sedimentary inputs. We might then expect to see roughly similar patterns of transport, with coarser material, higher rates of flux and greater variability in the transport record. At least four distinct phases of transport are discernible from the 1999 flood, although it can be assumed that with different bed material composition and changing hydraulic conditions, other phases would likely develop.

Chapter 5 Patterns of Bedload Transport

5.1 Discussion of Sediment Transport in O'Ne-ell Creek

A broad comparison of the 1998 and 1999 nival events shows that they both exhibit clear pulsating or unsteady transport patterns. Transport may falter or cease during flood stage, subject to channel conditions or sediment availability. The transport zone clearly widens as more material is set into motion, and then tapers as sediment transport declines. We observe that the transport zone may move considerably throughout an event. These patterns of activity are discussed in sections 5.2, 5.3 and 5.4, below.

Although a number of problems have arisen applying the signal processing algorithms (described in Chapter 3) to the analysis of the flood record, we have attempted to estimate the total transport volume based on the number of particles counted as they pass over the device. The assumptions and calculations involved with this estimate are found in Section 5.5. The estimates obtained are then compared with existing transport measurements taken at 3 study reaches within the Stuart-Takla watersheds.

5.2 Temporal Variation in Transport

In O'Ne-ell Creek we observe pulses on several time scales. Firstly, there are daily pulses observed, as sediment moves in response to the diurnal pattern of snow melt. As the melt water discharge rises in the late afternoon and peaks around midnight, rates of sediment movement generally increase proportionally. Secondly, pulses are clearly visible on a time-scale of tens of minutes. As the volume of sediment in transit reaches a certain threshold of congestion, the transport becomes unsteady and moves in pulses with

intervals of 10 to 30 minutes. Finally, at the instantaneous time scale, sediment is observed moving as clustered material.

The various types of short term, quasi-cyclic pulses discussed here are distinct from larger multi-event cycles of degradation and aggradation known as 'slugs', 'translational waves' or 'megaform pulses' which exist on a timescale of months or years (Nicholas *et al*, 1995). These may occur as a result of large, discrete sediment inputs, such as landslides and debris torrents, or from industrial activity such as mining. They are also associated with the development of gravel bars and other morphological features such as log jams.

With respect to variation in transport rates at the tens of minutes scale, this pattern has been reported in the literature for almost 70 years. Work done in the early 1930s with basket samplers was the first to provide clear indication that bedload transport occurs in waves rather than as a steady discharge. Ehrenberger (1931) documented the oscillatory behaviour of bedload discharge in the Danube and Inn rivers (Figure 40), taking repetitive samples from a limited number of fixed stations. Similarly, Mulhofer's (1933) and Nesper's (1937) data showed patterns that suggest a variable periodicity in sediment discharge rates even at constant water flow.

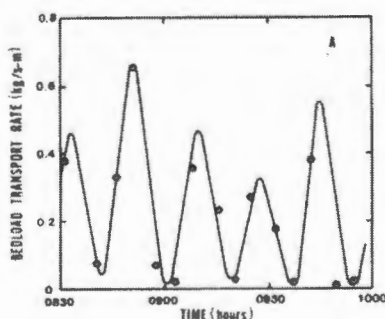


Figure 40 - Figure from Ehrenberger's bedload measurements, taken with a basket sampler on the River Danube at Vienna National Bridge, 24 June 1931 suggest a pulsating movement of bedload. Sampling time=100-300s. Mean transport rate = 0.236 kg/s/m. (Ehrenberger, 1931 - Fig. 6). Taken from Gomez, 1991.

Results from more recently developed, direct sampling apparatus such as slot traps with pressure pillows (Kuhnle, 1991; Harris and Richards, 1995), vortex tube traps (Klingeman and Milhous, 1970; Tacconi and Billi, 1989), and in situ magnetic sensor devices (Reid *et al.*, 1984; Ergenzinger and Custer, 1983; Bunte, 1996) have all clearly illustrated the passage of distinct pulses of sediment on a number of different time scales. Measurements taken by Bunte (1996) at Squaw Creek, Montana, are particularly clear, showing the presence of bedload pulses often followed by smaller 'secondary' and 'tertiary' pulses during a nival flood event (Figure 41).

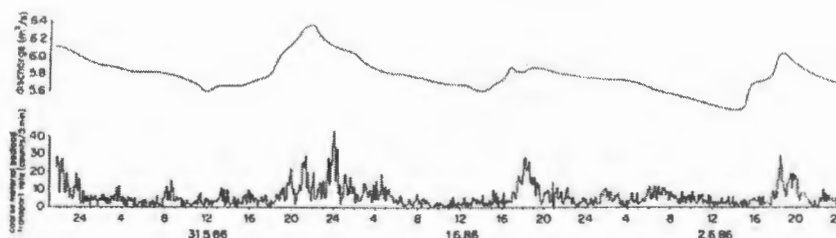


Figure 41 - Results from magnetic bedload detector at Squaw Creek, Montana (Bunte 1996).

Flume studies have amplified certain details of this phenomena, beginning with the work of Schoklitsch (1934) and Einstein (1937). Work by Hamamori (1962) sought to model the frequency of bedload pulses based on the movement of coherent bedforms such as ripples, dunes or bars. More recently, Iseya and Ikeda (1987), Kuhnle and Southard (1988), Gomez *et al.* (1989), Hoey and Sutherland (1991), Seminara *et al.* (1996) and others have all sought to model bedload waves in heterogeneous sediments

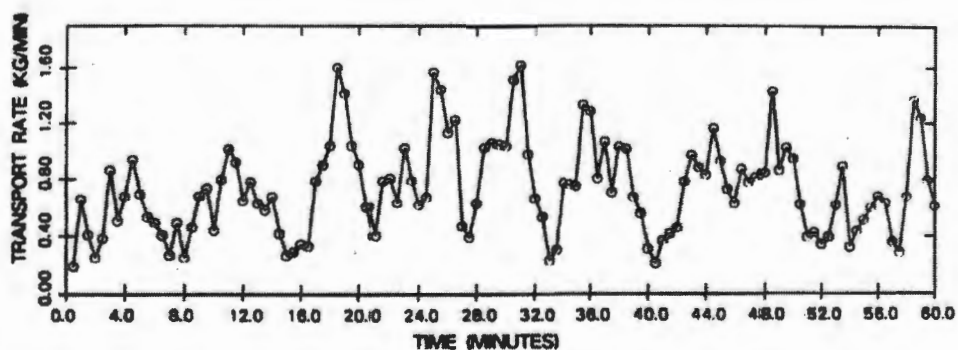


Figure 42 – Total transport rate versus time. Measurements were taken in a gravel-bed flume, showing transport fluctuations on the order of tens of minutes (Kuhnle and Southard, 1988).

based on contributing factors such as irregularities in streambed surface and variations in sediment supply. These functions operate at a number of time scales and within a number of different river types.

Part of the variable nature of sediment discharge is attributed to changes in the rate of sediment supply during the flood event. Supply may vary in response to the scour and fill cycles that take place upstream. Pulses may be caused by the periodic evacuation of storage structures such as step-pools and log jams. Exogenous inputs, such as collapse of the stream bank section noted above, are another typical source of sediment pulses.

Lateral and vertical grain sorting effects will also affect sediment supply. Gomez (1983) points out that the development of an armour coat may eventually lead to the exhaustion of mobile material. Kuhnle and Southard (1988) note that the episodic dislodging of larger structural clasts from their stable position will cause variability in transport rates as well, since all the imbricated clasts around them immediately become available for transport. Large woody debris, bed armouring and bar development undoubtedly play a role as well.

Braided rivers present a special case of pulsing sediment transport. Kang (1982) and Southard *et al.* (1984) have both suggested that the basic processes of braiding produce bedload pulses as a matter of course. Scour occurring in anabranch confluences may also produce bedload pulses (Ashmore, 1988).

Perturbations or roughness elements along the streambed lead to instability of flow and sediment transport. As sediment discharge increases, the transport rate becomes out of phase with the existing bedforms. As sediment accumulates or disperses along the channel, the bed surface is altered, in turn changing the flow patterns and shear stresses exerted by water. As material is transferred from one reach to the next in greater and greater volumes, traffic jams begin to occur.

Numerous field studies have related this pattern to the migration of distinct bedforms such as dunes or sheets of sediment (Klingeman and Milhous (1970); Tacconi and Billi (1987), and Gomez *et al.* (1983, 1989, 1997), although such coherent forms are not often observed in coarse gravel systems such as O’Ne-ell Creek. Whiting *et al.* (1988) observed the transport of fine gravels, under conditions where the bed could be clearly seen. They noted that the bed material was organized into waves with distinct coarse fronts, traveling as a “bedload sheet” or moving carpet. The sheets are coarsest at the leading edge, the length of which is much greater than the height, and the height of which is less than three coarse-grain diameters. This spatial and temporal organization of moving sheets was further analyzed by Seminara *et al.* (1996) in flumes, with a view to understanding the sorting function they perform in heterogeneous sediments as they migrate along the channel. These sheets usually develop in streams with sand and fine gravels.

5.3 Pulsations in the 1999 transport record

Figure 43 shows a typical data record, this one recorded on June 15, which exemplifies the pulsing nature of the bedload transport in O’Ne-ell Creek. The peak of the hydrograph occurs at about 23:00 (off the graph). The lower portion of the graph is the output from a single sensor, located 3.4m from right bank. This roughly corresponds to the locus of transport for this period, and gives a good indication of the general pattern of movement. Pulses seem to occur every 5-20 minutes

The upper portion of the graph shows the spatial variation of the transport intensity. The stream width is measured from the east (right) bank of the study site. The active transport zone is mostly confined to a 1 m lane, although activity can be seen along the whole length of the device.

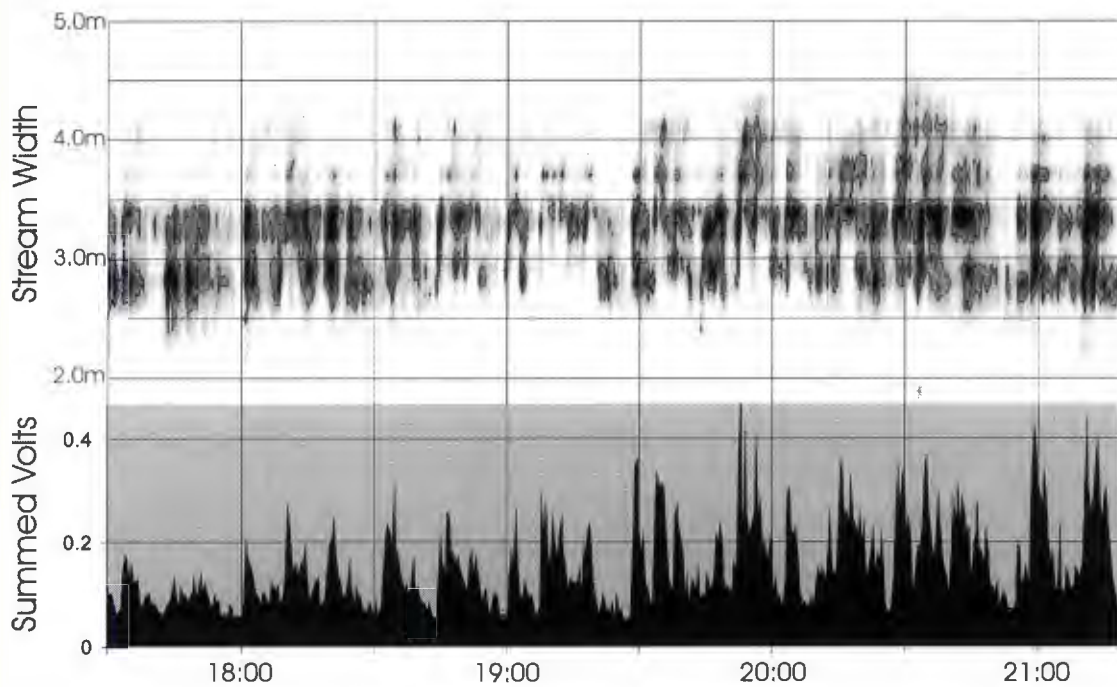


Figure 43 - Figure showing the pulsing nature of bedload transport. The upper portion of the graph displays the width of the stream over the course of 4 hours on June 15. The lower half of the graph is the voltage from a sensor located 3.4 meters from the right bank of the creek.

5.4 Lateral Instability - The Shifting Locus of Transport

The variability of transport conditions shown within the record includes not only temporal variations in intensity, but also in the lateral migration of the **locus of transport**. Distinct from the thalweg, which is defined as the thread of deepest water (Leopold, 1994), the locus of transport is a term used to denote the portion of the channel that accommodates the most material in transit (Church, 2000 personal communication). Leopold (1994) points out that in many mountain streams, 80 percent of bedload moves in 40 percent of the channel width. It is therefore important in modeling rates of transport with empirical equations to understand where the majority of bedload is moving.

The following figure was calculated by summing up activity in each BMD file to determine which sensor lane experienced the most activity. As one may observe, the principal area of activity shifted considerably throughout the course of the flood. At first,

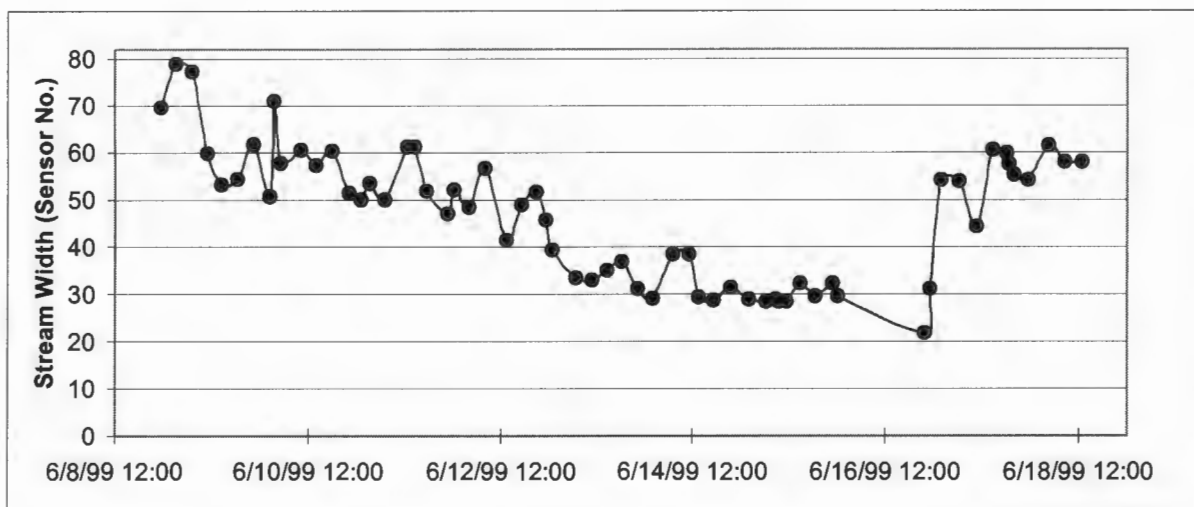


Figure 44 – The wandering locus of transport – the locus of transport is defined here as the zone of maximum bedload activity throughout each data file from the 1999 Nival event. The locus of transport moved substantially throughout the event, starting within roughly 1 m of the right bank (see Figure 34, June 11th) and drifting to within 2 m of the right bank (June 15-16).

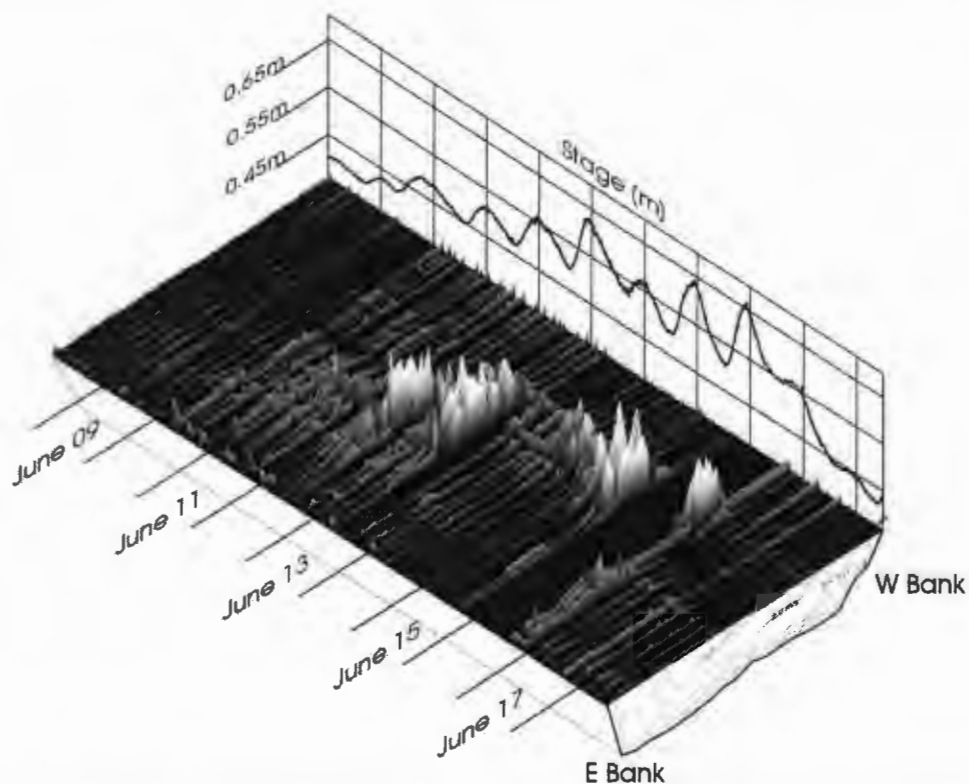


Figure 45 - The total activity across each sensor is summed for every BMD file. File lengths are usually 3-4 hours. Summed values were divided by the length of the file to ensure compatible numbers. The cross section profile (see Figure 33) adds the context of channel geometry.

most of the material was carried along the deeper, eastern portion of the creek, where flows were swifter. As the flood progresses, we see the activity shifting towards the center, and eventually over to the western side of the creek.

Figure 45 shows this activity trend in three dimensions. Summations from each file are plotted along the length of the 8 day event, showing the relative amount of activity at each sensor. The active zone changes from a relatively narrow band at the beginning to a broader field of motion mid-event, which then constricts again to a small lane of transport towards the end of the flood.

5.5 Transport Volumes – A Transport Estimate from the 1999 Nival Event

Ideally, the BMD would be used as a device to determine the instantaneous rate of sediment transport across the stream width. With the proper calibration and improved design, it is hoped that we might be able to collect information on the size of passing particles, providing vital information about sedimentological processes occurring during a flood event. This is difficult with the existing record because much of the record from the 1999 event is contaminated with background interference from the electrical systems, thus complicating much of the signal processing work. The high variability of magnetic intensity of particles further complicates the modeling.

However, an order-of-magnitude estimate for the bulk transport over the course of the event can be made by making a number of simplifying assumptions and using the particle size distribution from the bed material bulk samples to estimate the total number of grains in a single kilogram of bedload. The simplifying assumptions are:

- *The bedload material has the same particle size distribution as the bed material.*
As flood stage rises in a gravel-bed river, researchers have noted that the number of particles transported in each grain-size class may vary by nearly two orders of

magnitude (Parker, Klingeman and Maclean, 1982; Bunte, 1992). Particle size distributions vary with changing hydraulic conditions, sediment availability and clustering or hiding effects. However, since we are looking at the smaller end of the scale (ie. particles smaller than **45 mm**), this material is less subject to selective transport, and we may assume that the bed material distribution is a useful approximation.

- *Variation in magnetic intensity is uniform for various size clasts, and is similar in character to the bed material.* Although lithologies tend to disintegrate and become sorted at different rates, we assume here that each lithologic group, with its distinct magnetic properties, is uniformly distributed throughout all size ranges of bedload material at O'Ne-ell Creek. We may further assume that since most of the transported material is endogenous to the creek channel, it has a magnetic character that is statistically similar to the samples taken from the stream bed.
- *The volume of particles is similar to that of spheres of the same caliber.* The larger clasts are subrounded to subangular and generally have 70% of the volume of equivalent spheres (n=442, St.Dev.=10.3%, see Figure 46). However, since the sieving process selects particles by their b- and c- axes, it is likely that their volume averages that of a sphere. With smaller sized materials, grains will increasingly approach sphericity.

Figure 46- Distribution of grain geometries based on a sampling of material >50 mm The average sphericity of particles is 0.7.

- *The density of particles is uniform (2.65).* This density value is for the most common minerals such as feldspar and quartz, but there are a number of lithologies in the stream that are denser such as andesite, and ultramafic rocks that likely range closer to 3.0.

- *Only particles larger than 4 mm are able to induce a sufficiently large voltage response to exceed the threshold of detection.* Since the volumetric estimate is based on the *number* of particles passing, this is certainly the most sensitive variable in the equation. While 2 mm particles have been detected in the laboratory, this case is generally rare; a threshold of 4 mm appears to be a better approximation.

Figure 47 - Size distribution of the theoretical bedload material used in the calculations. The proportions are based on the 4 bulk samples of bed material taken at the site. The coarsest material is 45 mm (5.5 ψ), and the assumed threshold of detection is 4 mm (2.0 ψ).

Based on random bedload sampling with a 10-inch (25 cm) basket sampler throughout the course of the event, the largest clast captured had an a-axis of 6.6 ψ (100 mm). By far the majority of the material did not exceed the medium gravel size range (>12 mm).

During periods of marginal transport, we observe particle counts at rates of up to 35 per second. At the peak of transport activity, rates reach up to 100 or 150 per second (Figure 48). Theoretically, the detection algorithm can detect up to 600 events/ sec. However, there may be times where the sensors are overwhelmed by multiple events. On the other hand, there are a few points in the records where random noise interferes with particle counting, and this may add up to 25% more particles than were actually passing.

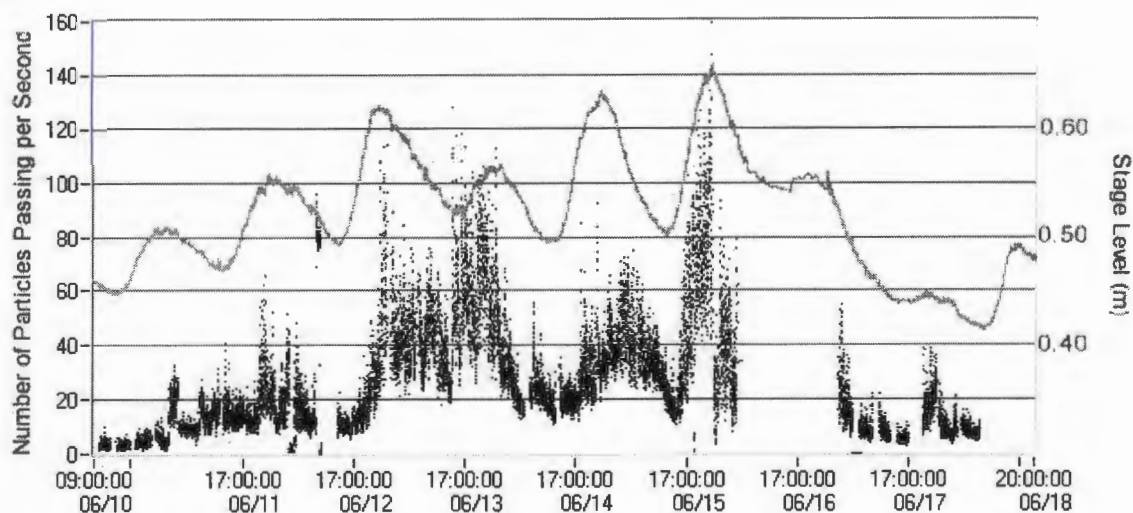


Figure 48 – Rates of particle transport (number of events per second) over the course of the flood.

Assuming that the device is only able to distinguish individual particles larger than 4 mm in size, there are approximately 5647 particles per kilogram of the bed material (Table 2). Of those particles, we assume that only 30% are sufficiently magnetic to initiate a voltage signal over the threshold of detection. Furthermore, since particles must generally pass over the more sensitive 6 cm central diameter of the sensor to register (the sensors are spaced at 10 cm intervals), there is a further exclusion of 40% of the sample. Therefore, a correction factor of $(0.30) \times (0.60) = 0.18$ is applied to this value. The total number of detectable particles per kilogram is thus 1017.

Other complicating factors include cases where two signals arise on adjacent sensors from a larger clast passing between them, and sections of mostly static, where sand grains are passing in large volumes.

Sieve Size (mm)	% of Sample Weight	Proportional Weight	Density kg/m ³	Single Grain Volume (m ³)	Single Grain Weight (kg)	# of Grains in 1kg Sample
45.3	17.78	0.1778	2650	3.02E-05	8.01E-02	2.22
32.0	15.99	0.1599	2650	1.07E-05	2.82E-02	5.66
22.6	11.22	0.1122	2650	3.76E-06	9.97E-03	11.25
16.0	8.75	0.0875	2650	1.33E-06	3.53E-03	24.79
11.3	9.52	0.0952	2650	4.71E-07	1.25E-03	76.32
8.0	14.70	0.1470	2650	5.32E-08	1.41E-04	1042.71
4.0	7.35	0.0735	2650	6.18E-09	1.64E-05	4484.20
2.0	8.95	0.0895	2650	1.49E-09	3.94E-06	- Not
0.83	3.05	0.0305	2650	1.55E-10	4.11E-07	Included -
0.5	2.69	0.0269	2650	6.54E-11	1.73E-07	----
	100.00 %					5647.15
					x 18% detected =	1016.49

Table 2 - An estimate of the total number of grains per kilogram of bed material from O'Ne-ell Creek, based on 4 bulk samples taken at the study site.

Over the course of 6 days (June 10 to June 15), some 14×10^6 particle events were registered. Typical rates for a day were 1.7×10^5 on June 10 (low) and 4.2×10^6 on June 13 (high). Making the gross assumption that the particle distributions for these days were similar, and that 1016.5 events marked the passage of 1 kg of material, the volumes break down as follows:

Date	# of Particles	Tons of Material	Unit Trans. Rate
June 10	171859	0.169	0.023 kg/m-s
June 11	1203123	1.184	0.164
June 12	1504929	1.480	0.206
June 13	4202050	4.134	0.574
June 14	2058716	2.025	0.281
June 15	3230275	3.178	0.441
June 16	1271613	1.251	-----
June 17	771466	0.759	0.057
Total	14414031	14.18	

Table 3 - Daily particle counts, with associated bulk sediment transport estimates. The record from June 16th is incomplete.

This would imply that at the height of transport activity, bedload was moving at a rate of 2.87 kg/s, or 0.574 kg/m-s, given an active transport zone width of 5.0m. In terms of the volume of material passing during the flood, assuming an aggregate density of 1.8, 14.18 tonnes equals 7.88 m³ of material passing over the device

5.5.1 Magnitude of Error

Although larger particles are not likely in motion during the early part of the event, we are assuming a static distribution of material throughout. With marginal amounts of material moving, the inclusion of larger clasts (i.e. 45 mm) does affect the volumetric estimate somewhat, even through they comprise such a small fraction of the particle count. By changing the largest-sized clast assumed to be in motion to 22.6 mm, for example, the volumetric estimate for the given period declines to 66% of our original estimate.

The calculations are rather more sensitive to the decision of the minimum size clast detectable. If a smaller size limit is chosen, the calculated volume decreases greatly. If we had chosen a detection threshold of 0.833 mm instead of 4 mm for instance, the

transport estimate for the nival event would have been 781 kg - just over 5% of the present weight estimate of 14 180 kg. With a threshold of 8 mm, however, the estimate would be 68 857 kg, almost 5 times the present value. The assumption of minimum threshold of detection is thus of considerable importance in these calculations.

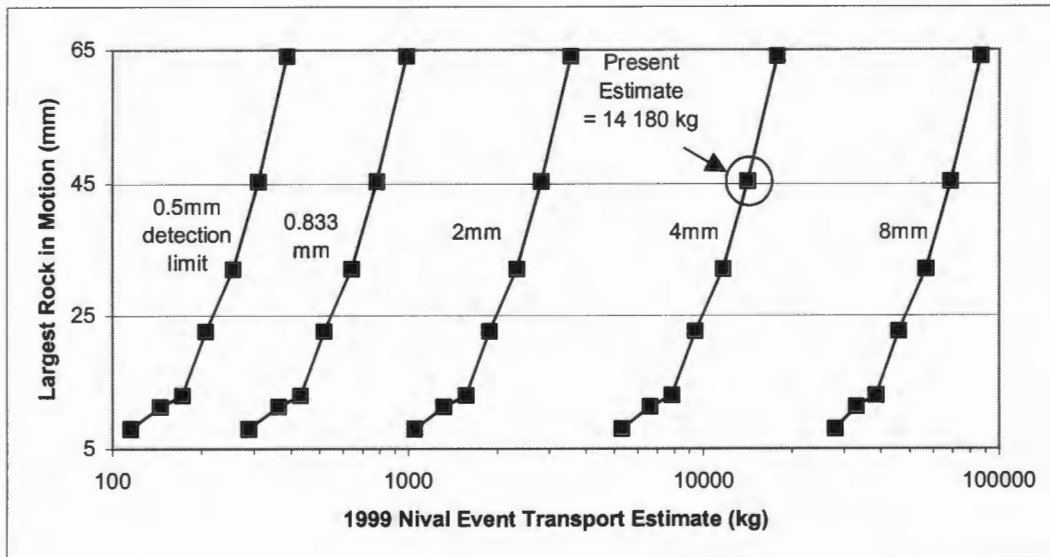


Figure 49 - The effect of two important parameters in the volumetric transport estimate. As the assumed threshold of detection by a BMD sensor increases from 0.5 mm to 8 mm, the estimate of transported material grows by several orders of magnitude. The assumptions regarding the largest particle in motion (y-axis) affect the volumetric estimate as well - as the assumed size moves from 8 mm to 64 mm, the estimate increases by a factor of 3.

Ideally, data from basket sampling should be paired with the BMD calculations so that some estimate of the largest grain in motion can be made for as many periods of the record as possible. We could then adjust the estimate to reflect the different conditions encountered throughout the flood event.

5.5.2 Stream Efficiency

Table 4 shows some of the hydraulic parameters at the BMD site. The water-surface slope was not adequately measured, and is thus assumed to be similar to the bed slope of 0.013. Unit stream power is defined as the product of the unit weight of water, velocity, depth and slope ($\omega = \gamma V D S$). The mean shear stress at the bed is defined as the

product of the unit weight of water depth, and slope ($\gamma DS = \omega/V$). The **stream efficiency** is the unit bedload-transport rate (estimated in Table 3) divided by unit stream power (Emmett, 1976).

It is interesting to note that Leopold and Emmett (1975) have developed a relationship between bedload transport rates and stream power, based on the hypotheses of Bagnold (1973). They suggest that as stream power increases, and sediment is set in motion, the stream efficiency will approach a constant. The efficiency rating generally found in coarse gravel rivers (32-64 mm) is 2-3 percent, barring any effects such as armouring, that further diminish the transport capacity of the stream. These values are close to the range of the present transport estimates, 0.2% to 4.8%.

Date	Stage (m)	Q (m ³ /s)	Mean Flow Velocity (m/s)	Unit Stream Power (kg/m-s)	Mean Shear Stress (g/cm ²)	Stream Efficiency %
June 10	0.52	10.55	1.5	10.14	0.676	0.2316
June 11	0.55	11.73	1.6	11.44	0.715	1.4370
June 12	0.62	14.49	2.0	16.12	0.806	1.2756
June 13	0.57	12.52	1.6	11.856	0.741	4.8427
June 14	0.63	14.88	2.0	16.38	0.819	1.7173
June 15	0.64	15.27	2.1	17.472	0.832	2.5261
June 16	-	-	-	-	-	-
June 17	0.44	7.41	1.4	8.01	0.572	0.7152

Table 4 - Summary of hydraulic parameters at O'Ne-ell 1950.

5.6 Comparison with Existing Data

The best available data on rates of bedload transport in O'Ne-ell Creek have been collected by Gottesfeld (1998) and Poirier (2000) (See Section 1.3). Based on their measurements taken over the course of the 1996 and 1997 floods at O'Ne-ell Creek, we are able to determine approximate volumes of material carried through a given reach. The reaches chosen for comparison are O'Ne-ell 1550 and O'Ne-ell 950², roughly 400m and 1000m downstream of the BMD site (O'Ne-ell 1950), respectively. Tsitsutl Creek joins O'Ne-ell at approximately 1750, adding substantial flow to that of O'Ne-ell. Combined with a subdued gradient ($>.005$), somewhat finer material and different years of measurement, we would expect the transport estimates from these reaches to vary appreciably. Data from Forfar Creek (see Figure 3) is also shown for comparison. The flood discharge ($\sim 10 \text{ m}^3/\text{s}$) and slope (0.015) of Forfar 1545 are close to that of the O'Ne-ell BMD site.

By measuring the typical travel distances of tracer sediment particles, Gottesfeld was able to determine an average step length of clasts within the study reaches. The smallest particles that were used as tracers were 50 mm (i.e. mostly larger than the gravel and sand material that was measured by the BMD in 1999). The travel distances measured are referred to later as 'Tracer Step Lengths'.

From topographic surveys of the stream bed, Poirier was able to determine loci of deposition and erosion, corresponding closely to pool-riffle units within each study reach. The lengths between these points are referred to in the calculations as 'Morphological Step Lengths'. These agree substantially with the Tracer Step Lengths measured by Gottesfeld. The volumes of cut and fill surveyed by Poirier represent the net amount of material moved, i.e. the lowest possible estimate of transport.

² Reach labels refer to the chainage distance measured from the mouth of the creek.

To convert these reach transport estimates to at-a-point transport estimates, the total amount of material transported within the reach is divided by the number of step-lengths. The ‘tracer’ and ‘morphological’ values offer slightly different estimated transport volumes, but they are largely in agreement with the BMD estimates. If anything, the 7.88 m³ moved during the 1999 flood event appears slightly low. This may be attributed to the lower magnitude flood that passed through the study reach in 1999.

	<i>Cut / Fill Vol. (m³)</i>	<i>Reach Length</i>	<i># Pool/Riffle Units (Morph. Step Length)</i>	<i># Tracer Steps (T. Step Length)</i>	<i>Transport Vol Estimates (m³)</i>
O’Ne-ell 1550 Nival Flood ‘96	30.87	68 m	3.5 (19.42 m)	2.5 (26.78 m)	8.82
O’Ne-ell 1550 Nival Flood ‘97	32.07				12.35
O’Ne-ell 925 Nival Flood ‘96	15.82	37 m	2 (18.5 m)	--	9.16
O’Ne-ell 925 Nival Flood ‘97	11.21				12.83
Forfar 1545 Nival Flood ‘96	7.51	47 m	2.5 (23.5 m)	4.8 (9.65 m)	7.91
Forfar 1545 Nival Flood ‘97	11.60				5.61
					3.00
					1.56
					4.64
					2.42

Table 5 – Calculations of net transport rates through three reaches in the Stuart-Takla Watersheds. Cut/Fill Volumes are taken from morphological estimates made by Poirier (2000). Morphological Step Lengths and Tracer Step Lengths provide two estimates of transport distances within the reach. Cut/Fill volumes are accordingly divided by the number of step lengths in the reach, providing two estimates of transport volumes.

Chapter 6 Future Directions and Conclusion

There are two major components to be undertaken for the completion of the BMD project. The first is the proper calibration of this device, likely in a flume with video capabilities. We are presently only able to guess at the effectiveness of this device – further work must be done toward generating accurate volumetric estimates. The second is the device installation, which must be improved in a number of respects. This section will examine some of the opportunities and barriers that face the project at this point.

6.1 Flume Studies

The next stage for calibrating the BMD is to place it on the bed of a laboratory flume, and pass known quantities of material over the sensors and relate this to the volume of passing sediment. Church (2000, personal communication) has suggested that the proper methodology to accomplish this is to cast sediment particles out of concrete with varying amounts of magnetite mixed into them. By controlling the magnetic content of the particles in this way, and measuring velocities by means of a video camera system, all the variables should be accounted for.

Another important calibration experiment will be to place a conventional sampler such as the Helley-Smith device downstream of the BMD during a transport event, and compare the BMD record with the volumes of sediment retrieved from the flow.

6.2 Device Installation

Several improvements for the device have been suggested over the course of our investigative work (1998-2000). Since the velocity of individual particles is far from certain throughout the course of a flood event, a second row of sensors would be extremely helpful in interpreting particle trajectory. This could be placed directly

downstream of the present row, with a 10 cm distance from center to center. Data from the two rows of sensors could be convolved to estimate a mean particle transport velocity. The second row of sensors would double the number of channels in the data acquisition system (and thus the data storage requirements), so some thought must be given as to how to implement this.

It is presumed that if this type of bedload movement detector were to be installed in a stream with clasts of uniform magnetic permeability, then the summed voltage signals could be interpreted as transport mass per unit time.

The device has been described as somewhat of a 'sieve', since particles passing between sensors may register much less of a signal than those passing directly over a sensor (see section 2.1). What is required is a 'discrete' field such that a passing particle would induce the same signal no matter which way it passed over the device.

As a compensatory measure, the second row of sensors could be placed in a staggered position, such that a particle passing between sensors on one row would pass directly over the next sensor downstream. At whichever point that it passes along the device, the sum of the upstream and downstream signals may theoretically be constant.

Further additions to the study apparatus should include some device for measuring the instantaneous shear stress close to the boundary layer, so that the subtle turbulent fluctuations may be recorded in conjunction with flow velocities. A number of strategies involving Pitot tubes or pressure transducers have been suggested, although the implementation of these devices in the active transport zone presents some problems.

6.3 Automation and Signal Processing

We have not yet been able to capture a summer or fall flood, of which there are usually few that will initiate bedload transport. It is hoped that some means of automating

the device will be developed in the future. We have experimented with a “knock detector,” a piezoelectric device that emits a voltage signal when triggered by vibration. This will provide an acceptable cue to start recording, however, we have not been able to arrange a failsafe computer system that will initialize itself and begin recording.

Ultimately, the BMD must be able to process the incoming data ‘on the fly’, and provide a summarized record of a flood event, rather than spooling hundreds of gigabytes of data that need to be processed. If the magnetic character of the stream bed sediments is known, it may be possible to set the data acquisition software to the task of ‘counting’ events and estimating their frequency. As better signal processing and spectral analyses tools evolve, it will become easier to provide a statistical summary that need not be larger than a gigabyte in total, even for several weeks of monitoring. The only remaining logistical problem then is the power supply.

The power supply is certainly the weak link in the installation. In sections, the data is so badly degraded from sources such as a running generator (or possibly a VGA monitor) that the data are unsalvageable. The generator needs to be shielded from the data acquisition’s power supply, perhaps by connecting it to the last battery in the array, rather than the same charge/discharge terminals as it is presently configured. Despite this measure, it may still be quite difficult to isolate the data acquisition system from the voltage irregularities of a solar system. As far as automating power supply, some means of triggering the generator when power runs low must be found.

Conclusions

The UNBC BMD is a novel instrument for measuring the passage of bedload material in a coarse gravel bed creek. With newly patented sensor technology devised at the University of Northern British Columbia, and a high-speed data acquisition system, the instantaneous observation of particle motion along an alluvial channel is now possible. Initial data sets recorded from nival events in 1998 and 1999 show transport dynamics that are consistent with a century of field observations, with a spatial and temporal resolution never achieved before.

In light of existing technologies that have been used for measuring bedload, the BMD presents several advantages. The device provides a continuous record, and samples the full width of the stream. It is able to detect 30 percent of the material in transit, with minimal interference of the sediment passage. It is expected that the sensors are capable of detecting a higher percentage of the material - there is always the potential of filtering the data in order to *reduce* the quantities detected, and thus simplify processing.

The BMD is a semi-permanent installation, requiring considerable effort to install the footings, frame, cables, and wiring. The power requirements are substantial. An array of solar panels and a backup generator are required to run the computers and data logging equipment. The device still requires extensive calibration in order to better relate the signals recorded to the actual quantities of sediment in transport. It is hoped that with a better data acquisition system and faster computer systems, the device will be a viable instrument for sediment transport studies.

The calibration work that has been performed shows that there exists a strong relationship between the size of passing clasts and the period of the signal that they generate. The confounding factor is velocity; as particles move more quickly, the period is proportionally shortened. If an assumption is made about the likely transport velocity

of particles, there are a number of signal processing tools for calculating the frequency of the recorded signals. A rough volumetric estimate may then be made.

The results from the data recorded over the course of two nival flood events offer a wealth of information on bedload transport. Bedload sampling has never been achieved at this resolution, and thus we are uniquely capable of verifying hypotheses regarding the rates and distribution of sediment moving along the bed. The flood records clearly show how the locus of transport varies from one side of the creek to the other, and that the response of transport rates to water discharge can be quite variable. The semi-quantitative data collected on pulsations and bedload streets raise new questions about the transport processes in gravel bed rivers such as O'Ne-ell Creek.

It is anticipated that as the device is refined, gathers more and more data, and becomes applied to different fluvial environments, a more comprehensive picture of sediment transport will emerge.

References

- Andrews, E.D. 1983. 'Entrainment of gravel from naturally sorted riverbed material.' *Geol. Soc. Am. Bull.* **94**. 1225-1231.
- Andrews, E.D. and G. Parker. 1987. 'Formation of a coarse surface layer as the response to gravel mobility.' *In*: C.R. Thorne, J.C. Bathurst and R.D. Hey (Eds). *Sediment Transport in Gravel Bed Rivers*. Wiley, Chichester. 43-79.
- Ashmore, P.E. 1988. 'Channel morphology and bedload pulses in braided, gravel-bed streams', *Geogr. Annlr.* **73A(1)**, 37-52
- Ashmore, P.E. and M.A. Church. 1999. 'Sediment transport and river morphology: a paradigm for study.' *In*: *Gravel Bed Rivers in the Environment*. P. Klingeman, P. Komar, W. Bradley (Eds). John Wiley & Sons, Chichester. 115-148.
- Ashworth, P.J. and R.I. Ferguson. 1989. 'Size-selective entrainment of bed load in gravel bed streams.' *Water Resour. Res.* **25** (4). 627-634.
- Bagnold, R.A. 1966. 'An approach to the sediment transport problem from general physics.' *US Geol. Surv. Pap.* 422-1.
- Banziger, R. and H. Burch, 1990. Acoustic sensors (hydrophones) as indicators for bed load transport in a mountain torrent. *In*: *Hydrology in Mountainous Regions (Proc. Lausanne Symp., August 1990)* 207-214. IAHS Publ. no. 193.
- Beaudry, P. 2000. 'Fine sediments in the Stuart-Takla Watersheds.' *Stuart-Takla Fish-Forestry Interaction Study: 10 Year Report. In press*
- Beschta, R.L. 1987. 'Conceptual models of sediment transport in streams'. *In*: C.R. Thorne, J.C. Bathurst and R.D. Hey (Eds). *Sediment Transport in Gravel Bed Rivers*. Wiley, Chichester. 378-408.
- Billi, P. and P. Tacconi. 1987. 'Bedload transport processes monitored at Virginio Creek Measuring Station, Italy'. *In*: V. Gardiner (Ed). *International Geomorphology*. Wiley, Chichester. 549-559.
- Bridge, J.S. and S.J. Bennett. 1992. 'A model for the entrainment and transport of sediment grains of mixed sizes, shapes and densities.' *Water Resour. Res.* **28** (2). 337-363.

- Bunte, K. 1992. 'Particle number grain-size composition of bedload in a mountain stream.' *In*: Billi, P., Hey, R.D., Thorne, C.R., and Tacconi, P., (Eds), *Dynamics of Gravel Bed Rivers*. John Wiley & Sons, Chichester, 55-68.
- Bunte, K. 1996. 'Analyses of the Temporal Variation of Coarse Bedload Transport and Its Grain Size Distribution', General Technical Report RM-GTR-288, USDA Forest Service, Fort Collins, 123 pp.
- Butler, P.R. 1977. 'Movement of cobbles in a gravel-bed stream during a flood season.' *Geol. Soc. Am. Bull.* **88**. 1072-1074.
- Carling, P.A., 1987. 'Bed stability in gravel streams with reference to stream regulation and ecology.' *In*: K Richards (Ed). *River Channels, Environment and Process*. Blackwell, Oxford, 272-294.
- Carling, P.A., Williams, J.J., Kelsey, A., Glaister, M.S. and Orr, H.G. 1998. 'Coarse bedload transport in a mountain river', *Earth Surf. Proc. Landf.* **23**, 141-157.
- Chacho, E.F., R.L. Burrows and W.W. Emmett. 1988. 'Detection of coarse sediment movement using radio transmitters.' *International Association for Hydraulic Research XXIII Congress August 21-25, 1989, Ottawa, Canada*. 1989. p B367-B373.
- Church, M.A. 1978. 'Palaeohydrological reconstructions from a Holocene valley fill.' *In*: *Fluvial Sedimentology*. A.D. Miall (Ed.) *Mem. Can. Soc. Pet. Geol.* **5**. 743-772.
- Church, M.A., D.G. McLean and J.F. Wolcott. 1987. 'River bed gravels: sampling and analysis.' *In*: C.R. Thorne, J.C. Bathurst and R.D. Hey (Eds). *Sediment Transport in Gravel Bed Rivers*. Wiley, Chichester. 43-79.
- Church, M.A., Wolcott, J.F., and Fletcher, W.K. 1991. 'A test of equal mobility in fluvial sediment transport: behavior of the sand fraction.' *Water Resour. Res.* **27**. 2941-2951.
- Church, M.A. and M.A. Hassan. 1998. 'Stabilizing self-organized structures in gravel-bed stream channels: Field and experimental observations.' *Wat. Resour. Res.* **34**(11). 3169-3179.
- Colby, B.R., 1964. Scour and fill in sand bed rivers. *US Geol. Surv. Pap.* 462-D, 32 pp.
- Crickmore, M.K. 1967. 'Measurement of sand transport in rivers with special reference to tracer methods.' *Sedimentology.* **8**. 175-228.
- Custer, S.G. 1991. A review of natural gravel transport detection experiments at Squaw Creek, Montana, 1981-1991. *Unpublished manuscript*. Dept. of Earth Sciences, Montana State University, Bozeman, MT.

- Custer, S.G., Bunte, K., Spieker, R., and Ergenzinger, P. 1986. 'Timing and location of coarse bedload transport: Squaw Creek, Montana.' *EOS, Trans. Am. Geophys. Union.* **67**(44). 943.
- Custer, S.G., Ergenzinger, P., Bugosh, N., and Anderson, B.C. 1987. 'Electromagnetic detection of pebble transport in streams: a method for measurement of sediment transport waves.' In Ethridge, F. and Flores, R. (Eds.) *Recent Development in Fluvial Sedimentology. Soc. Paleont. Mineralog. Sp. Pub.* 39: 21-26.
- Dingman, S.L. 1984. *Fluvial Hydrology.* W.H. Freeman & Co. N.Y.
- Dietrich, W.E., J.W. Kirchner, H. Ikeda and F. Iseya. 1989. 'Sediment supply and the development of the coarse surface layer in gravel bedded rivers.' *Nature.* **340.** 215-217.
- Dinehart, R.L. 1989. 'Dune migration in a steep, coarse-bedded stream.' *Water Resour. Res.* **25**(5). 911-923.
- Dinehart, R.L. 1992. 'Evolution of coarse bed forms: field measurements at flood stage.' *Water Resour. Res.* **28**(10). 2667-2689.
- Ehrenberger, R. 1931. 'Direkte geschiebemessungen an der Donau bei wein und deren bisherige Ergebnisse [Direct bedload measurement on the Danube at Vienna and their results to data]'. Vienna, Die Wasserwirtschaft, Issue 34, p.1-9. Translation no.39-20, U.S. Waterways Expt. Sta., Vicksburg, Miss.
- Einstein, H.A., 1937. 'Der Geschiebetrieb als Wahrscheinlichkeitsproblem [Bedload transport as a probability problem]'. *Mitt. Versuchsanst. Wasserbau Eidg. Tech. Hochschule., Verlag Rascher, Zurich.* [English Translation in: H.W. Shen (ed), 1972. *Sedimentation. Water Resour. Publ., Fort Collins, C1-C105*].
- Einstein, H.A. 1950. 'The bedload function for sediment transportation in open channel flows'. *U.S. Dept. of Agriculture Tech. Bull.* 1026. 71pp.
- Emmett, W.W. 1976. 'Bedload transport in two large, gravel-bed rivers, Idaho and Washington.' *Proc. 3rd Fed. Int. Sed. Conf.* 4-101 - 4-114.
- Emmett, W.W. 1980. 'A field calibration of the sediment-trapping characteristics of the Helley-Smith bedload sampler.' *U.S. Geol. Surv. Prof. Pap.* 1139. 28pp.
- Ergenzinger, P., and J. Conrady, 1982. 'A new tracer technique for measuring bedload in natural channels.' *Catena.* **9.** 76-93.

- Ergenzinger, P., and S. Custer, 1982. 'First experiences measuring coarse bedload material transport with a magnetic device.' *In: Mechanics of Sediment Transport. Proc. Euromech.* **156.** 223-227.
- Ergenzinger, P and S.G. Custer. 1983. 'Determination of bedload transport using naturally magnetic tracers: first experiences at Squaw Creek, Gallatin County, Montana.' *Water Resour. Res.* **19(1).** 187-193.
- Ergenzinger, P., C. de Jong, and G. Christaller. 1994. 'Interrelationships between bedload transfer and river-bed adjustment in mountain rivers: an example from Squaw Creek, Montana.' *In: Kirby, M.J., (ed). Process Models and Theoretical Geomorphology.* John Wiley & Sons. Chichester. 141-158.
- Fenton, J. and J.E. Abbott. 1977. 'Initial movement of grain on a stream bed: The effect of relative protrusion.' *Proc. R. Soc. London, Ser. A.* **352.** 523-537.
- Ferguson, R.I., and Ashworth, P.J., 1992. 'Spatial patterns of bedload transport and channel change in braided and near-braided rivers.' in Billi, P., Hey, R.D., Thorne, C.R., and Tacconi, P., (Eds), *Dynamics of Gravel Bed Rivers.* John Wiley & Sons. Chichester. 477-495.
- Gintz, D., M.A. Hassan and K-H Schmidt. 1996. 'Frequency and magnitude of bedload transport in a mountain river.' *Earth Surf. Proc. Landf.* **21.** 433-445.
- Goff, J.R. and P.E. Ashmore. 1994. 'Gravel transport and morphological change in braided Sunwapta River, Alberta, Canada.' *Earth Surf. Proc. Landf.* **19.** 195-212.
- Gomez, B. 1983. 'Temporal variations in bedload transport rates: the effect of progressive bed armouring.' *Earth Surf. Proc. Landf.* **8.** 41-54.
- Gomez, B., R.L. Naff, and D. Hubbell. 1989. 'Temporal variations in bedload transport rates associated with the migration of bedforms'. *Earth Surf. Proc. Landf.* **14.** 135-156.
- Gomez, B. 1991. 'Bedload transport'. *Earth-Science Reviews.* **31.** 89-132.
- Gomez, B. and Troutman, B.M., 1997. 'Evaluation of process errors in bed load sampling using a dune model'. *Water Resour. Res.* **33(10).** 2387-2398.
- Gottesfeld, A.S., 1998. 'Bedload transport during sockeye redd excavation and by floods in the Stuart-Takla experimental watersheds, British Columbia'. In Brewin, M.K. and Monita, D.M.A. (tech. coords). *Forest-fish conference: land management practices affecting aquatic ecosystems. Proc. Forest-Fish Conf., May 1-4, 1996, Calgary, Alberta. Nat. Resour. Can. For. Serv., North. For. Cent.* Edmonton, Alberta. Inf. Rep. NOR-X-356. 249-258.

- Govi, M., F. Maraga and F. Moia. 1993. 'Seismic detectors for continuous bed load monitoring in a gravel stream'. *Hydr. Sci. J.* **38** (2), 123-132.
- Grass, 1971. 'Structural features of turbulent flow over smooth and rough boundaries.' *J. Fluid Mech.* **50**. 233-255.
- Griffiths, G.A. 1979. 'Recent sedimentation history of the Waimakariri River, New Zealand'. *J. Hydrol. N.Z.* **18**. 6-28.
- Hamamori, A. 1962. 'A theoretical investigation on the fluctuations of bedload transport.' *Delft Hydraulics Laboratory Rept.*, **R4**.
- Harris, T. and K.S. Richards. 1995. 'Design and calibration of a recording bedload trap.' *Earth Surf. Proc. Landf.* **20**. 711-720.
- Hassan, M.A., 1990. 'Scour, fill and burial depth of coarse material in gravel bed streams'. *Earth Surf. Processes Landf.*, **15**. 341-162.
- Hayward, J.A. and A.J. Sutherland. 1974. 'The Torlesse Stream vortex-tube sediment trap.' *J. Hydrol.* **13** (1). 41-53.
- Helley, E.J. and W. Smith. 1971. 'Development and calibration of a pressure-difference bedload sampler.' *U.S. Geol. Surv. open-file report*, 18 pp.
- Hoey, T. and A.J. Sutherland. 1991. 'Channel morphology and bedload pulses in braided rivers: a laboratory study.' *Earth Surf. Processes Landf.* **16**. 447-462.
- Hoey, T. 1992. 'Temporal variations in bedload transport rates and sediment storage in gravel-bed rivers.' *Prog. in Phys. Geog.* **16** (3). 319-338.
- Hollingshead, A.B. 1971. 'Sediment transport measurements in a gravel river'. *Journal of the Hydraulics Division, ASCE*. Nov 1971, **97** (HY11), 1817-1834.
- Hubbell, D.W. 1964. 'Apparatus and techniques for measuring bedload.' *U.S. Geol. Surv. Water-Supply Pap.* 1748.
- Hubbell, D.W. 1987. 'Bedload sampling and analysis.' *In*: C.R. Thorne, J.C. Bathurst and R.D. Hey (eds). *Sediment Transport in Gravel Bed Rivers*. John Wiley and Sons. Chichester. 90-120.
- Iseya, F. and H. Ikeda, 1987. 'Pulsations in bedload transport rates induced by a longitudinal sediment sorting: a flume study using sand and gravel mixtures.' *Geogr. Annlr.* **69A**. 15-27.
- Jackson, R.G. 1976. 'Sedimentological and fluid-dynamic implications of the turbulent bursting phenomenon in geophysical flows.' *J. Fluid Mech.* **77**. 531-560.

- Jackson, W.L. and R.L. Beschta. 1982. 'A model of two-phase bed load transport in an Oregon Coast Range stream.' *Earth Surf. Proc. Landf.* **7**. 517-527.
- Kang, S. 1982 'Sediment transport in a small glacial stream: Hilda Creek, Alberta'. MSc thesis. 265 pp. Univ. of Ill. at Chicago.
- Klingeman, P.C. 1981. 'Short-term considerations on river gravel supply.' *In: Salmon-Spawning Gravel: A Renewable Resource in the Pacific Northwest?* Water Research Center, Washington State University. Pullman, Washington. 123-139.
- Klingeman, P.C. and R.T. Milhous. 1970. 'Oak Creek vortex bed load sampler.' *17th Annual Pacific North-West Meeting of the Am. Geophys. Union*, University of Puget Sound. Tacoma, Washington. 17 pp.
- Knighton, D. 1998. *Fluvial Forms and Processes: A New Perspective*. John Wiley and Sons Inc. New York. 383 pp.
- Kondolf, G.M. and W.V.G. Matthews. 1986. 'Transport of tracer gravels on a coastal California river.' *J. Hydrol.* **85**. 265-280.
- Kuhnle, R.A. and J.B. Southard. 1988. 'Bedload transport fluctuations in a gravel bed laboratory channel.' *Water Resour. Res.* **24**(2). 247-260.
- Kuhnle, R.A., 1991. 'Bedload transport on two small streams', *Proc. of the 5th Fed. Interagency Sed. Conf.* **1**. 4-139 – 4-146.
- Kuhnle, R.A., 1992. 'Bedload transport during rising and falling stages on two small streams'. *Earth Surf. Proc. Landf.* **17**. 191-197.
- Lane, S.N., K.S. Richards and H. Chandler. 1994. 'Development in the monitoring and terrain modeling small-scale bed topography'. *Earth Surf. Proc. Landf.* **19**. 349-368
- Lane, S.N., K.S. Richards and H. Chandler. 1995. 'Morphological estimation of the time-integrated bed load transport rate.' *Water Resour. Res.* **31**(3). 761-72.
- Laronne, J.B. and M.A. Carson. 1976. 'Interrelationship between bed morphology and bed material transport in a small, gravel-bed channel'. *Sedimentology.* **23**. 67-85.
- Laronne, J.B., D.N. Outhet, P.A. Carling and T.J. McCabe (1994). Technical note - scour chain deployment in gravel bed rivers. *Catena.* **22**(4). 299-306.
- Leopold, L.B. 1994. *A View of the River*. Harvard University Press. Cambridge, Massachusetts.

- Leopold, L.B., W.W. Emmett, and R.M. Myrick, 1966. *Fluvial Processes in Geomorphology*. Freeman. San Francisco, CA.
- Leopold, L.B. and W.W. Emmett. 1976. 'Bedload measurements, East Fork River, Wyoming.' *Proc. Nat. Acad. Sci.* **73**. 1000-1004.
- Macdonald, J.S., Scrivener, J.C., and Smith, G. 1992. 'The Stuart-Takla Fisheries/Forestry Interaction project: study description and design'. *Can. Tech. Rep. Fish. Aquat. Sci.* No. 1899.
- Montgomery, D.R., J.M. Buffington, R.D. Smith, K.M. Schmidt and G. Pess. 1995. 'Pool spacing in forest channels.' *Water Resour. Res.* **31**(4). 1097-1105.
- Mühlhofer, L. 1933. 'Untersuchungen über der Schwebstoff und Geschiebeführung des Inn nächst Kirchbichl, Tirol' [Investigations into suspended load and bedload of the River Inn, near Kirchbichl, Tirol]. *Wasserwirtschaft*, Heft 1-6.
- Nesper, F. 1937. 'Ergebnisse der Messungen über die Geschiebe- und Schlammführung des Rheins an der Brugger Rheinbrücke [Results of bedload and silt movement observations on the Rhine at the Brugg Bridge]. *Schweiz. Bauz.*, Heft 100.
- Nicholas, A.P., P.J. Ashworth, M.J. Kirkby, M.G. Macklin and T. Murray. 1995. 'Sediment slugs: large-scale fluctuations in fluvial sediment transport rates and storage volumes.' *Prog. Phys. Geog.* **10** (4). 500-519.
- Parker, G. and P.C. Klingeman. 1982. 'On why gravel bed streams are paved.' *Water Resour. Res.* **18**. 1409-1423.
- Nino, Y. and M.H. Garcia. 1996. 'Experiments on particle-turbulence interactions in the near-wall region of an open channel flow: implications for sediment transport.' *J. Fluid Mech.* **326**. 285-319.
- Parker, G., P.C. Klingeman and D.L. McLean. 1982. 'Bedload and size distribution in paved gravel bed streams.' *J. Hydraul. Eng.* **108**. 544-571.
- Poirier, Ronald W. 2000. The effects of sockeye spawning on streambed morphology. M.Sc. thesis. University of Northern British Columbia. Prince George, B.C., Canada (*in preparation*).
- Powell, D.M. and Ashworth, P.J. 1995. 'Spatial pattern of flow competence and bedload transport in a divided gravel bed river.' *Water Resour. Res.* **31**(3). 741-752.
- Qian, S. and D. Chen. 1996. *Joint Time-Frequency Analysis*. Prentice Hall, New York.
- Rathbun, R.E. and C.F. Nordin. 1971. 'Tracer studies of sediment transport processes.' *Proc. ASCE, J. Hydraul. Div.* **97 HY9**. 1305-16.

- Reid, I., J.T. Layman, and L.E. Frostick. 1980. 'The continuous measurement of bedload discharge.' *J. Hydraul. Res.* **18**(3). 243-249.
- Reid, I., A.C. Brayshaw and L.E. Frostick. 1984. 'An electromagnetic device for automatic detection of bedload motion and its field applications.' *Sedimentology*. **31**. 269-276.
- Reid, I., L.E. Frostick, and J.T. Layman. 1985. 'The incidence and nature of bedload transport during flood flows in coarse grained alluvial channels.' *Earth Surf. Proc. and Landf.* **10**. 33-44.
- Reid, I. and Frostick, L.E., 1994. 'Fundamental properties of fluids and their relation to sediment transport processes.' *In: Pye, K. (Ed.), Sediment Transport and Depositional Processes.* Blackwell Scientific Publications. Boston. 25-60.
- Rice, S.P. 1994. 'Towards a model of changes in bed material texture at the drainage basin scale.' *In: Kirkby, M.J. (Ed.). Process Models and Theoretical Geomorphology.* John Wiley and Sons. Chichester. 159-172.
- Rouse, H.L., 1994. 'Measurement of bedload gravel transport: the calibration of a self-generated noise system.' *Earth Surf. Proc. Landf.* **19**. 789-800.
- Ryder, J.M. 1995. 'Stuart-Takla watersheds: terrain and sediment sources.' *Res. Br., BC Min. For.* Victoria, BC. Work. Pap. 03/1995.
- Sayre, W.W. and D.W. Hubbell, 1965. 'Transport and dispersion of labeled bed material, North Loup River, Nebraska.' *U.S. Geol. Surv. Prof. Pap.* 433-C.
- Schmidt, K-H. and P. Ergenzinger. 1992. 'Bedload entrainment, travel lengths, step lengths, rest periods-studied with passive (iron, magnetic) and active (radio) tracer techniques.' *Earth Surf. Proc. Landf.* **17**. 147-165.
- Schoklitsch, A., 1934. Der geschiebetrieb und die geschiebefracht [Bedload and bedload movement]. *Wasserwirtschaft*, Heft 4.
- Seminara, G., M. Columbini and G. Parker. 1996. 'Nearly pure sorting waves and formation of bedload sheets.' *J. Fluid Mech.* **312**. 253-278.
- Shields, A. 1936. Anwendung der Aehnlichkeitsmechanik der Turbulenzforschung auf die Geschiebebewegung, *Mitt. Preuss. Versuchsanst. Wasserbau Schiffbau.* **36**. 5-24. (English translation by W.P. Ott and J.C. van Uchelen, 43 pp., U.S. Dept. of Agric. Soil Conser. Serv. Coop. Lab., Calif. Inst. of Technol., Pasadena, 1950).

- Sobocinsky, R.W., T.E. Cerling, S.J. Morrison and I.L. Larsen. 1990. 'Sediment transport in a small stream based on ^{137}Cs inventories of the bed load fraction.' *Water Resour. Res.* **26**(6). 1177-1187.
- Spieker, R. and Ergenzinger, P. 1987. 'New developments in measuring bedload by the magnetic tracer technique.' *In: Erosion, Transport and Deposition Processes. Proceedings of the Jerusalem Workshop, March-April 1987.* IAHS Publ. No. 189. 169-178.
- Sutherland, A.J. 1987. 'Static armour layers by selective erosion.' *In: C.R. Thorne, J.C. Bathurst and R.D. Hey (Eds). Sediment Transport in Gravel Bed Rivers.* John Wiley and Sons. Chichester. 243-260.
- Southard, J.B., N.D. Smith and R.A. Kuhnle. 1984. 'Chutes and lobes: newly identified elements of braiding in shallow gravelly streams.' *In: Koster, E.H. and Steel, R.J. (Eds). Sedimentology of Gravels and Conglomerates. Can. Soc. Petr. Geol. Mem.* **10**. 51-59.
- Tacconi, P. and P. Billi. 1987. 'Bedload transport measurement by the vortex trap on Virginio Creek, Italy.' *In: C.R. Thorne, J.C. Bathurst and R.D. Hey (Eds). Sediment Transport in Gravel Bed Rivers.* John Wiley and Sons. Chichester. 583-616.
- Thoms, M.C. 1992. 'A comparison of grab- and freeze-sampling techniques in the collection of gravel-bed river sediment.' *Sediment. Geol.* **78**. 191-200.
- Thorne, P.D., J.J. Williams, A.D. Heathershaw. 1989. 'In situ acoustic measurements of marine gravel threshold and transport.' *Sedimentology.* **36**. 61-74.
- Whiting, P.J., W.E. Dietrich, L.B. Leopold, T.G. Drake and R.L. Shreve. 1988. 'Bedload sheets in heterogeneous sediment.' *Geology.* **16**. 105-108.
- Wilcock, P.R. and J.B. Southard. 1989. 'Experimental study of incipient motion in mixed-size sediment.' *Water Resour. Res.* **24**. 1137-1151.
- Willetts, B.B., J.K. Maizels and J. Florence. 1987. 'The simulation of stream bed armouring and its consequences.' *Proc. Inst. Civ. Eng., Part 1,82.* 799-814.
- Williams, J.J., P.D. Thorne, A.D. Heathershaw. 1989. 'Comparisons between acoustic measurements and predictions of the bedload transport of marine gravels.' *Sedimentology.* **36**. 973-979.
- Yilmaz, Ozdogan. 1987. Seismic Data Processing. S. Doherty (Ed). *Society of Exploration Geophysicists.* Tulsa.

Appendix A – Glossary

a-, b- and c- axes: 3 measurements describing the dimensions of a clast. The a-axis of a clast is the longest axis of the grain, and the longest axis orthogonal to that is the b-axis. The two dimensional area described by the a-b plane of a clast is its maximum projection. The c-axis is normal to the a-b plane.

Aggradation: The process of building up a surface by deposition.

Allochthonous: Derived from outside a system, for instance, colluvial material from a cliff face contributing to the bedload of a stream.

Anabranching River: Multiple channels separated by stable islands which are large relative to the size of the channels, and which divide the flow at discharges up to and including bankfull. Consequently the flow patterns in adjacent channel segments are essentially independent of one another, unlike those in **braided channels** (Knighton, 1998).

Armour layer: Erosion-resistant layer of relatively large particles on the surface of a streambed. Such layers typically result from removal of finer particles by erosion.

Autochthonous: Derived from within a system, for instance, sediment transported from one gravel bar to the next.

Bankfull: Most commonly defined as the point at which discharge in the creek has filled the channel to capacity, occurring on the average once every 1.5 years.

Bioturbation: Disturbance of a natural system by an organism; in this case, the disruption of the streambed gravels by spawning salmon.

BMD: The Bedload Movement Detector, developed at UNBC. The device consists of an array of magnetic sensors housed in an aluminum beam. The beam is set into the stream bed such that its upper surface is flush with the gravel bed, and signals from the sensors are recorded during a bedload transport event. An estimate of bedload transport may then be obtained.

Braided Stream: Stream that forms an interlacing network of branching and recombining channels separated by bars and contained within a dominant pair of floodplain banks.

Competence: A threshold of stream discharge at which particles may be entrained and carried with the flow.

DFO: The Department of Fisheries and Oceans, recently renamed Fisheries and Oceans Canada (FOC).

Equal Mobility: A hypothesis stating that coarse sediment particles will resist entrainment due to their being hidden or **imbricated**. Once flows reach a critical threshold, however, the resistance of the larger, structural stones is overcome, and all size ranges of material become available for transport at roughly the same time.

Fast Fourier Transform (FFT): A fast method for calculating the Discrete Fourier Transform. It is used when the number of samples in a time series is a power of 2.

Fluvial Entrainment: Suspension and transport of solid materials by stream flow.

Fourier Transform: Usually referred to as the Discrete Fourier Transform or DFT. A mathematical process whereby a time series, or signal, is uniquely and completely described as a sum of a number of sinusoids, each with a unique peak amplitude, frequency, and a phase lag (relative alignment). The resultant series provides a representation of frequencies present within the original signal.

Freeze Core Sampling: A method of sampling streambed gravels. The device used in the present study consisted of a 1m long, 5 cm diameter, hollow aluminum standpipe with a bowl-like flared open end. The pipe has a pointed tip that is driven into the streambed some 30 cm. Acetone is then poured into the large flared end, filling the standpipe, and dry ice is placed in the bowl. As the acetone cools, the interstitial water and sediment next to the pipe are quickly frozen (10-20 min) and then removed as a core.

Hilbert Transform: The Hilbert Transform (\mathcal{H}) returns a complex helical sequence, sometimes called the *analytic signal*, from a real data sequence. The analytic signal has a real part, which is the original data, and an imaginary part, which contains the Hilbert Transform. The imaginary part is a version of the original real sequence with a 90° phase shift. Sines are therefore transformed to cosines, and vice versa. The Hilbert transformed series has the same amplitude and frequency content as the original real data and includes phase information that depends on the phase of the original data (Mitra, 1990).

Hydraulic Efficiency: The ratio of the mean velocity of water discharge through the sampler to the mean velocity of the water discharge which would have occurred through the area occupied by the opening in the sampler nozzle had the sampler not been there (Hubbell, 1964).

Imbrication: The interlocking, or “shingling” of particles, as they are naturally deposited in similar orientations. Freshly deposited material becomes more tightly packed as marginal flows shake and settle them into place.

JTFA: Joint Time-Frequency Analysis. A method of analysis that simultaneously provides both time and frequency information. It shows how the frequency spectrum of a signal varies with time.

Large Woody Debris (LWD): Any large piece of woody material that intrudes into a stream channel, whose smallest diameter is greater than 10 cm, and whose length is greater than 2m. LWD is important for providing fish habitat and in influencing channel morphology.

Locus of Transport: The portion of a stream cross-section that exhibits the highest rates of bedload transport.

Low Pass Filter: A filter that passes frequencies below a certain cutoff frequency. It passes low frequencies but attenuates high frequencies.

MOF: The British Columbia Ministry of Forests.

Nival Flood: The spring flood event, generated by snow-melt, in mountain catchments.

Nyquist Frequency: Half of the sampling frequency. The Nyquist theorem states that to recover an analog signal from its samples, the sampling frequency should be at least twice the highest frequency in the signal. Therefore, in order to capture signals up to 50Hz, the BMD sampled the voltage data at a rate of 100 Hz.

Phi (ϕ) Scale: A logarithmic scale used to describe the size of sediment grains. The relation between grain size (D) and phi (ϕ) units is as follows:

$$\phi = -\log_2 D(\text{mm}) = -3.3219 \log_{10} D(\text{mm})$$

Pool-Riffle Morphology: Pool-riffle channels have an undulating bed that defines a sequence of bars, pools and riffles. Pools are topographic depressions within the channel, spaced every five to seven channel widths. Riffles are shallow sections of the stream with rapid currents and a surface broken by gravel, rubble, or boulders.

Psi (ψ) Scale: The inverse (negative) representation of the logarithmic **Phi (ϕ) Scale**.

Redd: Nest made in gravel, consisting of a depression hydraulically dug by a fish for egg deposition (and then filled) and associated gravel mounds.

Shear Stress: The product of the unit weight of water (1000 kg/m^3), depth (m) and slope (m/m), and is a parameter useful in predicting the maximum size of bedload particles that may be entrained.

Short Time Fourier Transform (STFT): The term for taking a Fourier transform of shorter time intervals of samples of a signal, rather than on the entire set of samples. Also known as the windowed Fourier transform.

Stage Level: The depth of stream flow at a monitoring station. The stage level is usually calibrated to previous measurements of discharge.

Stream Efficiency: Expressed as the unit bedload transport rate divided by unit **stream power**.

Stream Order: A number from 1 to 6 or higher, ranked from headwaters to river terminus, that designates the relative position of a stream or stream segment in a drainage basin. First-order streams have no discrete tributaries; the junction of two first-order streams produces a second-order stream; the junction of two second-order streams produces a third-order stream; etc.

Stream Power: The product of the unit weight of water (1000 kg/m^3), velocity (m/s), flow depth (m) and slope (m/m). This is a useful parameter in presenting the transport rate of bedload sediment.

Stream Reach: A relatively homogeneous section of a stream having a sequence of repeating structural characteristics (or processes) and fish habitat types.

Thalweg: A line connecting the deepest parts of a stream channel.

Third Order Tributary: (see **Stream Order**)

Appendix B – Gravel sampling data

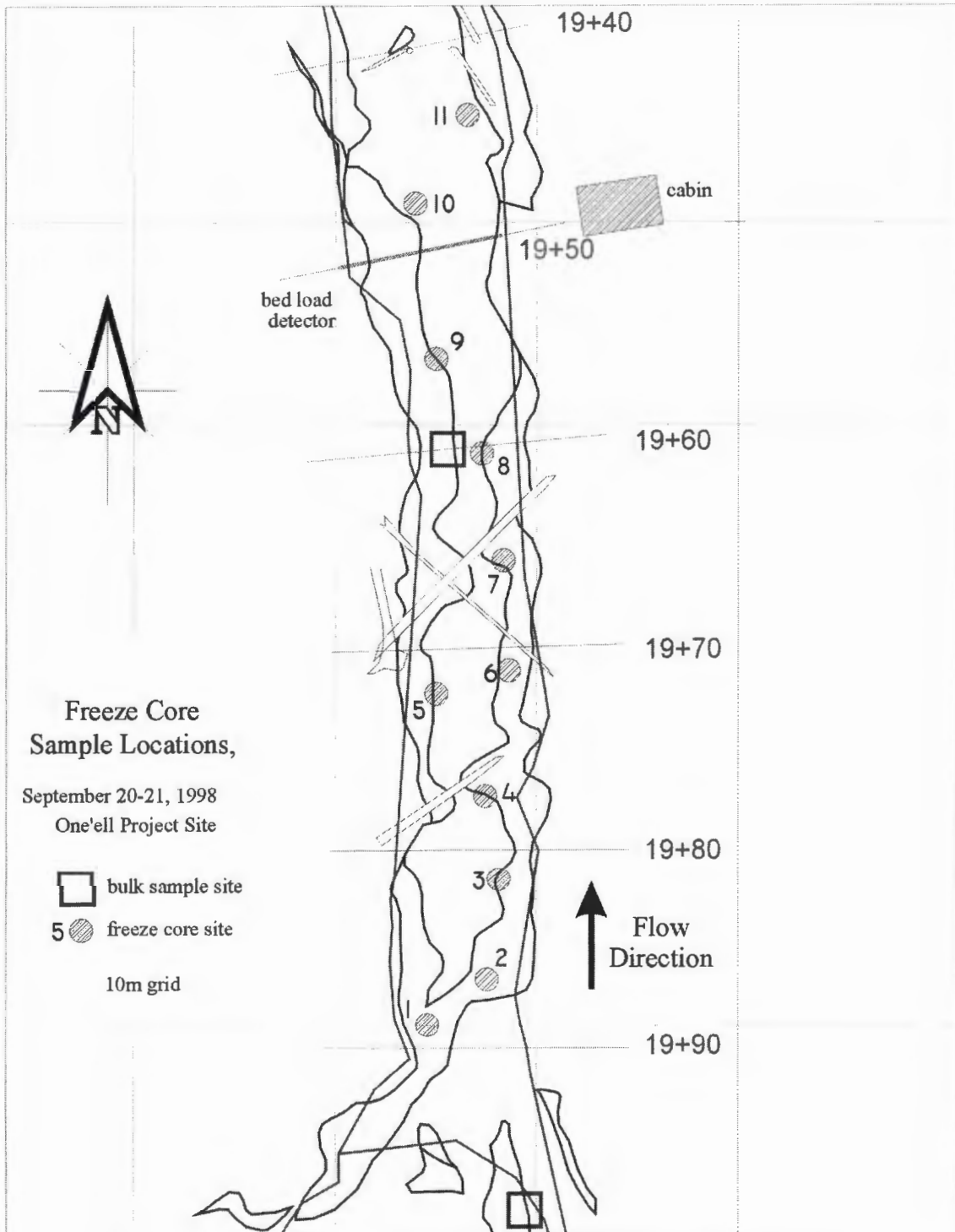


Figure 50 - Locations of gravel sampling sites at the BMD study site.

Table 6 - Freeze Core sample data

Date	Total Sample Weight (g)	Total Sample Weight (g)	Split (y/n)	Total												Sum of Sieve fractions
				0.0 - 0.075mm (g)	.075 - 0.3mm (g)	0.3 - 1.18mm (g)	1.18 - 2.36mm (g)	2.36 - 5.6mm (g)	5.6 - 9.5mm (g)	9.5 - 12.5mm (g)	12.5 - 25mm (g)	25 - 50 mm (g)	> 50mm (g)			
98/09/20	-8325.4	7324.3	n	6.3	61.3	57.4	130.4	254.8	224.7	142.5	909.5	1054.4	4485.5	7326.8		
98/09/20	-7426.8	6449.5	n	8.5	72.8	240.1	379.1	595.4	469.9	297.1	773.2	412.0	3199.1	6447.2		
98/09/20	-5040.1	4542.1	n	3.0	41.9	60.2	91.7	190.8	186.5	95.2	446.7	712.5	2714.0	4542.5		
98/09/20	-9289.3	8274.9	n	8.2	62.2	643.2	644.8	543.3	502.5	351.8	1734.6	1313.9	2469.9	8274.4		
98/09/20	-14699.2	13204.7	n	13.8	56.9	348.4	541.4	582.4	429.4	278.0	1401.6	1116.7	8431.0	13199.6		
98/09/20	-8600.6	7618.5	n	8.0	59.0	278.1	416.1	563.8	452.6	278.3	1266.9	918.0	3377.8	7618.6		
98/09/20	-7077.0	6113.1	n	6.9	28.9	156.6	221.3	246.7	287.3	272.2	1910.2	1309.4	1673.4	6112.9		
98/09/20	-5226.2	4709.0	n	3.7	17.0	22.1	28.8	27.1	41.9	45.0	1034.7	663.5	2825.3	4709.1		
98/09/20	-8148.3	7162.0	n	6.5	45.8	147.6	142.3	128.0	160.0	131.4	518.8	1153.9	4728.1	7162.4		
98/09/20	-3616.8	3119.6	n	11.3	133.3	283.7	272.5	332.2	305.5	182.2	915.7	683.0	0.0	3119.4		
98/09/20	-9241.0	8235.7	n	12.7	90.2	694.2	627.1	546.9	565.4	377.8	1854.6	1400.9	2064.4	8234.2		
98/09/20	-13245.4	11784.0	n	28.2	207.5	918.4	910.2	1275.7	910.2	533.3	2308.0	2081.2	2609.6	11782.3		
98/09/21	-8534.7	7568.3	n	9.7	65.6	390.5	579.3	636.3	487.0	286.9	1230.4	935.0	2946.5	7567.2		
98/09/21	-12663.1	11177.8	n	31.3	214.0	969.0	627.0	900.6	828.3	484.5	2245.8	1552.2	3324.7	11177.4		
98/09/20	-13018.3	11534.8	n	37.7	215.3	1349.1	978.0	1364.2	1058.4	654.0	2236.9	854.4	2783.2	11531.2		
98/09/20	-7781.9	6776.7	n	7.9	64.2	310.3	324.2	447.8	381.5	220.7	906.1	958.4	3155.3	6776.4		
98/09/20	-10234.2	8750.3	n	43.3	276.5	997.5	788.0	1090.0	842.3	501.5	2175.4	1382.2	651.8	8748.5		
98/09/20	-10960.6	9464.0	n	10.5	83.0	662.3	638.6	674.3	526.9	377.8	1854.9	1751.7	2883.2	9463.2		
98/09/20	-3477.1	2990.0	n	0.7	1.4	5.4	12.2	32.4	46.7	62.9	640.1	692.7	1498.3	2992.8		
98/09/20	-15371.6	13868.1	n	20.4	144.1	881.3	855.2	1133.3	961.6	599.5	2476.2	1397.2	5393.0	13861.8		
98/09/20	-11962.7	10961.6	n	8.6	59.6	274.5	358.1	357.5	355.6	236.4	1324.8	348.2	7637.4	10960.7		
98/09/20	-10502.7	9525.4	n	20.7	183.7	543.0	553.1	583.1	553.4	399.8	1895.6	810.6	3979.0	9522.0		

Table 7 - Bulk Sample (15 cm deep) Sieve Data - cont on next page

Sample #1 taken from gravel bar near bank failure, 70m upstream
Sample #2 taken from gravel bar 50m downstream from kitchen
Sample #3 taken from Wside bar, 10m upstream of the detector

Coarse	Split four ways, so multiplied by 4									
	64.0 Passed #1	45.0 Passed #2	32.0 Passed #3	22.6 Passed #4	16.0 Passed #5	11.3 Passed #6	8.0 Passed #7	2.0 Passed #8	0.833 Passed #9	0.5 Passed #10
5438.8	5086.8	4439.2	5866.5	5990.0	7404.8	31224.0	9591.2	3655.2	3005.6	
3520.3	4580.8	4481.7	6346.0	4837.7	6853.9					
5032.0	5050.1	4437.0	6380.0	2459.0						
6251.5	3986.2	4708.4								
6631.2	4134.3	4852.8								
7784.2	4358.9	3528.9								
6744.1										
4670.2										
102176.7	46072.3	27197.1	18592.5	13286.7	14258.7	31224.0	9591.2	3655.2	3005.6	
TOTAL:										
										295508.0

7034.2	7644.6	7580.4	6563.2	6435.8	6468.9	40626.0	17964.0	5337.2	6398.4
9428.5	7728.8	7875.6	7495.0	5378.3	6132.3				
9762.5	8324.1	8017.5	6035.9	3891.2	3659.0				
4850.6	4542.4	5468.5							

34126.0 31075.8 28239.9 28942.0 20094.1 15705.3 16260.2 40626.0 17964.0 5337.2 6398.4 244768.9

Coarse Passed #1 Passed #2 Passed #3 Passed#4 Passed#5 Passed#6 Passed #7 Passed#8 Passed#9 Passed #10
10518.6 8680.0 9277.6 8006.0 7456.0 5705.0 31326.0 14497.2 5164.4 3473.2
11667.0 9493.2 6851.7 5802.0 4433.1 6121.3
9820.0 8675.0 3333.8 1932.7
10149.7

81219.0 42155.3 26848.2 19463.1 13808.0 11889.1 13759.0 31326.0 14497.2 5164.4 3473.2 263602.5

Table 8 - Bulk sample (30 cm deep) Sieve Data

Sieve Work - August 4-6, 1998
All weights measured in grams (g)

Sieve Size	0.833 mm	1.18 mm	2.36 mm	2.70 mm	5.60 mm	5.80 mm	8.65 mm	9.5 mm	12.3 mm	24.08 mm	50 mm
Weight (g)	10736.8	5315.4	5768.0	3892.0	3039.6	7720.8	820.8	6851.0	1954.6	8307.6	136087.2
Weight (g)	6914.7	5680.1		4929.5		8461.6	1354.3	5218.5	4925.2	8860.2	
Weight (g)	5395.8	251.5		5288.3					6300.7	8004.8	
Weight (g)				4254.6					6566.0	9346.8	
Weight (g)				3591.3					4913.6	8172.5	
Weight (g)									6600.0	10116.2	
Weight (g)									5231.3	9784.8	
Weight (g)									3605.4	9090.6	
Weight (g)									6995.5	6967.8	
Weight (g)	23047.3	11247.0	5768.0	21955.7	3039.6	16182.4	2175.1	12069.5	40096.8	85646.8	136087.2

	<u>Weight of Fraction (g)</u>	<u>Percentage By Weight</u>
1.18 mm	23047.3	6.45
2.36 mm	11247.0	3.15
2.70 mm	5768.0	1.61
5.60 mm	21955.7	6.14
5.80 mm	3039.6	0.85
8.65 mm	16182.4	4.53
9.50 mm	2175.1	0.61
12.3 mm	12069.5	3.38
24.08 mm	40096.8	11.22
50 mm	85646.8	23.97
Total Sample	136087.2	38.09
Total Sample	357315.4	

Table 9.- Sample of Magnetic Sampling Data (All clasts < 50mm)

Rock #	phi	Equiv. Sieve Size (mm)	Caliper Measure (mm)			Sphericity	Roundness (mm)	Magnetic Intensity			Intensity Value	Weight (g)	Note: C.C. = cache creek metamorphics Lithology
			A	B	C			Min	Max	Avg			
1	-5.95	61.66	111.6	77.9	39.2	0.56	12	-0.533	-0.029	-0.141	0.392	452.1	Greeny UM
2	-5.94	61.48	86	74.4	45	0.68	5	-0.492	-0.473	-0.483	0.009	346.4	Andesite
3	-6.58	95.97	154.4	119.2	64.9	0.61	13	-0.521	-0.494	-0.509	0.012	1703.3	Meta-shale
4	-6.15	71.18	108.4	78.1	63.5	0.78	23	-0.595	-0.419	-0.474	0.121	714.1	Grano-diorite
5	-6.18	72.44	128.9	88.5	51.6	0.62	15	-0.343	-0.032	-0.076	0.267	1022.7	Quartzose
6	-6.90	119.67	157.2	141.2	93.3	0.73	14	-0.612	-0.560	-0.593	0.019	2232.7	Greywacke
7	-6.69	103.51	155.3	116	89.3	0.76	18	-0.193	-0.073	-0.129	0.064	1742.3	C.C. Quartzite
8	-6.48	89.12	134.1	106.5	67.4	0.69	14	-0.225	-0.080	-0.152	0.073	1510.2	Rhyolite w/Quartz bands
9	-6.30	78.70	122.2	96.7	55.1	0.64	9	-0.456	-0.388	-0.424	0.032	840.7	Grano-diorite
10	-6.40	84.74	95	87.4	82	0.93	24	-0.454	-0.419	-0.437	0.017	710.6	Grano-diorite
11	-6.48	89.26	153	99.8	77.3	0.73	27	-0.448	-0.425	-0.440	0.008	1796.0	Meta-greywacke
12	-5.93	60.95	117.1	64.4	57.3	0.76	17	-0.544	-0.442	-0.498	0.046	693.6	Andesite
13	-6.55	93.88	118.7	104.5	81.9	0.82	18	-0.010	0.056	0.024	0.034	1036.6	Rhyolite
14	-6.54	92.90	133	109.9	72	0.71	23	-0.526	-0.513	-0.521	0.005	1559.4	Grano-diorite
15	-5.87	58.42	78.2	68.5	46.2	0.74	27	-0.445	-0.424	-0.437	0.008	332.8	Grano-diorite
16	-6.11	68.96	113.2	78.7	57.6	0.72	8	-0.524	-0.510	-0.517	0.007	595.2	C.C. Quartzose
17	-5.82	56.59	88.3	67.5	43	0.68	12	-0.497	-0.489	-0.494	0.003	257.4	Mudstone
18	-6.19	72.93	106.5	81.2	63.6	0.78	7	-0.484	-0.471	-0.479	0.005	542.6	Volcanic
19	-6.19	73.15	145.4	95.4	40	0.49	7	-0.433	-0.404	-0.422	0.011	909.0	Greywacke
20	-6.14	70.39	91.1	77.4	62.6	0.82	6	-0.514	-0.503	-0.510	0.004	505.5	Meta-green?
21	-5.87	58.65	134	68	47.5	0.63	13	-0.619	-0.146	-0.441	0.178	678.0	Greeny UM
22	-6.71	105.01	155.2	125.3	79.7	0.69	25	-0.484	-0.463	-0.471	0.013	2367.2	Grano-diorite
23	-6.11	68.88	117.21	81.2	53.8	0.68	18	-0.673	-0.664	-0.669	0.004	641.7	Meta-shale
24	-6.34	81.06	101.3	96.3	62.2	0.74	7	-0.548	-0.535	-0.543	0.005	707.7	C.C. Green
25	-5.79	55.40	85.1	65.1	43.6	0.70	10	-0.499	-0.463	-0.478	0.021	301.4	Rhyolite
26	-6.11	68.94	96.2	78	58.5	0.77	12	-0.485	-0.475	-0.480	0.005	580.5	Diorite

Rock #	phi	Equiv. Sieve Size (mm)	Caliper Measure (mm)			Sphericity	Roundness	Magnetic Intensity			Intensity Value	Weight (g)	Note: C.C. = cache creek metamorphics Lithology
			A	B	C			Min	Max	Avg			
27	-5.80	55.83	83.5	68.7	38.9	0.64	8	-0.428	-0.412	-0.418	0.010	299.7	Grano-diorite
28	-6.83	113.98	189.2	116.6	111.3	0.83	13	-1.243	-0.067	-0.661	0.582	2909.2	Greeny UM (Meta?)
29	-5.84	57.47	108.8	70.3	40.8	0.60	11	-0.555	-0.519	-0.535	0.020	474.0	Grano-diorite
30	-5.99	63.57	100.3	75.18	49.3	0.69	8	-0.501	-0.485	-0.492	0.009	506.8	Grano-diorite
31	-6.35	81.38	97.8	93.5	67.1	0.79	4	-0.519	-0.508	-0.514	0.005	711.0	C.C. Quartzose
32	-6.00	64.11	90.1	72.9	53.9	0.76	15	-0.562	-0.510	-0.541	0.021	575.7	Meta-greywacke
33	-5.75	53.98	85.8	67	36.6	0.62	14	-1.016	-0.103	-0.538	0.478	274.5	Andesite
34	-6.14	70.61	95.4	83.8	54.3	0.72	11	-0.713	-0.686	-0.703	0.010	501.7	C.C. Quartzose
35	-5.69	51.73	62.3	64.4	34.7	0.67	13	-0.703	-0.624	-0.660	0.043	191.7	Greenstone
36	-5.73	53.14	68.2	55.2	51	0.89	8	-2.584	-0.127	-0.696	1.888	311.2	Porph Andesite
37	-5.80	55.67	85.8	69.7	36.6	0.61	7	-0.683	-0.647	-0.666	0.017	352.7	Andesite
38	-5.96	62.34	90.9	78.72	39.7	0.61	13	-0.721	-0.709	-0.716	0.005	323.2	Grano-diorite
39	-5.95	61.77	86.16	67.7	55.2	0.81	5	-0.920	-0.555	-0.710	0.210	325.7	Dacite
40	-5.71	52.34	78.7	65	35.4	0.63	14	-3.046	0.062	-0.881	2.165	259.1	Porph Andesite
41	-6.71	104.64	152.5	113.8	94.6	0.80	32	-0.488	-0.474	-0.481	0.007	2362.8	Grano-diorite
42	-6.34	81.04	109	96.9	61.2	0.71	10	-0.092	-0.060	-0.075	0.017	714.9	Grano-diorite
43	-5.66	50.45	77.8	55.2	45.2	0.78	9	-2.160	-0.042	-0.643	1.517	300.5	Andesite
44	-6.27	77.07	123.1	94.5	54.3	0.64	12	-0.699	-0.671	-0.688	0.011	865.5	Grano-diorite
45	-5.77	54.49	85.8	68.5	35.3	0.60	5	-0.035	0.053	0.009	0.044	299.7	C.C. Quartz
46	-6.16	71.74	108.7	84.8	55.7	0.70	6	-0.538	-0.137	-0.415	0.123	526.8	C.C. Green
47	-5.67	50.91	82.1	57.6	43.2	0.74	9	-0.466	-0.445	-0.455	0.011	252.1	C.C. Green
48	-6.39	84.06	151.4	102.8	59.7	0.61	22	-0.471	-0.449	-0.460	0.011	1364.8	Grano-diorite
49	-5.87	58.54	83.6	72.4	40.15	0.65	6	-0.458	-0.441	-0.451	0.007	261.3	Grano-diorite
50	-6.67	101.51	141.3	115.9	84.7	0.76	7	-0.482	-0.465	-0.472	0.010	1633.5	Meta-Quartz ?
51	-5.86	58.23	103.1	73	38.1	0.58	13	-0.422	-0.402	-0.412	0.010	374.6	C.C. Green
52	-6.43	86.14	106.2	97.9	72.5	0.80	11	-0.525	-0.492	-0.510	0.015	767.1	Grano-diorite
53	-5.93	60.79	119.2	69.2	51	0.68	13	-0.482	-0.458	-0.472	0.010	569.7	Dacite
54	-6.60	97.05	130	112.1	79.2	0.76	22	-0.398	-0.381	-0.387	0.011	1660.0	Grano-diorite
55	-5.87	58.37	87.7	70.7	42.6	0.67	10	-2.970	0.125	-0.659	2.311	330.3	Meta-Quartz ?
56	-6.78	110.20	145	117.3	102.6	0.85	16	-0.527	-0.498	-0.508	0.019	1620.8	Grano-diorite

Rock #	phi	Equiv. Sieve Size (mm)	Caliper Measure (mm)			Sphericity	Roundness	Magnetic Intensity			Intensity Value	Weight (g)	Note: C.C. = cache creek metamorphics Lithology
			A	B	C			Min	Max	Avg			
57	-5.87	58.48	98.2	61.5	55.3	0.80	12	-0.502	-0.472	-0.484	0.018	454.9	Meta-Sandstone
58	-5.93	61.09	82.4	78.9	35.2	0.58	4	-0.492	-0.464	-0.476	0.016	296.4	Mudstone
59	-5.61	48.91	87.7	59.9	34.6	0.61	6	-0.706	-0.668	-0.679	0.027	234.9	C.C. Green
60	-5.97	62.73	87.1	72.8	50.7	0.74	8	-0.758	-0.530	-0.668	0.090	423.0	C.C. Green
61	-5.92	60.51	88.4	69.3	50.2	0.75	21	-1.025	-1.005	-1.011	0.014	413.3	Meta-Sed-Quartzose
62	-5.96	62.44	88.4	70.7	52.9	0.77	8	-0.678	-0.661	-0.671	0.007	392.1	Green/Mafic
63	-6.37	82.58	116.1	100.5	59.5	0.67	18	-0.803	-0.513	-0.652	0.151	931.5	Porph Andesite
64	-6.21	74.16	109.2	83.4	63.6	0.77	22	-0.725	-0.634	-0.686	0.039	755.2	Porph Dacite
65	-6.14	70.58	106.5	84.2	53.6	0.69	9	-0.753	-0.551	-0.696	0.057	586.2	C.C. Green
66	-6.24	75.82	97.3	89.8	58.6	0.73	11	-0.704	-0.690	-0.697	0.007	662.4	Grano-diorite
67	-5.53	46.12	105.8	53.5	37.3	0.63	8	-0.713	-0.701	-0.708	0.005	265.5	Meta-Sandstone
68	-5.80	55.87	71.9	64.1	46.2	0.78	15	-0.713	-0.701	-0.710	0.003	292.9	Quartzite
69	-5.85	57.57	101.2	64.8	49.3	0.72	6	-0.729	-0.718	-0.723	0.006	388.9	Dacite
70	-6.11	68.95	87.7	79.4	56.6	0.77	8	-0.718	-0.703	-0.710	0.008	433.7	C.C. Quartzose
71	-5.90	59.57	90.7	71.6	44.4	0.67	4	-0.693	-0.636	-0.676	0.017	310.5	Meta-Sed.
72	-6.12	69.54	131.9	80.56	56.4	0.67	13	-0.907	-0.443	-0.720	0.187	679.0	Serpentine
73	-5.70	52.15	87.5	66.1	32.7	0.57	14	-0.931	-0.431	-0.726	0.205	243.7	Greenstone/Quartzose
74	-5.92	60.65	105	75.5	40.7	0.60	3	-0.713	-0.699	-0.706	0.007	450.9	Meta-Shale
75	-6.27	77.42	131.7	88.4	64.6	0.71	17	-0.725	-0.692	-0.703	0.022	1020.7	C.C. Green
76	-6.04	65.72	99.5	73.8	56.5	0.76	3	-1.122	-0.463	-0.825	0.297	441.6	UM Green
77	-5.98	62.94	104.2	67.7	57.8	0.78	8	-0.797	-0.783	-0.790	0.007	547.8	Grano-diorite
78	-5.97	62.66	122.6	72.4	51.1	0.67	18	-0.809	-0.767	-0.784	0.025	620.3	Grano-diorite
79	-6.26	76.39	96.4	89.9	59.9	0.75	13	-0.858	-0.777	-0.800	0.058	654.8	Grano-diorite
80	-6.19	72.92	102.9	88.4	53.1	0.68	16	-1.844	-0.111	-0.874	0.970	722.4	UM Green
81	-5.98	63.20	94.9	83.3	32.4	0.51	5	-0.565	-0.539	-0.554	0.011	355.3	Meta-Sed.
82	-5.81	56.06	76.5	56.8	55.3	0.89	6	-0.780	-0.762	-0.772	0.008	259.7	C.C. Quartzose
83	-5.89	59.26	94.4	66.5	51	0.75	6	-3.030	0.101	-0.602	2.428	342.7	Porph Andesite
84	-6.00	64.02	102.14	78.1	45.8	0.64	4	-0.782	-0.767	-0.776	0.006	466.2	C.C. Meta-Sed.
85	-6.18	72.58	111.06	85.5	56.8	0.70	8	-0.868	-0.626	-0.773	0.095	550.5	Greenstone
86	-6.30	78.73	108.8	96.7	55.2	0.66	5	-1.967	-0.041	-0.944	1.023	657.8	Greeny UM

Rock #	phi	Equiv. Sieve Size (mm)	Caliper Measure (mm)			Sphericity	Roundness	Magnetic Intensity			Intensity Value	Weight (g)	Note: C.C. = cache creek metamorphics Lithology
			A	B	C			Min	Max	Avg			
87	-5.65	50.07	89.4	59.5	38.4	0.65	4	-0.754	-0.733	-0.745	0.009	278.6	Porph Dacite
88	-6.49	90.06	174.2	105.8	70.9	0.65	19	-0.805	-0.724	-0.778	0.027	1793.8	Grano-diorite
89	-6.33	80.39	123.1	89.3	70.36	0.77	9	-0.760	-0.730	-0.747	0.013	895.5	Rhyolite
90	-6.02	65.07	91.3	76.4	51.3	0.72	12	-0.929	-0.530	-0.079	0.850	485.9	C.C. Green
91	-5.64	49.97	68.2	51.5	48.4	0.87	7	-0.817	-0.723	-0.779	0.038	235.5	C.C. Quartzose
92	-5.78	54.84	70.2	67.5	38.2	0.68	8	-0.727	-0.710	-0.720	0.007	215.3	Greywacke
93	-6.25	76.11	109.8	104.8	24.54	0.38	5	-0.749	-0.729	-0.741	0.008	364.5	Quartzite
94	-6.21	74.18	169.5	85.7	60.5	0.63	10	-0.732	-0.657	-0.694	0.038	1153.5	C.C. Meta-Sed.
95	-5.88	58.84	87.3	78.6	27.3	0.48	5	-0.655	-0.642	-0.649	0.006	247.8	Soapstone
96	-6.36	82.23	93	88.1	75.9	0.89	8	-0.739	-0.730	-0.734	0.005	684.7	Grano-diorite
97	-6.27	77.13	116.1	97.6	48.7	0.60	12	-0.678	-0.666	-0.672	0.006	729.3	Meta-Quartz Sandstone
98	-6.06	66.90	88.2	85.6	40.3	0.60	5	-0.878	-0.864	-0.870	0.008	460.5	C.C. Quartzose
99	-6.00	63.85	84	81	39.9	0.62	7	-0.868	-0.857	-0.862	0.006	338.4	Dacite
100	-5.93	60.81	110.5	61.6	60	0.81	4	-0.896	-0.883	-0.889	0.007	492.7	Meta-Quartz Sandstone
101	-6.38	83.14	140.2	92.1	73.1	0.75	20	-0.783	-0.698	-0.722	0.061	1605.2	C.C. Meta Quartzose
102	-5.83	56.97	83.6	58.5	55.4	0.86	5	-0.908	-0.512	-0.784	0.124	381.5	Greeny UM
103	-6.49	89.63	130.5	95.8	83	0.82	14	-0.689	-0.636	-0.667	0.022	1254.4	Grano-diorite
104	-5.61	48.96	73.1	64.3	25.7	0.52	8	-0.625	-0.613	-0.619	0.006	153.8	Meta-mudstone
105	-6.50	90.74	121.1	106.7	71.3	0.74	27	-0.646	-0.618	-0.635	0.011	1227.3	Rhyolite
106	-5.92	60.41	88.8	71.8	46.3	0.70	11	-0.598	-0.576	-0.586	0.012	378.9	Quartzite
107	-6.41	85.04	128.2	99.6	67.4	0.71	7	-2.287	-0.030	-0.591	1.696	853.6	Greeny UM
108	-5.83	57.05	87.3	74.2	31.7	0.54	6	-0.756	-0.733	-0.745	0.011	278.0	Porph Andesite
109	-6.27	76.95	105.1	80.8	72.9	0.86	6	-0.656	-0.634	-0.645	0.011	735.2	Greenstone
110	-5.69	51.52	82.6	61.6	38.9	0.67	3	-0.623	-0.595	-0.611	0.012	230.5	Meta-Sed.
111	-5.85	57.76	102.8	66.1	48	0.70	7	-0.624	-0.592	-0.599	0.025	442.5	Grano-diorite
112	-6.11	68.96	91.1	80.4	55.2	0.75	6	-0.647	-0.616	-0.626	0.021	587.2	C.C. Green
113	-5.88	58.90	84.5	78.3	28.4	0.50	6	-0.654	-0.644	-0.649	0.005	227.2	Grano-diorite
114	-5.60	48.51	95.4	58.4	36	0.62	6	-0.716	-0.626	-0.696	0.020	278.8	C.C. Green
115	-5.83	56.87	80	63	50	0.79	11	-0.712	-0.702	-0.708	0.004	322.2	Meta-conglomerate
116	-6.38	83.57	117.1	85.5	81.6	0.87	19	-0.669	-0.624	-0.648	0.021	1220.7	Grano-diorite

Rock #	phi	Equiv. Sieve Size (mm)	Caliper Measure (mm)			Sphericity	Roundness	Magnetic Intensity			Intensity Value	Weight (g)	Note: C.C. = cache creek metamorphics Lithology
			A	B	C			Min	Max	Avg			
117	-5.80	55.84	73.8	69	38.4	0.66	8	-0.633	-0.600	-0.617	0.016	236.9	Grano-diorite
118	-5.68	51.10	69.9	58.6	42.3	0.76	5	-0.649	-0.635	-0.641	0.008	238.0	Meta-greywacke
119	-6.22	74.37	80.8	84.3	62.9	0.84	5	-0.710	-0.596	-0.658	0.052	532.1	C.C. Volcanic (?)
120	-5.65	50.21	75.1	66.2	25.7	0.51	3	-0.648	-0.626	-0.634	0.014	216.8	Meta-Sed.
121	-5.72	52.57	78.1	64.6	36.8	0.65	5	-0.646	-0.636	-0.641	0.005	233.8	Dacite
122	-5.84	57.09	89.3	67.5	44.3	0.69	3	-0.867	-0.493	-0.695	0.172	300.6	C.C. Green
123	-6.08	67.44	139.3	71.6	63	0.74	5	-0.660	-0.608	-0.641	0.019	845.1	C.C. Quartzose
124	-5.75	53.63	80	67.5	34.6	0.61	7	-0.627	-0.609	-0.619	0.008	275.0	Meta-Sed.
125	-6.11	69.11	94.7	91.6	34.1	0.52	9	-0.631	-0.608	-0.621	0.010	359.1	Grano-diorite
126	-5.57	47.47	66.5	63.9	20.6	0.47	8	-0.623	-0.607	-0.616	0.007	138.4	Andesite
127	-5.71	52.22	126.8	62.4	39.5	0.59	6	-0.644	-0.598	-0.618	0.026	409.0	C.C. Green
128	-6.23	75.04	113.2	88.8	58.1	0.70	15	-0.774	-0.587	-0.704	0.070	641.3	C.C. Conglomerate
129	-5.67	50.89	82.1	55.1	46.3	0.78	1	-1.283	-0.394	-0.696	0.587	347.9	Rhyolite
130	-5.82	56.39	82.8	65	46.2	0.74	9	-1.094	-0.531	-0.750	0.344	395.3	Greeny UM
131	-6.46	88.10	156.1	104	68.6	0.66	21	-0.716	-0.690	-0.706	0.010	1593.8	Grano-diorite
132	-5.65	50.32	77.4	56	43.9	0.77	6	-0.723	-0.691	-0.707	0.016	261.9	C.C. Granitic
133	-5.92	60.68	76.1	73	45.1	0.72	9	-0.734	-0.685	-0.714	0.020	310.7	Greenstone
134	-5.82	56.60	80.8	67	43.8	0.71	5	-0.744	-0.716	-0.730	0.014	343.8	C.C. Green
135	-6.07	67.01	93.6	86	39.8	0.58	11	-0.699	-0.671	-0.683	0.016	415.9	Grano-diorite
136	-5.86	57.96	80.4	71.2	40.6	0.66	5	-0.828	-0.575	-0.713	0.115	248.3	Grano-diorite
137	-5.87	58.48	84.9	68.6	46.2	0.72	10	-0.685	-0.659	-0.674	0.011	357.7	Greywacke
138	-5.69	51.80	81.9	51.9	51.7	0.86	7	-1.443	-0.292	-0.684	0.759	333.2	Greeny UM
139	-6.09	68.14	100.6	70.4	65.8	0.85	11	-0.698	-0.675	-0.689	0.009	621.0	Grano-diorite
140	-6.25	76.23	123.6	89.7	59.8	0.69	9	-0.546	-0.471	-0.518	0.028	779.6	Grano-diorite
141	-5.96	62.47	102.5	70.3	53.5	0.74	4	-0.513	-0.471	-0.493	0.020	480.7	Grano-diorite
142	-5.71	52.38	86.3	65.6	34.4	0.60	2	-0.516	-0.464	-0.497	0.019	196.0	Meta-Quartz
143	-6.33	80.33	127.9	99.9	54.1	0.61	6	-0.499	-0.458	-0.478	0.021	778.5	C.C. Quartzose
144	-6.07	67.09	106.3	77.1	55.3	0.72	9	-0.457	-0.431	-0.446	0.011	587.9	Dacite
145	-6.13	70.27	108.6	86.4	49.1	0.64	5	-0.864	-0.072	-0.451	0.413	516.1	Greeny UM
146	-6.47	88.42	124.8	107.3	64.2	0.68	8	-0.811	-0.069	-0.635	0.176	814.7	C.C. Green

Rock #	phi	Equiv. Sieve Size (mm)	Caliper Measure (mm)			Sphericity	Roundness	Magnetic Intensity			Intensity Value	Weight (g)	Note: C.C. = cache creek metamorphics Lithology
			A	B	C			Min	Max	Avg			
147	-5.81	56.09	76.3	67.9	41	0.69	8	-0.631	-0.610	-0.618	0.013	307.5	Grano-diorite
148	-5.85	57.71	87.7	63.8	50.9	0.78	8	-0.884	-0.315	-0.596	0.288	352.7	Meta'd UM
149	-6.37	82.54	108.7	92.5	71.2	0.80	14	-0.599	-0.581	-0.592	0.007	877.1	Porph Rhyolite
150	-6.56	94.26	144.2	111.6	72.9	0.69	11	-0.602	-0.565	-0.577	0.025	1537.4	Grano-diorite
151	-5.81	55.99	87.7	70	37	0.61	5	-0.586	-0.563	-0.575	0.011	255.2	Dacite, w/quartz
152	-5.59	48.33	66.4	51	45.5	0.85	15	-0.630	-0.616	-0.622	0.008	230.5	Grano-diorite
153	-5.62	49.11	76.7	56.2	40.8	0.73	7	-0.642	-0.621	-0.634	0.008	216.5	Meta-Quartz Sandstone
154	-6.05	66.18	100.9	83.13	43	0.61	7	-0.625	-0.606	-0.616	0.009	442.0	C.C. Sed
155	-6.50	90.49	130.3	103.7	75	0.75	10	-0.632	-0.603	-0.618	0.014	1039.3	Greywacke
156	-5.66	50.69	71.2	63.8	32.7	0.62	6	-0.678	-0.599	-0.625	0.053	212.3	Rhyolite
157	-6.44	86.90	126.3	102.3	68.1	0.71	8	-0.661	-0.569	-0.614	0.047	1011.6	Dacite
158	-6.12	69.58	98	73.7	65.2	0.84	10	-0.641	-0.583	-0.618	0.023	613.7	Diorite
159	-5.87	58.54	94.1	69.3	45.3	0.68	5	-0.676	-0.659	-0.670	0.006	329.3	Quartzite
160	-6.38	83.19	124.7	95	69.4	0.74	13	-0.711	-0.670	-0.680	0.031	1151.3	Meta-Greywacke
161	-6.10	68.76	115.4	78.2	57.8	0.72	3	-0.879	-0.622	-0.733	0.146	611.2	Diorite w/ Greenstone
162	-6.40	84.61	118.4	102.1	62.4	0.69	8	-0.729	-0.678	-0.695	0.034	775.2	Meta-Sandstone
163	-6.08	67.74	93.9	78.5	54.9	0.74	3	-0.767	-0.662	-0.699	0.068	566.2	C.C. Quartzose
164	-6.35	81.83	120.3	95.2	65.8	0.73	19	-0.603	-0.582	-0.591	0.012	920.0	Grano-diorite
165	-5.87	58.56	100.3	66.7	49.1	0.71	5	-0.629	-0.562	-0.610	0.019	342.9	C.C. Green
166	-6.40	84.37	128.1	94	73.5	0.77	7	-0.619	-0.585	-0.603	0.016	964.1	Meta-Greywacke
167	-6.17	72.10	88.6	82.8	59.5	0.79	8	-0.911	-0.039	-0.587	0.324	485.6	Greeny UM
168	-5.81	56.10	79.1	67	42.5	0.70	5	-0.614	-0.594	-0.606	0.008	265.5	Grano-diorite
169	-6.33	80.24	99.5	91.8	66.7	0.79	13	-0.615	-0.603	-0.609	0.006	661.4	Grano-diorite
170	-6.26	76.45	140.9	93.2	54.8	0.61	11	-0.604	-0.592	-0.599	0.005	909.4	Andesite
171	-5.77	54.56	103	64.2	42.8	0.65	8	-0.621	-0.611	-0.616	0.005	286.1	Meta-Quartz Sandstone
172	-5.87	58.66	87.8	62.8	54.2	0.81	8	-0.643	-0.617	-0.630	0.013	334.5	Dacite
173	-6.26	76.88	104.9	90.8	59.8	0.72	13	-0.642	-0.629	-0.635	0.007	593.7	Greywacke
174	-6.17	72.22	94.7	80.7	62.6	0.80	7	-0.784	-0.547	-0.654	0.130	327.0	Grano-diorite
175	-5.88	58.85	89.3	72.2	41.4	0.65	6	-0.585	-0.566	-0.577	0.008	418.3	C.C. Mafic
176	-5.62	49.22	73.4	60.4	34.6	0.65	4	-0.821	-0.606	-0.709	0.112	214.6	Dacite

Rock #	phi	Equiv. Sieve Size (mm)	Caliper Measure (mm)			Sphericity	Roundness	Magnetic Intensity		Intensity Value	Weight (g)	Note: C.C. = cache creek metamorphics Lithology
			A	B	C			Min	Max	Avg		
177	-5.93	60.85	86	76.3	39.8	0.63	5	-0.736	-0.707	-0.720	315.1	Rhyolite w/Quartz bands
178	-5.72	52.76	115	60.4	43.8	0.65	8	-0.731	-0.706	-0.717	411.3	C.C. Quartzose
179	-6.01	64.43	80.9	80.7	42.3	0.65	7	-0.689	-0.675	-0.680	382.7	Grano-diorite
180	-5.95	61.78	74.9	69	53.6	0.82	13	-0.691	-0.681	-0.686	320.9	C.C. Volcanic
181	-6.19	73.13	117.2	75.2	71	0.83	10	-0.688	-0.666	-0.674	851.8	Grano-diorite
182	-6.26	76.56	115.8	97.4	47.3	0.59	9	-0.710	-0.686	-0.697	709.5	Grano-diorite
183	-6.19	73.00	108.2	91.4	48	0.62	3	-0.778	-0.637	-0.696	492.4	Meta-Sed.
184	-5.92	60.55	89.3	75.5	40.4	0.63	8	-0.750	-0.600	-0.692	353.5	Granitic (?)
185	-6.14	70.32	97.7	90.7	40.8	0.58	5	-0.730	-0.693	-0.714	411.0	Porph Rhyolite
186	-5.99	63.67	75.8	73.8	51.6	0.78	12	-0.773	-0.509	-0.718	350.7	C.C. Quartzose
187	-5.54	46.69	103.7	53.5	38.7	0.65	6	-0.744	-0.692	-0.720	299.8	C.C. Sed
188	-5.93	61.02	120.5	66.9	54.5	0.72	7	-0.890	-0.808	-0.854	585.3	Porph Dacite
189	-5.69	51.64	96.4	62.3	38.1	0.63	3	-4.359	0.785	-0.670	281.9	Greeny UM
190	-5.92	60.60	93.8	65.8	54.9	0.79	14	-0.850	-0.827	-0.839	516.6	Diorite
191	-5.81	56.02	83.5	67.6	41.3	0.67	3	-0.842	-0.825	-0.835	275.4	C.C. Quartzose
192	-6.29	78.01	143.18	84.7	70.7	0.75	5	-0.811	-0.762	-0.788	1235.0	Meta-Greywacke
193	-6.70	103.93	139.4	125.5	76.5	0.70	21	-0.819	-0.778	-0.801	192.6	Grano-diorite
194	-6.13	70.03	123.6	81.2	56.7	0.69	15	-0.784	-0.768	-0.776	918.2	C.C. Sed
195	-5.61	48.99	71	61.6	31.7	0.62	3	-0.782	-0.773	-0.778	190.2	C.C. Conglomerate
196	-5.62	49.18	66.4	50.8	47.5	0.88	10	-4.994	1.556	-0.575	199.2	Greeny UM
197	-5.91	60.24	111.3	74.9	40.6	0.59	3	-3.999	1.226	-0.816	428.5	Greeny UM
198	-5.76	54.33	81.2	74	20.7	0.42	1	-0.771	-0.754	-0.767	133.2	C.C. Volcanic
199	-5.73	52.98	83.1	63.6	39.6	0.67	6	-0.771	-0.760	-0.766	293.1	C.C. Sed
200	-5.67	50.76	117.6	51.5	50	0.75	3	-0.772	-0.761	-0.765	388.1	C.C. Quartz/Sed
201	-5.69	51.52	71.2	56.5	46	0.81	5	-0.871	-0.608	-0.748	250.4	Diorite
202	-5.67	50.99	101.9	58.4	42.3	0.67	3	-0.932	-0.612	-0.702	354.1	C.C. Quartz/Sed
203	-6.09	68.26	90.6	83.7	48.1	0.68	6	-0.811	-0.793	-0.800	373.5	Porph Dacite
204	-6.56	94.57	137.8	118.4	62.2	0.62	9	-0.799	-0.756	-0.787	1226.3	Granitic (light col.)
205	-6.16	71.37	127.5	83.5	56.7	0.67	8	-0.777	-0.732	-0.753	911.3	Greywacke
206	-6.69	102.91	145.7	111.2	93.9	0.82	6	-0.792	-0.712	-0.758	1765.1	Grano-diorite

Rock #	phi	Equiv. Sieve Size (mm)	Caliper Measure (mm)			Sphericity	Roundness	Magnetic Intensity			Intensity Value	Weight (g)	Note: C.C. = cache creek metamorphics Lithology
			A	B	C			Min	Max	Avg			
207	-6.42	85.48	121.2	93.6	76.5	0.80	2	-0.727	-0.717	-0.723	0.004	668.8	C.C. Sed
208	-5.83	57.05	77.3	65	47.8	0.77	5	-0.680	-0.670	-0.676	0.004	311.5	Grano-diorite
209	-5.72	52.78	79.9	61.7	42	0.71	5	-0.738	-0.482	-0.669	0.069	297.4	Porph Dacite
210	-5.89	59.34	85.2	72.3	42.6	0.67	4	-0.828	-0.626	-0.723	0.105	301.8	C.C. Quartzose
211	-6.03	65.32	98.3	83.7	39.1	0.57	3	-0.769	-0.597	-0.705	0.064	367.7	Grano-diorite
212	-5.97	62.64	101.1	80.9	36.1	0.55	2	-0.823	-0.624	-0.783	0.040	388.5	C.C. Sed
213	-5.49	45.02	83.9	53.9	33.9	0.64	5	-0.780	-0.764	-0.772	0.008	260.2	Grano-diorite
214	-5.73	53.02	92.4	63.1	40.5	0.66	4	-0.781	-0.746	-0.768	0.013	305.9	C.C. Quartzose
215	-5.69	51.45	69	50.9	52	0.92	5	-1.282	0.064	-0.763	0.519	212.8	Greeny UM
216	-6.04	65.82	99.9	84	40.1	0.58	4	-0.751	-0.717	-0.733	0.018	396.4	Andesite (pink, v. fine)
217	-6.16	71.47	116.3	84.4	55.6	0.68	2	-0.815	-0.483	-0.710	0.105	550.2	C.C. UM (?)
218	-5.69	51.47	79.9	52.8	50.1	0.84	9	-0.776	-0.745	-0.764	0.012	320.3	C.C. Quartzose, Porph
219	-5.97	62.88	100.9	73.6	49.9	0.70	4	-1.184	0.212	-0.742	0.442	585.4	C.C. UM
220	-6.06	66.67	81.6	77.7	53.4	0.77	13	-0.753	-0.737	-0.744	0.009	426.8	Grano-diorite
221	-5.93	60.77	94.4	68.8	51.5	0.74	3	-0.742	-0.697	-0.723	0.019	388.5	Quartzite
222	-5.65	50.28	80.1	55.3	44.7	0.77	2	-0.705	-0.685	-0.697	0.008	243.8	Dacite (greenish)
223	-5.57	47.37	102	59.6	30.6	0.54	4	-0.695	-0.670	-0.683	0.012	316.8	Quartzite
224	-5.78	54.97	84.6	69	35.8	0.61	3	-0.748	-0.559	-0.681	0.067	270.5	C.C. Andesite
225	-5.82	56.31	94.1	66.5	43.8	0.68	1	-0.681	-0.636	-0.652	0.029	390.5	C.C. Quartzose
226	-5.99	63.51	85.8	74	50.9	0.74	7	-0.690	-0.465	-0.616	0.074	450.7	C.C. UM
227	-5.63	49.65	71.2	55.2	43.4	0.78	5	-0.609	-0.583	-0.593	0.016	265.3	C.C. Quartzose
228	-5.63	49.44	79.5	57	40.5	0.72	8	-0.600	-0.577	-0.590	0.010	287.1	Meta-Sandstone
229	-5.70	51.83	73.1	59	43.5	0.76	4	-0.619	-0.547	-0.585	0.034	232.7	Grano-diorite
230	-5.73	52.90	70	61.7	42.3	0.75	2	-0.768	-0.751	-0.761	0.007	268.6	Porph Dacite
231	-5.72	52.81	72.9	62.1	41.5	0.73	4	-0.766	-0.754	-0.750	0.016	259.2	C.C. Quartz/Sed
232	-5.88	58.70	83.1	75	35.6	0.59	5	-0.772	-0.736	-0.756	0.016	233.0	Dacite
233	-5.66	50.56	96.9	61.3	36.8	0.61	4	-0.851	-0.660	-0.753	0.098	261.5	C.C. Quartz/UM
234	-5.59	48.15	80.8	52.8	43	0.76	3	-0.753	-0.730	-0.743	0.010	239.3	Diorite w/Quartz bands

Appendix C – Laboratory calibration data

Tests were done on the BMD sensors using 6 rocks of varying size and lithology. The rocks were affixed to a pendulum and passed over two sensors at varying speeds. Three positions were tested: across the middle of sensor 1, at one quarter the width of sensor 1 (toward sensor 2), and exactly between the two sensors. The position is indicated by the picture at the top of each set of diagrams. The clasts were passed at three speeds: 1.4 m/s, 0.8 m/s and 0.4 m/s. Note that the voltage scale is the same for all diagrams.

The rocks used were as follows:

Sample	Weight	Short Circumf.	Long Circumf.	Rock Type
A	214 g	15.2 cm	18.7 cm	Metapyroxinite
B	388 g	17.5 cm	22.8 cm	Andesite
C	22.1 g	7.0 cm	8.9 cm	Serpentine (+?)
D	1355 g	30.4 cm	34.9 cm	Granodiorite
E	552 g	19.5 cm	30.2 cm	Greenstone
F	69.1 g	17.3 cm	14.6 cm	Serpentine (+?)

Table 10 - Characteristics of rock samples used in pendulum experiments.

